To the Graduate Council:

I am submitting herewith a dissertation written by Geoffrey St. John Canright entitled "Hot Electrons and Core Hole Screening." I have examined the final copy of this document for form and content and recommend that it be accepted in partial fulfillment of the requirements for the degree of Doctor of Philosophy, with a major in Physics.

Gerald D. Mahan, Major Professor

We have read this dissertation
and recommend its acceptance:

Accepted for the Council:

Vice Provost
and Dean of the Graduate School

Hot Electrons and Core Hole Screening

A Dissertation
Presented for the
Doctor of Philosophy
Degree
The University of Tennessee, Knoxville

Geoffrey St. John Canright
December 1987

Acknowledgements

I am greatly indebted to Dr. Gerald Mahan for serving as my thesis advisor; he has created an environment in which I could discover my own abilities to seek out and solve interesting problems, while remaining in touch with my efforts so as to provide help at crucial points. It has been a pleasure to learn from someone who knows the Golden Mean between too much and too little interference.

I am no less indebted to the other members of my committee: Dr. Joachim Burgdörfer, Dr. J. O. Thomson, and Dr. M. O. Pace. Each has contributed in an important way to the progress of my work to this point. I also wish to express my deep appreciation for the support of my wife. Dian has managed to share the raising of a family and the tending of a farm, deliver and care for hundreds of babies, and (important!) feed me, while putting up with the needs and idiosyncracies of a Ph.D. student in physics. This is not an easy task and she has performed marvelously.

I wish also to thank Drs. Tom Callcott, Jim Thompson, Giovanni Vignale, and Mark Mostoller for conversations which helped me learn to think in the cryptic world of solid-state physics. I look forward to further interaction with all those persons named here.

I am further indebted to the University of Tennessee for significant financial support during the course of my work, in the form of a General Electric Scholarship, a Graduate School Fellowship award, and continuing support from the Science Alliance.

Abstract

Two problems are discussed with respect to the applicability of linear response theory. In Part I, high-field transport in solids is treated analytically in one dimension for optical phonon scattering, for arbitrary field strength. The problem is thus highly nonlinear in field, while linearized in the carrier concentration, which in turn implies neglecting carrier-carrier scattering. Results are obtained for a constant field profile. The results show the well-known velocity saturation behavior in a realistic way, thus emphasizing the critical role of optical phonons in this phenomenon. A Maxwellian distribution is found at all fields; in some cases the electron temperature is lower than the lattice temperature. Runaway is shown to result from forward (polar) scattering, but not for isotropic scattering. The formalism developed for the high-field problem is also applied to the transient relaxation of carriers under photoexcitation; the results are compared with experiment. In Part II, the dynamic screening of a suddenly-created core hole in a metal is examined in the linear approximation. The photoelectron is neglected; the results are thus valid for photon energies well above threshold. The time and space dependence of the screening charge, for high and low electron gas density, is obtained by numerical integration over the spectral function of the dynamic dielectric function. The integral is broken into a plasmon part and an electron-hole pair (e-h) part, from the corresponding regions of the spectral function. The e-h part is found to be more heavily damped, and much larger in amplitude ($\times 30$) than the plasmon part; however, both parts respond on essentially the same time scale given by the inverse plasma frequency. Addition of local-field corrections to the RPA is found to have little effect on the results. Transients in screening are found to be larger and more persistent for low density than for high density. However, in either case transients are not predicted to persist to times on the order of the core hole lifetime from x-ray emission.

Contents

List of Figures

Chapter 1

Overview

Linear response theory has a well-earned place in physics due to its general utility and applicability to a wide variety of physical problems [1]. The assumption of linear response generally makes a problem more tractable, and hence is employed whenever it is judged to be physically reasonable. In the following we will examine two somewhat different problems in physics: electron transport and impurity screening in solids. For the former problem we will find it possible to go beyond the linear approximation in an important way, obtaining a variety of realistic results pertinent to transport in large fields. In the latter problem we find new results for the time response of the electron gas, while remaining within linear response theory, leaving a more general treatment of the problem to a future theory.

In each case (charge transport, and screening) it is perhaps fair to say that the level of approximation which is employed is not far from what is needed to describe current experiments. More specifically: for the transport case, developments in semiconductor microfabrication techniques have resulted in the routine application of very large electric fields (normal voltages across very small distances), necessitating a theory which goes beyond the linear (in field) approximation. This need has been clear for some time, and a number of efforts have been made to meet it. In the case of impurity screening, static effects are generally observed experimen-

tally at nearest-neighbor distances or greater, for which linear response is not a bad approximation. Dynamic screening effects, on the other hand, are of interest in theories of x-ray absorption and emission in metals, in which the response of the conduction electrons to the charged core hole is important; but for this problem the time scale of the response is more significant than the amplitude. Here we rely on the argument that, to the extent linear response theory can correctly depict the frequency dependence of the spectral function of the electron gas, it can model the dynamic response accurately.

In the following two Parts we shall describe in more detail the background and motivation for the present work. The remainder of this chapter will be used to specify more precisely the problems which were attempted and solved in the course of this work.

The quantum-mechanical treatment of electron transport in the presence of arbitrarily strong, inhomogeneous electric fields, subject to the full variety of scattering mechanisms, is obviously impossible in its most general form. A wide variety of simplifying assumptions is possible, each having its own merits. We have chosen a subset which is intended to illuminate the large-field problem; the original formulation of the problem in this form and its partial solution were given by Mahan [2] in recent work.

As a first, and major, step, we start with a classical transport equation, the Boltzmann equation [3]. The Boltzmann equation treats electrons as particles with well-defined position and momentum. The effect of the lattice is incorporated in two ways: it renormalizes the electron mass, and acts as a source for phonons. Thus we model a gas of two species of interacting particles, with number conservation holding only for the electrons. The particle picture is adequate to the extent that a wave packet picture is adequate, with the packet being built from Bloch functions; the picture breaks down if the effective mean free path becomes too short (strong

scattering), or if the field varies on a length scale which is comparable with the wave-packet extension.

The Boltzmann equation describes the electron distribution function $f_e(k, r, t)$ and the phonon function f_p. Either can be written as

$$f = f^0 + \delta f$$

where f^0 is the equilibrium distribution and δf the change induced by the field. A linear theory would discard terms in δf beyond first order in field. We choose to retain the full field dependence of f_e in accord with our goal. We do however assume that f_e itself is small, that is, that the carriers are dilute. This enables two simplifications. First, terms in f_e^2 are discarded. Hence electron-electron scattering (which goes as f^2) is neglected. Second, since the field perturbs the phonon distribution only through its effect on f_e, we can set $\delta f_p = 0$, or $f_p = f_p^0$.

We further restrict the spatial dependence of f_e to one dimension, and seek only the steady-state solution. We consider scattering only by optical phonons with an Einstein spectrum, $\omega_q = \omega_0$. The full set of constraints chosen thus constitutes a reasonable model for transport in semiconductors in large fields. In these systems charge carriers are dilute, flow is commonly two-dimensional and often quasi-one-dimensional, and optical phonons are the dominant scattering mechanism.

With the model thus chosen, we can discretize the electron distribution as follows: change variables from momentum to energy, and then use the fact that, for dispersionless phonons, energy is gained or lost only in fixed increments of $\hbar\omega_0$. The problem then reduces to one of linear algebra (in infinite vectors and matrices). The solution employs the eigenvalues and eigenvectors found by Mahan [2]; some rather subtle considerations regarding boundary conditions remain which have yet to be fully resolved, except for the constant-field case. In the latter case the electron distribution is obtained for a variety of fields and lattice temperatures, thus yielding a description of electron heating, velocity saturation, and (in some cases) electron velocity runaway.

The one-spatial-dimension, steady-state problem is then shown to map onto the transient (one time dimension) problem which is spatially isotropic. Hence the same formalism may be applied to describe the transient relaxation via optical phonon scattering of dilute carriers under photoexcitation in semiconductors. This process, as studied experimentally via the luminescence of the recombining carriers, is in fact one in which the dominance of optical phonon scattering is clearly revealed by the observation of discrete (although broadened) lines in the luminescence spectra, which are evenly spaced at intervals of $\hbar\omega_0$. Boundary conditions are trivial in this (time-dependent) case, and results are obtained for both pulsed and steady illumination, the latter problem yielding a steady-state solution which may be compared with experiment. Thus a one-dimensional solution to the transport problem, first developed to describe high-field transport, yields as a bonus a description of the time relaxation of nonequilibrium carriers under photoexcitation.

We now shift our attention to metals, and raise the photoexcitation energy to the x-ray band, in order to study another relaxation process: the dynamical screening response of the electron gas. Here we assume that the absorption of an x-ray photon excites a core electron in a metal to an energy sufficient to ionize the core, leaving behind a positively-charged "impurity" (a core hole). The question is, how does the electron gas respond in real space and time to the creation of the hole? After a few approximations are made, the answer is obtained in the form of a double integral which is computed numerically.

The core hole is modeled as a featureless, point positive charge which is created instantaneously at $t = 0$, $r = 0$. This is not an unreasonable model since atomic (core) relaxation processes occur at significantly smaller time and spatial scales than those of interest in extra-atomic screening. We further assume that the ejected electron has no further effect on the screening response beyond leaving behind a charged hole; in other words, it is ejected with infinite velocity. The results thus obtained are clearly appropriate only for x-ray energies far above the ionization

threshold. For lower x-ray energies, the photoelectron will remain in the vicinity of the core hole on a time scale comparable to that of the screening cloud, and hence affect and be affected by the screening. This problem, while interesting, is not dealt with here and remains to be examined in future work.

Finally, as mentioned above, we assume that the screening charge is proportional to the perturbation, ie we assume linear response. This enables the exploitation of the well-developed machinery of linear screening theory using the wavevector- and frequency-dependent dielectric function $\epsilon(q,\omega)$ [4]. With a choice of ϵ one can then calculate the screening charge density $\rho(r,t)$ (actually the deviation from the uniform, unperturbed density n_0) induced by the core hole. The results obtained are essentially in agreement with previous ideas: we find that the transients in screening persist for a time ω_p^{-1}, where ω_p is the long-wavelength plasma frequency, and hence that dynamic effects of screening on the following core hole decay by x-ray emission (which occurs at times $\gg \omega_p^{-1}$) are expected to be small.

Part I

Hot Electrons in One Dimension

Chapter 2

Introduction to Part I

Whenever carriers in a solid are accelerated by an electric field their average energy is increased over the equilibrium value. The carriers reach a steady-state distribution (in steady field) when the input of energy and momentum from the field is balanced by equal fluxes of the same quantities to the lattice. For small fields the field-induced energy increment is negligible relative to the mean carrier energy. In this case we say that the carrier temperature is unchanged from the equilibrium (lattice) value. It follows that the transport coefficient of interest—ie the conductivity—takes, for small fields, the value appropriate to the equilibrium temperature; the response (current) is then linear in field. Hence we can define the linear-response regime as that in which the change in carrier energy is negligible [5].

Correspondingly, linear-response coefficients are inapplicable when the mean energy—or temperature—of the carriers becomes field-dependent. Since the mean energy is expected to increase with field, such carriers are called "hot electrons" (or holes). The study of high-field transport then involves the study of various hot-electron effects which are not seen in the linear regime. A good early introduction to the field was given by Conwell [6]; more recent references include [5,7,8,9,10]. Fröhlich [11] first introduced the concept of an electron temperature T_e greater than the lattice temperature T_l, in a study of the electrical breakdown process in

solids; we may regard this as the birth of the hot-electron concept. In the following we will briefly survey a variety of hot-electron phenomena.

One of the earliest experimental observations of a hot-electron effect was obtained in bulk semiconductors by Ryder and Shockley [12,13]. They observed the evolution of the current density from the linear regime, characterized by Ohm's Law, or

$$j = \sigma_0 F \tag{2.1}$$

with σ_0 a constant, through a region in field F where the current density j fell significantly below the value given by (2.1), to the saturation region characterized by

$$j \approx \text{constant} = j_s$$

at high fields. The fields required to reach saturation were temperature-dependent, being larger at higher temperature, and on the order of 10^3 V/cm for Ge, and 10^4 V/cm for Si. The saturation velocity, given by

$$v_s = j_s/nc,$$

with n the carrier density and e the electronic charge, was found to be only weakly temperature-dependent [13].

More recent observations of saturation include that of Fang and Fowler [14] for a (two-dimensional) inversion layer in Si; similarly, for holes in bulk p-Ge by Nougier and Rolland [15], and for electrons in SiO_2 by Hughes [16].

A simple picture involving optical phonons may be used to describe saturation at low temperatures. If we assume optical phonons are the principal scatterers, and that a phonon is emitted promptly by any carrier whose energy exceeds the phonon energy $\hbar\omega_0$, then clearly no carrier will be accelerated by the field to a velocity much greater than v_M, where

$$E(v_M) = \hbar\omega_0,$$

E being the carrier energy. The average carrier velocity at saturation, v_s, will then be proportional to v_M [17]. At higher temperatures the absorption of thermally generated phonons tends to retard the approach to saturation, while having a small effect on the saturation velocity.

It is also possible to observe the carrier velocity to reach a peak and then decrease with increasing field, giving rise to a region of negative differential mobility [5]. This occurs as the carriers acquire sufficient energy to transfer into a state with significantly larger effective mass. This latter state may be another valley in the conduction band (intervalley transfer), or, in the case of heterostructures, a high-mass valley in the conduction band of an adjacent layer (real-space transfer) [18].

At very high fields, the same optical phonons which are responsible for velocity saturation may be incapable of absorbing energy from the accelerated carriers at a rate sufficient for stabilizing the carrier population. The carriers then "run away" from the phonons for fields above a threshold field, where the power input from the field equals the maximum dissipation attainable with optical phonons. Runaway was predicted as early as 1937 [19],but not experimentally verified until very recently [20]. Above the runaway field the electrons accelerate until some other mechanism sets in at higher energies, such as impact ionization [21]. It is interesting to note that Thornber and Feynman, using path-integral techniques in a fully quantum-mechanical transport theory, were able to model all three regions (linear, saturation, and runaway), at arbitrary temperature, in a single calculation [22].

Other hot-electron effects involve small devices, in which a steady-state distribution is not attained due to the short conduction channel. One then must consider current transients in space; for example, the carrier velocity may rise above the steady value (that expected at $x \rightarrow \infty$) at the injection end of the channel (velocity overshoot) [23]. In the extreme case, injected electrons may traverse an ultrashort channel without scattering at all, thus exhibiting ballistic transport [24,25].

Finally we mention a phenomenon which has not been experimentally verified,

and perhaps cannot be termed a "hot"-electron effect. Several theoretical calculations have predicted that, for certain values of field and lattice temperature T_l, the carrier population may be ascribed a temperature which is lower than T_l [24,26,27,28]. A credible argument for such an effect is as follows: assuming the only strong scatterers (optical phonons) have an energy which is large compared to a typical (equilibrium) carrier energy, we can expect the field to impart a significant center-of-mass (CM) momentum to the carrier population. Viewing the carrier energy in the CM frame can then lead to a low temperature if the carriers are strongly clustered about the CM momentum.

Early calculations [26,27] assumed a CM momentum $\vec{k_0}$, and a temperature T_e, related by

$$f(\vec{k}) = a \exp\left(-\frac{(\vec{k}-\vec{k_0})^2}{2mk_BT_e}\right) \tag{2.2}$$

where m is the effective mass and k_B is Boltzmann's constant. Eq. (2.2) is called the "displaced Maxwellian" form for the distribution function (DF). We shall find in Chapter 3, for a model which only considers optical phonons, that cooling is also predicted. The model of Chapter 3, however, does not assume any specific form for the DF; and, contrary to [21-23], in this work energy is defined in the "lab" frame, ie relative to the lattice.

Another means of exciting hot carriers in semiconductors is by photoexcitation [29], which allows a control over the excited population density and energy distribution which is not possible in electric fields. The study of the time relaxation of the excited population has provided a great deal of information on scattering mechnisms and lifetimes in semiconductors [30,31]. Where a typical experiment consists of "excite-and-probe", an electric field or photoexcitation can serve as the exciting agent, and the latter as the probe. In the most general case, hot electrons, hot holes, and hot phonons [32,33] all present significant effects.

We next briefly review previous theoretical work on hot carriers. The Boltzmann Transport Equation (BTE) has been the traditional theoretical tool, capable in

principle of incorporating all but quantum effects. It is [5, Ch. 11]

$$\frac{\partial f}{\partial t} + \vec{v} \cdot \frac{\partial f}{\partial \vec{r}} + \vec{F} \cdot \frac{\partial f}{\partial \vec{p}} = \left(\frac{\partial f}{\partial t} \right)_c \tag{2.3}$$

where $f = f(\vec{r}, \vec{p}, t)$ is the DF giving the occupation of the state with momentum $\vec{p}$ at location $(\vec{r}, t)$. The left-hand terms represent continuous streaming of f in phase space; the right-hand term incorporates the effects of scattering. There are various methods of solving the BTE [6]; [5, Ch. 11]. The relaxation-time approximation [24,33,34] replaces the scattering term with

$$\left(\frac{\partial f}{\partial t} \right)_c = - \left(\frac{f - f_0}{\tau} \right) \tag{2.4}$$

where f_0 is the equilibrium DF and τ is a relaxation time. Other methods involve assuming a parameterized form (spherical harmonic expansion [35], Maxwellian, or drifted Maxwellian [26,27]) for the DF and then using energy and momentum balance equations to solve for the parameters. Numerical solutions are also frequently employed [15,24,27,33], since analytical solutions are generally limited in scope. Finally, there are Monte-Carlo techniques [36,37].

Clearly the model of point particles with independent, instantaneous collisions which is implicit in the classical BTE must break down for sufficiently small devices, large fields, or strong scattering. Considerable work has been done towards a quantum-mechanical transport theory [28,38–42]. Some authors [38,39] have found that the BTE, as tested against a quantum transport theory, should be valid for a wide range of experimental conditions, including very high fields [39]. This work, along with the considerable efficacy of the BTE as found in previous work through comparison with experiment, justifies continued reliance on the BTE for many high-field problems.

The remainder of Part I consists of three chapters. Chapter 3 presents an analytical solution to the BTE in one spatial dimension, in steady state for arbitrary field and temperature; most of this work has been published [43]. Chapter 4 is a published article [44] on the runaway problem, using the theory of Chapter 3.

Finally, Chapter 5 presents another paper [45] which maps the one-dimensional, steady-state problem onto the transient, homogeneous case, enabling the analysis of relaxation under photoexcitation.

Chapter 3

High-field Transport

3.1 Formulation of the Problem

The Boltzmann equation may be written

$$Df = \left(\frac{\partial f}{\partial t}\right)_c \tag{3.1}$$

where

$$Df = \frac{\partial f}{\partial t} + \dot{\vec{r}} \cdot \frac{\partial f}{\partial \vec{r}} + \dot{\vec{k}} \cdot \frac{\partial f}{\partial \vec{k}} \tag{3.2}$$

contains all the terms from the continuous streaming of f in phase space, and $\left(\frac{\partial f}{\partial t}\right)_c$ describes the effect of collisions. Here and from now on we let $\hbar = 1$ and k_B (Boltzmann's constant) $= 1$. Next we restrict to one dimension and steady state, obtaining

$$v\frac{\partial f}{\partial x} - \frac{\partial V}{\partial x}\frac{\partial f}{\partial k} = \left(\frac{\partial f}{\partial t}\right)_c \tag{3.3}$$

where V is the electrostatic potential energy. Now introduce the total energy

$$E = \frac{k^2}{2m} + V(x) = E(k, x).$$

Since E is a function of both k and x, we must transform both partial derivatives on the lhs of (3.3); in matrix form

$$\begin{pmatrix} \frac{\partial f}{\partial x} \\ \frac{\partial f}{\partial k} \end{pmatrix} = \begin{pmatrix} \frac{\partial x}{\partial x} & \frac{\partial E}{\partial x} \\ \frac{\partial x}{\partial k} & \frac{\partial E}{\partial k} \end{pmatrix} \begin{pmatrix} \frac{\partial f}{\partial x} \\ \frac{\partial f}{\partial E} \end{pmatrix}$$

or

$$\frac{\partial f}{\partial x} = \frac{\partial f}{\partial x} + \frac{\partial V}{\partial x}\frac{\partial f}{\partial E}$$
$$\frac{\partial f}{\partial k} = \frac{k}{m}\frac{\partial f}{\partial E} = v\frac{\partial f}{\partial E}$$

giving, upon substitution into (3.3),

$$v\frac{\partial f}{\partial x} = \left(\frac{\partial f}{\partial t}\right)_c . \tag{3.4}$$

The collision term is normally written in the form

$$\left(\frac{\partial f(k,r,t)}{\partial t}\right)_c = \sum_{k'} |W_{kk'}|^2 \left[f_{k'}(1-f_k) - f_k(1-f_{k'})\right] \delta(E) \tag{3.5}$$

where $f_k = f(k,r,t)$, etc.

When we transform to an energy basis we must keep track of angular information. This is simple in one dimension, where the directional degrees of freedom collapse to two discrete values which we call (+,-). Thus f_E^+ denotes particles of energy E with velocity in the positive x-direction, and f_E^- particles traveling in the opposite direction. We decompose the matrix element $|W_{kk'}|^2$ into an energy dependence, $1/\tau_{EE'}$, a boson number factor (N_0 for phonon absorption and (N_0+1) for emission), and a directional dependence, for which we introduce the parameter α. The latter is defined so that, for a given (E,E'), the probability of a scattering event which reverses the velocity is α times the probability of the same event without reversal. N_0 is the Bose function, $(\exp(G)-1)^{-1}$, where $G = \omega_0/T$.

In this notation Eq. (3.5) becomes

$$\left(\frac{\partial f_E^+}{\partial t}\right)_c = \int_0^\infty dE' \frac{1}{\tau_{EE'}}$$

$$
\begin{aligned}
&\times \Big\{ N_0 \left[(f^+_{E'} + \alpha f^-_{E'})(1 - f^+_E)\delta(E' - E + \omega_0) \right. \\
&\left. - f^+_E \, (1 - f^+_{E'} + \alpha - \alpha f^-_{E'})\delta(E' - E - \omega_0) \right] \\
&+ (N_0 + 1) \left[(f^+_{E'} + \alpha f^-_{E'})(1 - f^+_E)\delta(E' - E - \omega_0) \right. \\
&\left. - f^+_E \, (1 - f^+_{E'} + \alpha - \alpha f^-_{E'})\delta(E' - E + \omega_0) \right] \Big\} . \qquad (3.6)
\end{aligned}
$$

The four terms in curly brackets denote, respectively, phonon absorption into final state E, absorption from initial state E, emission into E, and emission out of E. Each term contains a forward-scattering term, and a backscattering term which is multiplied by α. The analogous equation for f^-_E is Eq. (3.6) with all the (+,-) superscripts exchanged.

Now divide Eq. (3.4) by v and let

$$
\frac{1}{v(E)} \frac{1}{\tau_{EE'}} \equiv \frac{1}{\ell_0}
$$

where ℓ_0 is the mean free path for phonon scattering in the forward direction, assumed constant. Then, combining (3.4) and (3.6),

$$
\begin{aligned}
\ell_0 \frac{\partial f^+_E}{\partial x} = \\
&N_0 \left[f^+(E - \omega_0) + \alpha f^-(E - \omega_0) \right] (1 - f^+_E)\Theta(E - \omega_0) \\
&- N_0 f^+_E \left[1 - f^+(E + \omega_0) + \alpha - \alpha f^-(E + \omega_0) \right] \\
&+ (N_0 + 1) \left[f^+(E + \omega_0) + \alpha f^-(E + \omega_0) \right] (1 - f^+_E) \\
&- (N_0 + 1) f^+_E \left[1 - f^+(E - \omega_0) + \alpha - \alpha f^-(E - \omega_0) \right] \Theta(E - \omega_0) \qquad (3.7)
\end{aligned}
$$

Here the corresponding equation for f^-_E has a minus sign, since $v(-) = -v(+)$.

Now we linearize the equation by neglecting terms quadratic in f, which is reasonable for low carrier concentrations. This gives

$$
\begin{aligned}
\ell_0 \frac{\partial f^+_E}{\partial x} &= N_0 \left[f^+(E - \omega_0) + \alpha f^-(E - \omega_0) \right] \Theta(E - \omega_0) \\
&\quad - N_0 f^+_E (1 + \alpha)
\end{aligned}
$$

$$+ (N_0+1)\left[f^+(E+\omega_0) + \alpha f^-(E+\omega_0)\right]$$
$$- (N_0+1) f_E^{\pm}(1+\alpha)\Theta(E-\omega_0) \tag{3.8}$$

Mahan [2] solved the above equation for $\alpha = 0$. In this work we take $\alpha = 1$, ie back- and forward-scattering equally probable. The case for general α, while also soluble, is more complicated and has not been treated.

Equation (3.8) clearly describes a discrete set of energy levels. There is a lowest level, and a set of levels spaced ω_0 apart. Thus, as long as scattering is only by dispersionless phonons, we find the carrier population divided according to energy into noninteracting subsets. An electron of energy E will mix with a population of electrons of $E \pm n\omega_0$ (n an integer) only; carriers of energy $E + \delta$ ($\delta \neq n\omega_0$) do not enter the problem. We proceed by solving for one subset which scatters among energies $\varepsilon_0 + l\omega_0$, $l = 0, 1, 2, \ldots$

The lowest energy ε_0 is essentially irrelevant to the solution and is hence dropped from the notation; thus

$$f_E^{\pm} \Longrightarrow f_l^{\pm}$$

In this notation, Eq. (3.8) and its analog for f^- become, with $\alpha = 1$,

$$\ell_0 \frac{\partial f_l^+}{\partial x} = N_0(f_{l-1}^+ + f_{l-1}^-)\Theta(l-1) - 2N_0 f_l^+ + (N_0+1)(f_{l+1}^+ + f_{l+1}^-) - 2(N_0+1) f_l^+ \Theta(l-1) \tag{3.9}$$

$$\ell_0 \frac{\partial f_l^-}{\partial x} = -N_0(f_{l-1}^- + f_{l-1}^+)\Theta(l-1) + 2N_0 f_l^- - (N_0+1)(f_{l+1}^- + f_{l+1}^+) + 2(N_0+1) f_l^- \Theta(l-1) \tag{3.10}$$

The sum and difference of these two equations give

$$\ell_0 \frac{\partial F_l}{\partial x} = -2N_0 G_l - 2(N_0+1) G_l \Theta(l-1) \tag{3.11}$$

$$\ell_0 \frac{\partial G_l}{\partial x} = 2N_0 F_{l-1}\Theta(l-1) - 2N_0 F_l - 2(N_0+1)F_{l+1} - 2(N_0+1)F_l\Theta(l-1) \tag{3.12}$$

where

$$F_l = f_l^+ + f_l^-$$

and

$$G_l = f_l^+ - f_l^-.$$

More compactly,

$$\vec{F}' = -M_1\vec{G} \tag{3.13}$$

$$\vec{G}' = -M_2\vec{F} \tag{3.14}$$

where the prime signifies $\partial/\partial z$, $z = 2x/l_0$,

$$M_1 = Diag(N_0, 2N_0+1, 2N_0+1, \ldots) \tag{3.15}$$

$$M_2 = \begin{pmatrix} N_0 & -N_0-1 & 0 & 0 & \cdots \\ -N_0 & 2N_0+1 & -N_0-1 & 0 & \cdots \\ 0 & -N_0 & 2N_0+1 & -N_0-1 & \cdots \\ 0 & 0 & -N_0 & 2N_0+1 & \cdots \\ 0 & 0 & 0 & -N_0 & \cdots \\ \vdots & \vdots & \vdots & \vdots & \ddots \end{pmatrix}. \tag{3.16}$$

The matrix M_2 is identical to the matrix M obtained by Mahan [2] for the $\alpha = 0$ problem.

Finally we write Eqs. (3.13), (3.14) in the most compact form,

$$\vec{X}' = -A\vec{X} \tag{3.17}$$

or

$$\begin{pmatrix} \vec{F} \\ \vec{G} \end{pmatrix}' = -\begin{pmatrix} 0 & M_1 \\ M_2 & 0 \end{pmatrix}\begin{pmatrix} \vec{F} \\ \vec{G} \end{pmatrix} \tag{3.18}$$

Eq. (3.17) is a linear, homogeneous, first-order vector differential equation with constant coefficient matrix A. Hence the solution may be written as

$$\vec{X} = \sum_i a_i e^{-\lambda_i z}\vec{x}_i \tag{3.19}$$

where λ_i and $\vec{x}_i$ satisfy

$$A\vec{x}_i = \lambda_i \vec{x}_i, \tag{3.20}$$

ie they are respectively the eigenvalues and eigenvectors of A. Hence the solution of the Boltzmann equation in the form of Eq. (3.17) reduces to first finding the spectrum of A, and then using boundary conditions to determine the constants a_i. These two parts of the solution are described in the following two sections.

3.2 Eigenvalues and Eigenvectors of A

We suspect that A has a zero eigenvalue whose eigenvector $\vec{x^0}$ is the equilibrium solution; ie it satisfies

$$(\vec{x^0})' = -A\vec{x^0} = \vec{0}$$

We can expand $|A|$ in cofactors, using the elements of M_1, to obtain

$$|A| = N_0(2N_0+1)(2N_0+1)\cdots(2N_0+1)|M_2|.$$

However we know that $|M_2| = 0$ from Mahan's [2] work. Hence $|A| = 0$, and so $\lambda = 0$ is an eigenvalue of A. The eigenvector $\vec{x^0}$ satisfies

$$A\vec{x^0} = \begin{pmatrix} 0 & M_1 \\ M_2 & 0 \end{pmatrix} \begin{pmatrix} \vec{y} \\ \vec{z} \end{pmatrix} = \vec{0} \tag{3.21}$$

or, written out,

$$\begin{pmatrix} N_0 z_0 \\ (2N_0+1)z_1 \\ (2N_0+1)z_2 \\ \vdots \\ M_2\vec{y} \end{pmatrix} = \begin{pmatrix} 0 \\ 0 \\ 0 \\ \vdots \\ \vec{0} \end{pmatrix} \tag{3.22}$$

The upper half of (3.22) gives $z_l = 0$ for all l. The lower half is satisfied by

$$y_l = ke^{-Gl},$$

as shown by Mahan [2]. Thus

$$\vec{x}^0 = k \begin{pmatrix} e^{-Gl} \\ \vec{0} \end{pmatrix}. \tag{3.23}$$

Now we show that all powers of λ in the secular equation,

$$|A - \lambda I| = 0,$$

are *even*, or equivalently that the eigenvalues λ_A occur in pairs of opposite sign. Assume

$$A\vec{x} = \lambda_A \vec{x} \tag{3.24}$$

Then

$$\begin{aligned} A^2\vec{x} &= \begin{pmatrix} 0 & M_1 \\ M_2 & 0 \end{pmatrix} \begin{pmatrix} 0 & M_1 \\ M_2 & 0 \end{pmatrix} \vec{x} \\ &= \begin{pmatrix} M_1 M_2 & 0 \\ 0 & M_2 M_1 \end{pmatrix} \vec{x} \\ &= \lambda_A^2 \vec{x} = \lambda_A^2 \begin{pmatrix} \vec{y} \\ \vec{z} \end{pmatrix}. \end{aligned} \tag{3.25}$$

Thus

$$M_1 M_2 \vec{y} = \lambda_A^2 \vec{y}$$

$$M_2 M_1 \vec{z} = \lambda_A^2 \vec{z}$$

Let λ_{12} be an eigenvalue of $M_1 M_2$, and similarly for λ_{21} and $M_2 M_1$. Then we have

$$\lambda_A^2 = \lambda_{12} = \lambda_{21}$$

or

$$\lambda_A = \pm(\lambda_{12})^{1/2} = \pm(\lambda_{21})^{1/2}. \tag{3.26}$$

Let us find the eigenvalues λ_{21} of M_2M_1. For convenience we will drop the subscripts on λ_{21}.

$$M_2M_1 = \begin{pmatrix} a^2 & -bc & 0 & 0 & \\ -a^2 & c^2 & -bc & 0 & \\ 0 & -ac & c^2 & -bc & \\ 0 & 0 & -ac & c^2 & \\ & & & & \ddots \end{pmatrix} \tag{3.27}$$

where

$$a = N_0 = \frac{1}{e^G - 1} \tag{3.28}$$

$$b = N_0 + 1 = \frac{e^G}{e^G - 1} \tag{3.29}$$

$$c = 2N_0 + 1 = \frac{e^G + 1}{e^G - 1} \tag{3.30}$$

We want λ such that

$$(M_2M_1 - \lambda I)\vec{z} = \vec{0}$$

or

$$(a^2 - \lambda)z_0 - bcz_1 = 0 \tag{3.31}$$

$$-a^2z_0 + (c^2 - \lambda)z_1 - bcz_2 = 0 \tag{3.32}$$

$$-aczz_{l-1} + (c^2 - \lambda)z_l - bcz_{l+1} = 0,\ l > 1 \tag{3.33}$$

Rewrite the $l > 1$ equation as

$$z_{l+1} = \frac{c - \lambda/c}{b} z_l - \frac{a}{b} z_{l-1} \tag{3.34}$$

This recursion relation (3.34) is identical to that solved by Mahan [2] in obtaining the eigenvalues λ' of M_2, if λ/c is replaced by λ'. Hence we find

$$\lambda_{21} = c\lambda'$$

or

$$\lambda_A = \pm\{(2N_0+1)[2N_0+1-2(N_0+1)e^{-G/2}\cos\theta]\}^{1/2} \tag{3.35}$$

where θ is a continuous parameter verying from $-\pi$ to π. This continous parameterization of λ_A arises from the infinite dimensionality of A, which demands an infinite number of eigenvalues and eigenvectors.

We shall describe the details of the solution of (3.31–3.34) since they are needed to obtain the eigenvectors $\vec{x}$. Let $w_{l+1} \equiv z_l$. Then (3.34) becomes

$$\begin{pmatrix} z_{l+1} \\ w_{l+1} \end{pmatrix} = \begin{pmatrix} e & f \\ 1 & 0 \end{pmatrix} \begin{pmatrix} z_l \\ w_l \end{pmatrix} \equiv N \begin{pmatrix} z_l \\ w_l \end{pmatrix} \tag{3.36}$$

where

$$e = (c-\lambda')/b \tag{3.37}$$

$$f = a/b \tag{3.38}$$

The matrix N has two eigenvalues; call them Λ_1 and Λ_2. Let us try a solution to (3.36) of the form

$$z_l = \Lambda_i^l \tag{3.39}$$

where i can be 1 or 2. Then

$$\begin{aligned} N \begin{pmatrix} z_l \\ w_l \end{pmatrix} &= \begin{pmatrix} e & f \\ 1 & 0 \end{pmatrix} \begin{pmatrix} \Lambda^l \\ \Lambda^{l-1} \end{pmatrix} = \Lambda^{l-1} \begin{pmatrix} e\Lambda - f \\ \Lambda \end{pmatrix} \\ &\stackrel{?}{=} \begin{pmatrix} z_{l+1} \\ w_{l+1} \end{pmatrix} = \begin{pmatrix} \Lambda^{l+1} \\ \Lambda^l \end{pmatrix} = \Lambda^{l-1} \begin{pmatrix} \Lambda^2 \\ \Lambda \end{pmatrix} \end{aligned}$$

We can satisfy the equality if

$$\Lambda^2 = e\Lambda - f$$

which is equivalent to

$$|N - \Lambda I| = 0. \tag{3.40}$$

Thus if Λ_i is an eigenvalue of N, (3.39) is a solution of (3.36); and since the latter equation is homogeneous, the most general solution is the linear combination

$$z_l = \alpha\Lambda_1^l + \beta\Lambda_2^l. \tag{3.41}$$

Hence let us find $\Lambda_{1,2}$. They satisfy (3.40) and so are given by

$$\Lambda = \frac{e}{2} \pm [(\frac{e}{2})^2 - f]^{1/2} \tag{3.42}$$

Now guess (to be verified by self-consistency) that $(e/2)^2 < f$; and use the fact that $f = \exp(-G)$ to write (3.42) as

$$\Lambda_{1,2} = e^{-G/2}\{\frac{e}{2}e^{+G/2} \pm i[1 - (\frac{e}{2}e^{G/2})^2]^{1/2}\} \tag{3.43}$$

$$= e^{-G/2}e^{\pm i\theta} \tag{3.44}$$

where

$$\cos\theta = \frac{e}{2}e^{G/2}. \tag{3.45}$$

Rearranging (3.37) gives λ' as a function of θ; and hence we get (3.35).

Following our supposition we have obtained complex eigenvalues $\Lambda_{1,2}$; in order for z_l to be real, we set $\alpha = \beta^*$, or

$$\alpha = \frac{1}{2}e^{i\phi}; \beta = \frac{1}{2}e^{-i\phi} \tag{3.46}$$

and we use a "boundary condition" [Eq. (3.32)] to determine ϕ. From (3.41), (3.44), and (3.46) we have

$$z_l = \frac{1}{2}e^{i\phi}(e^{-Gl/2}e^{il\theta}) + \frac{1}{2}e^{-i\phi}(e^{-Gl/2}e^{-il\theta})$$

or

$$z_l = e^{-Gl/2}\cos(l\theta + \phi) \tag{3.47}$$

We note that (3.47) is true for $l \geq 1$ only, since it was obtained from (3.34) which does not contain z_0. Hence we have two equations (3.31), (3.32) to specify ϕ and z_0. First rewrite (3.32) so that it takes the form of (3.33):

$$-ac\left[\frac{a}{c}z_0\right] + (c^2 - \lambda)z_1 - bcz_2 = 0$$

Since this is of the form (3.33) which is solved by (3.47), it is satisfied if the quantity in square brackets is (3.47) evaluated at $l = 0$. Thus

$$\frac{a}{c} z_0 = \cos\phi$$

$$z_0 = \frac{2N_0 + 1}{N_0} \cos\phi = (1 + e^G)\cos\phi \tag{3.48}$$

The generalization of (3.47) and (3.48) is

$$z_l = (1 + e^G \delta_{l=0}) e^{-Gl/2} \cos(l\theta + \phi) \tag{3.49}$$

These are the (infinitely many) eigenvectors of $M_2 M_1$, parameterized by θ; and thus, by Eq. (3.26), we have specified half of the components of the eigenvectors of A—once we pin down ϕ. Let us do that first: Eq. (3.31) is now

$$(a^2 - \lambda_{21})(\frac{c}{a}\cos\phi) - bce^{-G/2}\cos(\theta + \phi) = 0$$

whose solution is

$$\tan\phi = [\cos\theta + \frac{\lambda_{21} e^{G/2}}{ab} - \frac{a e^{G/2}}{b}]/\sin\theta$$

or, using (3.28–3.30),

$$\tan\phi = [e^{G/2}(2 + e^G) - \cos\theta(2e^G + 1)]/\sin\theta \tag{3.50}$$

Now we want the upper half ($\vec{y}$) of the eigenvector $\vec{x}$ in Eq. (3.25). Rewrite (3.24) as

$$\begin{pmatrix} 0 & M_1 \\ M_2 & 0 \end{pmatrix} \begin{pmatrix} \vec{y} \\ \vec{z} \end{pmatrix} = \lambda_A \begin{pmatrix} \vec{y} \\ \vec{z} \end{pmatrix} \tag{3.51}$$

Define

$$\varepsilon_l = 1 + e^G \delta_{l=0} \tag{3.52}$$

(a notation which will be used repeatedly) so that

$$(M_1)_{ll} = \frac{c}{\varepsilon_l} \tag{3.53}$$

Then the upper half of (3.51) is

$$\frac{c}{\varepsilon_l} z_l = \lambda_A y_l$$

or

$$y_l = \frac{c}{\varepsilon_l \lambda_A} z_l$$

so that

$$\vec{x}^{\pm}(\theta) = \begin{pmatrix} \vec{y}(\theta) \\ \vec{z}(\theta) \end{pmatrix} = \begin{pmatrix} \pm \frac{(2N_0+1)}{(\lambda_{21})^{1/2}} e^{-Gl/2} \cos(l\theta + \phi) \\ \varepsilon_l e^{-Gl/2} \cos(l\theta + \phi) \end{pmatrix} \tag{3.54}$$

Hence, for each θ, we get one eigenvector/eigenvalue pair for the square matrix $M_2 M_1$, and two [using (3.26),(3.54)] for the matrix A whose dimension is twice that of $M_2 M_1$.

Here we notice that putting $\lambda_{21} = 0$ into (3.26) does not give two eigenvalues; ie, for the matrix A, the $\lambda_A = 0$ eigenvalue has multiplicity two. Hence we need another eigenvector for a complete solution. Since A is not Hermitian, it is not necessarily true that there two linearly independent eigenvectors for a double eigenvalue [46]; and in fact, in finding $\vec{x}^0$, we found only one. There is not another eigenvector for A. To complete the solution we need to introduce a "generalized eigenvector" [46].

We want to solve an equation of the form (3.17), and $\lambda_j [= 0]$ is a double root of the characteristic equation. Modify (3.19) to read

$$\vec{X} = \sum_{i \neq j} a_i \vec{x}_i e^{-\lambda_i z} + b_j \vec{x}_j e^{-\lambda_j z} + a_j \vec{S} \tag{3.55}$$

$$\vec{S} = z \vec{S}_1 e^{-\lambda_j z} + \vec{S}_2 e^{-\lambda_j z} \tag{3.56}$$

We show that the vector $\vec{S}$ solves (3.17):

$$\begin{aligned} \vec{S}' &= (\vec{S}_1 - \lambda_j z \vec{S}_1) e^{-\lambda_j z} - \lambda_j \vec{S}_2 e^{-\lambda_j z} \\ &= -\lambda_j z \vec{S}_1 e^{-\lambda_j z} + (\vec{S}_1 - \lambda_j \vec{S}_2) e^{-\lambda_j z} \\ -A\vec{S} &= -A\vec{S}_1 z e^{-\lambda_j z} - A\vec{S}_2 e^{-\lambda_j z} \end{aligned}$$

Hence we have a solution if

$$-A\vec{S}_1 = -\lambda_j \vec{S}_1 \text{ and } -A\vec{S}_2 = \vec{S}_1 - \lambda_j \vec{S}_2$$

or

$$(A - \lambda_j I)\vec{S}_1 = \vec{0} \tag{3.57}$$

$$(A - \lambda_j I)\vec{S}_2 = -\vec{S}_1 \tag{3.58}$$

Thus $\vec{S}_1$ is the eigenvector corresponding to λ_j ; and $\vec{S}_2$ is the *generalized* eigenvector for λ_j. In our case, $\lambda_j = 0$, $\vec{S}_1 = \vec{x}^0$, and we seek $\vec{S}_2$ such that

$$A\vec{S}_2 = \begin{pmatrix} 0 & M_1 \\ M_2 & 0 \end{pmatrix} \begin{pmatrix} \vec{y}^S \\ \vec{z}^S \end{pmatrix} = -\vec{x}^0 = -k \begin{pmatrix} e^{-Gl} \\ \vec{0} \end{pmatrix}$$

giving

$$y_l^S = k' e^{-Gl}$$

and

$$z_l^S = \frac{-k\varepsilon_l e^{-Gl}}{c} \quad [\text{ using (3.53) }]$$

or

$$\vec{S}_2 = \begin{pmatrix} k' e^{-Gl} \\ \frac{-k\varepsilon_l}{2N_0+1} e^{-Gl} \end{pmatrix} \tag{3.59}$$

Now we can write the general form for the solution as

$$\begin{aligned} \vec{X}(z) &= b_0 \vec{X}^0 + a_0(z\vec{X}^0 + \vec{S}_2) \\ &= + \int_{-\pi}^{\pi} \frac{d\theta}{2\pi} \left[C(\theta)\vec{x}^+(\theta) + D(\theta)\vec{x}^-(\theta) \right] \end{aligned}$$

Now change notation [since we will not refer to Eqs. (3.28–3.30) again] as follows:

$$\begin{aligned} b_0 k + a_0 k' &\Longrightarrow b \\ a_0 k &\Longrightarrow -a(2N_0 + 1) \\ \lambda_{21} &\Longrightarrow \lambda \end{aligned}$$

and use the fact that, since $\phi(-\theta) = -\phi(\theta)$, $\vec{x}^{\pm}(\theta)$ are even in θ. These changes give the general solution as

$$F_l(z) = [b - a(2N_0 + 1)z]e^{-Gl}$$

$$+ (2N_0 + 1)e^{-Gl/2} \int_0^\pi \frac{d\theta}{\pi} \frac{\cos(l\theta + \phi)}{\sqrt{\lambda(\theta)}}$$
$$\times \left[C(\theta) e^{-\sqrt{\lambda(\theta)}z} - D(\theta) e^{+\sqrt{\lambda(\theta)}z} \right] \quad (3.60)$$

$$G_l(z) = \varepsilon_l a e^{-Gl} + \varepsilon_l e^{-Gl/2} \int_0^\pi \frac{d\theta}{\pi} \cos(l\theta + \phi)$$
$$\times \left[C(\theta) e^{-\sqrt{\lambda(\theta)}z} + D(\theta) e^{+\sqrt{\lambda(\theta)}z} \right] \quad (3.61)$$

3.3 Sum Rules and Orthogonality Relations

In this section we derive a number of results which are critical to obtaining and interpreting the solution to the transport problem. First we consider

$$\begin{aligned}
\Sigma_1 &= \sum_{l=0}^{\infty} \varepsilon_l e^{-Gl/2} \cos(l\theta + \phi) \\
&= \sum_{l=0}^{\infty} e^{-Gl/2} \cos(l\theta + \phi) + e^G \cos\phi \\
&= \Sigma_2 + e^G \cos\phi \\
\Sigma_2 &= \Re \sum_{l=0}^{\infty} e^{-Gl/2} e^{il\theta} e^{i\phi} \\
&= \Re \left\{ e^{i\phi} \left[\frac{1}{1 - e^{-G/2} e^{i\theta}} \right] \right\} \\
&= \frac{\cos\phi(1 - e^{-G/2}\cos\theta) - \sin\phi(e^{-G/2}\sin\theta)}{(1 - e^{-G/2}\cos\theta)^2 + (e^{-G/2}\sin\theta)^2} \\
&= \cos\phi \left[\frac{1 - e^{-G/2}\cos\theta - \tan\phi \sin\theta e^{-G/2}}{1 - 2e^{-G/2}\cos\theta + e^{-G}} \right]
\end{aligned}$$

where $\Re$ means the real part. Using (3.50), the numerator is

$$-e^G \cos\phi \left[e^{-G} + 1 - 2e^{-G/2}\cos\theta \right]$$

so that

$$\Sigma_2 = -e^G \cos\phi$$

or

$$\Sigma_1 = \sum_{l=0}^{\infty} \varepsilon_l e^{-Gl/2} \cos(l\theta + \phi) = 0 \quad (3.62)$$

We can use (3.62) and the fact that

$$\sum_{l=0}^{\infty} \varepsilon_l e^{-Gl} = \frac{e^G}{1-e^{-G}} \tag{3.63}$$

to obtain from (3.60) and (3.61) two important sum rules for F and G:

$$\begin{aligned} \Sigma_G &= \sum_{l=0}^{\infty} G_l(z) \\ &= \frac{ae^G}{1-e^{-G}} \end{aligned} \tag{3.64}$$

$$\begin{aligned} \Sigma_F &= \sum_{l=0}^{\infty} \varepsilon_l F_l(z) \\ &= [b - a(2N_0+1)z]\frac{e^G}{1-e^{-G}} \end{aligned} \tag{3.65}$$

We can comment on the physical meaning of these. The particle density $n(z)$ and particle current $j(z)$ are given from the DF $f(k,z)$ by

$$n(z) = \int_{-\infty}^{\infty} dk f(k,z) \tag{3.66}$$

$$j(z) = \int_{-\infty}^{\infty} dk \frac{k}{m} f(k,z) \tag{3.67}$$

or

$$\begin{aligned} n(z) &= \int_0^{\infty} dk[f(k,z) + f(-k,z)] \\ j(z) &= \int_0^{\infty} dk \frac{k}{m}[f(k,z) - f(-k,z)] \end{aligned}$$

In energy space

$$\begin{aligned} n(z) &= \int_0^{\infty} dE(\frac{m}{2E})^{1/2} F(E,z) \\ j(z) &= \int_0^{\infty} dE G(E,z) \end{aligned}$$

We have let $E = \varepsilon_0 + l\omega_0$. Thus

$$\int_0^{\infty} dE = \sum_{l=0}^{\infty} \int_0^{\omega_0} d\varepsilon_0$$

which gives

$$n(z) = (\frac{m}{2})^{1/2} \int_0^{\omega_0} d\varepsilon_0 \sum_{l=0}^{\infty} \frac{F_l(z)}{(\varepsilon_0 + l\omega_0)^{1/2}} \tag{3.68}$$

$$j(z) = \int_0^{\omega_0} d\varepsilon_0 \sum_{l=0}^{\infty} G_l(z) \tag{3.69}$$

The former is not in the form of a derived sum rule. The latter, however, is, giving

$$j(z) = \frac{a\omega_0 e^G}{1 - e^{-G}} \tag{3.70}$$

which may be regarded as a definition of a. Note that, since electron number conservation is built into the theory, the current is independent of z. We do not have a closed form for $n(z)$; however it clearly is determined by both constants b and a. Hence the two constants give us the freedom to specify both current and density (at some point) for the problem.

We will need an orthogonality relation to obtain the constants $C(\theta)$ and $D(\theta)$ from boundary conditions on F and G. We state it below:

$$\Sigma_\delta = \sum_{l=0}^{\infty} \varepsilon_l \cos(l\theta + \phi)\cos(l\theta' + \phi') = \frac{\pi}{2}\delta(\theta - \theta') \tag{3.71}$$

First we show that $\Sigma_\delta = 0$ if $\theta \neq \theta'$:

$$\begin{aligned}
\Sigma_\delta &= \sum_{l=0}^{\infty} \cos(l\theta + \phi)\cos(l\theta' + \phi') + e^G \cos\phi \cos\phi' \\
&= \Sigma_3 + e^G \cos\phi \cos\phi' \\
\Sigma_3 &= \lim_{\delta \to 0} \Re \sum_{l=0}^{\infty} \{\exp[il(\theta + \theta') + i(\phi + \phi') - l\delta] \\
&\quad + \exp[il(\theta - \theta') + i(\phi - \phi') - l\delta]\} \\
&= \lim_{\delta \to 0} \Re \left[\frac{e^{i(\phi+\phi')}}{1 - e^{i(\theta+\theta')}e^{-\delta}} + \frac{e^{i(\phi-\phi')}}{1 - e^{i(\theta-\theta')}e^{-\delta}} \right] \\
&= \frac{1}{2}\left[\frac{\cos s - \cos(S - s)}{2 - 2\cos S} + \frac{\cos d - \cos(D - d)}{2 - 2\cos D} \right]
\end{aligned}$$

where

$$s = \phi + \phi' \qquad S = \theta + \theta'$$

$$d = \phi - \phi' \qquad D = \theta - \theta'$$

After much algebra one obtains

$$\begin{aligned}\Sigma_3 &= \frac{2\cos\phi\cos\phi'[-2e^G(\cos\theta-\cos\theta')^2]}{4(\cos\theta-\cos\theta')^2} \\ &= -e^G\cos\phi\cos\phi'\end{aligned}$$

so that

$$\Sigma_\delta = \Sigma_3 + e^G\cos\phi\cos\phi' = 0$$

Next we examine the special point $\theta = \theta'$. As we are seeking a δ-function we will neglect all finite quantities.

$$\begin{aligned}\lim_{\theta-\theta'\to 0}\Sigma_\delta &= \lim_{\theta-\theta'\to 0}\Sigma_3 \\ &= \lim_{\theta-\theta'\to 0}\lim_{\delta\to 0}\Re\left[\frac{e^{i(\phi-\phi')}}{1-e^{i(\theta-\theta')}e^{-\delta}}\right] \\ &= \lim_{\delta\to 0}\Re\left[\frac{1}{\delta - i(\theta-\theta')}\right] \\ &= \lim_{\delta\to 0}\frac{\delta}{\delta^2+(\theta-\theta')^2} \\ &= \frac{\pi}{2}\delta(\theta-\theta')\end{aligned}$$

Actually we get

$$\Sigma_\delta = \frac{\pi}{2}[\delta(\theta-\theta') + \delta(\theta+\theta')]$$

but we will neglect the second term as we restrict the range to $0 \le \theta, \theta' \le \pi$.

Now we apply (3.71) to (3.61) in order to get the constants, $C(\theta)$ and $D(\theta)$, in terms of G:

$$\begin{aligned}2\sum_{l=0}^{\infty} G_l(z)e^{Gl/2}\cos(l\theta+\phi) = \\ 2\sum_{l=0}^{\infty}\varepsilon_l a e^{-Gl/2}\cos(l\theta+\phi) \\ + 2\int_0^\pi \frac{d\theta'}{\pi}[Ce^{-\sqrt{\lambda}z} + De^{\sqrt{\lambda}z}] \\ \times\sum_{l=0}^{\infty}\varepsilon_l\cos(l\theta'+\phi')\cos(l\theta+\phi)\end{aligned}$$

so

$$2\sum_{l=0}^{\infty} G_l(z)\epsilon^{Gl/2}\cos(l\theta+\phi) = C(\theta)e^{-\sqrt{\lambda(\theta)}z} + D(\theta)e^{\sqrt{\lambda(\theta)}z} \tag{3.72}$$

Similarly, using (3.60) we get

$$2\frac{\sqrt{\lambda(\theta)}}{2N_0+1}\sum_{l=0}^{\infty} F_l(z)\varepsilon_l\epsilon^{Gl/2}\cos(l\theta+\phi) = C(\theta)e^{-\sqrt{\lambda(\theta)}z} - D(\theta)e^{\sqrt{\lambda(\theta)}z} \tag{3.73}$$

Hence, given F and G at a point z, we can calcuate F and G for any z using (3.60), (3.61), (3.72), and (3.73).

3.4 Boundary Conditions

It would seem from the above that the problem is completely solved; but in fact it is not. The remaining difficulty is connected with the fact that there are many boundaries in the problem, rather than simply two; and each requires a set of boundary conditions to specify the complete solution.

The extra boundaries arise because any solution to Eq. (3.17) is only valid over a region for which the labeling of the discrete energy indices is valid. Such a region is limited because, as $V(z)$ varies with z by an amount equal to ω_0, new levels appear or disappear. The case for constant electric field is shown in Fig. 3.1. Note that, in this figure, we introduce a convention to be used henceforth, that current flow is to the right. Eq. (3.17) singles out the $l = 0$ level as that one which cannot *emit* a phonon. As soon as V changes by a sufficient amount, that constraint no longer holds, the particles on that level can emit a phonon, and hence the level must be relabeled so that (3.17) may again be applied to it.

The vertical lines in Fig. 3.1 denote those values z_j at which a new level appears, at which point the levels must be relabeled. Since the scattering conditions are not continuous across these boundaries z_j, a solution to Eq. (3.17) is valid only for the region between two adjacent boundaries. To get a feeling for the magnitudes

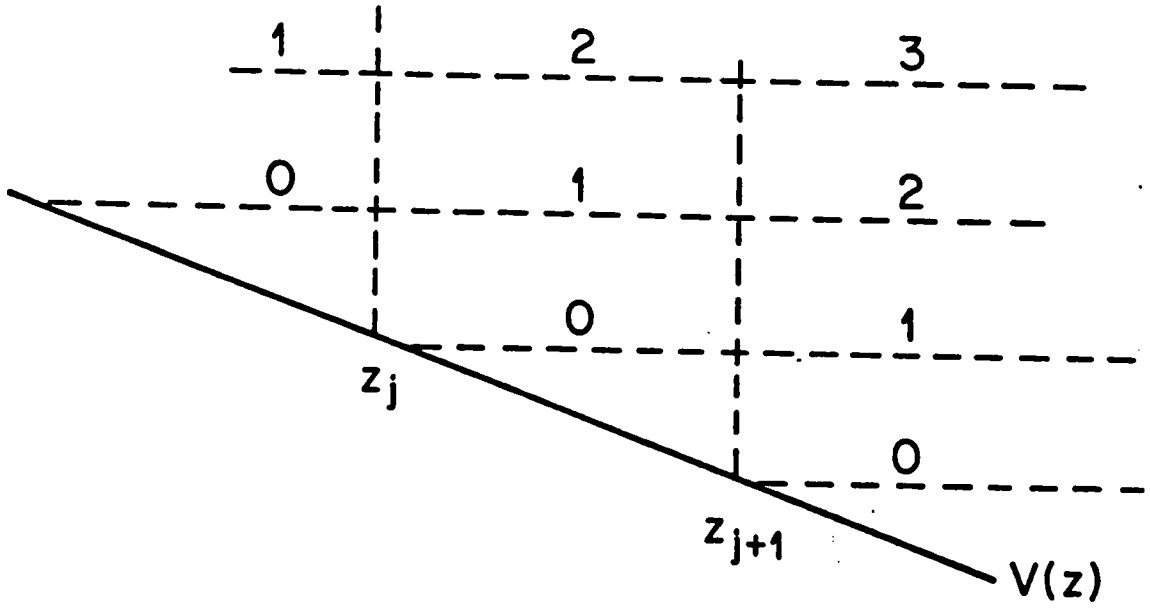

Figure 3.1: Staging for constant electric field. The potential profile $V(z)$ is shown for constant field as a solid line of constant slope. The horizontal lines are discrete energy levels spaced ω_0 apart; the vertical lines mark the stage boundaries, where new levels appear.

involved, suppose that a constant field of 10^4 V/cm is applied, and that $\omega_0 = .063$ eV [Si]. Then the width Δ_j between z_j and z_{j+1} is .063 μm. A 1-μm device (with one volt across it) would thus be divided into $\approx$16 stages.

In matching the solution across the stage boundaries, we assume that the magnitudes of F and G are continuous at the boundary. We cannot assume that the *derivatives* are continuous, however, since the scattering conditions change discontinuously at the boundary. We let F_l^- be the value just to the left of the boundary, F_l^+ that value just to the right, with V decreasing to the right as in Fig. 3.1; and similarly for G. The boundary condition is then

$$F_l^- = F_{l+1}^+ \tag{3.74}$$

$$G_l^- = G_{l+1}^+ \tag{3.75}$$

Clearly the (--) values determine all the (+) values except G_0^+ and F_0^+. We note that

$$\sum_{l=0}^{\infty} G_l^- = \sum_{l=0}^{\infty} G_l^+ = \frac{ae^G}{1-e^{-G}}$$

which gives, using (3.75),

$$G_0^+ = 0. \tag{3.76}$$

We cannot obtain a similar result for F_0^+ because the constants b are stage-dependent, reflecting the fact that the density $n(z)$ can vary with z. Hence we define b_j as the value appropriate for the region to the right of z_j. Since, in the expression (3.60) for F_l, the combination

$$b - a(2N_0 + 1)z$$

always occurs together, we can also absorb the constant $[-a(2N_0+1)z_j]$ into b_j, so that z measures the distance from the nearest match point to the left.

Now the sum rule (3.65) applied immediately to the left of z_{j+1} gives

$$e^G F_0^- + \sum_{l=0}^{\infty} F_l^- = [b_j - a(2N_0+1)\Delta_j]\frac{e^G}{1-e^{-G}}$$

where

$$\Delta_j \equiv z_{j+1} - z_j \tag{3.77}$$

and immediately to the right we have

$$e^G F_0^+ + \sum_{l=0}^{\infty} F_l^+ = b_{j+1} \frac{e^G}{1 - e^{-G}}$$

Taking the difference, and using (3.74) to cancel terms, we get

$$(1 + e^G) F_0^+ = e^G F_0^- + [b_{j+1} - b_j + a(2N_0 + 1)\Delta_j] \frac{e^G}{1 - e^{-G}} \tag{3.78}$$

which, assuming that the solution is known up to z_{j+1}, contains two unknowns, F_0^+ and b_{j+1}. Thus a solution for stage j does not determine the solution for stage $(j+1)$. We will have more to say about this in the Discussion; for now we wish to show that the solution is fully determined for the constant-field (CF) case.

By "constant field" we mean no variation in field over an infinite range in z; clearly a constant slope over a finite region would have perturbations in F and G in the finite region due to the boundaries. In the CF case, the solution is *not* independent of z, due to the discretization of the problem. The solution is however clearly periodic, with period $\Delta = z_{j+1} - z_j = \text{constant}$. This means that, since we have absorbed the constant z offsets into the b_j,

$$b_j = b_{j+1} \tag{3.79}$$

so that, using (3.55) and $F_0^- = F_1^+$, we get

$$F_0^+ = \frac{F_1^+}{1 + e^{-G}} + \frac{a\Delta}{(1 - e^{-G})^2}. \tag{3.80}$$

We thus have all the ingredients for a complete solution to the CF problem, for arbitrary field strength. The implementation of this solution will be described in the following section. We note here that the non-CF problem has so far not yielded a self-consistent solution, essentially due to the boundary-condition dilemma presented above.

3.5 Constant Field Solution

We concentrate on the solution $\vec{X}^{j+1}$ immediately to the right of the stage boundary. We wish to express this quantity in terms of the one immediately to the right of the previous stage boundary, $\vec{X}^j$. Having done so we will equate the two and thereby obtain a self-consistent solution to the CF problem. Schematically, we seek an expression of the form

$$\vec{X}^{j+1} = \vec{X}^{j+1}(\vec{X}^j, a, b, \Delta) \tag{3.81}$$

Given such a relation, we choose b (density) and Δ ($\propto 1/F$, where F is the electric field), and then impose periodicity:

$$\vec{X} = \vec{X}(\vec{X}, a, b, \Delta) \tag{3.82}$$

and self-consistently determine $\vec{X}$ and a.

First we derive an expression of the form (3.81). Basically this involves combining expressions like (3.60) and (3.61) with (3.72) and (3.73). For compactness we introduce the notation

$$F_l \equiv F_l^j(z_j + \delta) \tag{3.83}$$

$$F_l^- \equiv F_l^j(z_j + \Delta - \delta) \tag{3.84}$$

$$F_l^+ \equiv F_l^{j+1}(z_{j+1} + \delta) \tag{3.85}$$

where δ is infinitesimal; and similarly for G. We can also choose $z_j = 0$. Then Eqs. (3.60–3.61) become, at $z = \Delta$,

$$\begin{aligned} F_l^- &= [b - a(2N_0 = 1)\Delta]e^{-Gl} + (2N_0 + 1)e^{-Gl/2} \\ &\quad \times \int_0^\pi \frac{d\theta}{\pi}[\bar{C} - \bar{D}]\frac{\cos(l\theta + \phi)}{\sqrt{\lambda}} \end{aligned} \tag{3.86}$$

$$\begin{aligned} G_l^- &= \varepsilon_l a e^{-Gl} + \varepsilon_l e^{-Gl/2} \\ &\quad \times \int_0^\pi \frac{d\theta}{\pi}[\bar{C} + \bar{D}]\cos(l\theta + \phi) \end{aligned} \tag{3.87}$$

where

$$\begin{aligned}\bar{C} &= Ce^{-\sqrt{\lambda}\Delta} \\ \bar{D} &= De^{\sqrt{\lambda}\Delta}\end{aligned}$$

Evaluating (3.72) and (3.73) at $z = 0$ gives

$$\begin{aligned}C(\theta) &= \sum_{l=0}^{\infty} e^{Gl/2}\cos(l\theta+\phi)[G_l + \varepsilon_l F_l \frac{\sqrt{\lambda}}{2N_0+1}] \\ D(\theta) &= \sum_{l=0}^{\infty} e^{Gl/2}\cos(l\theta+\phi)[G_l - \varepsilon_l F_l \frac{\sqrt{\lambda}}{2N_0+1}]\end{aligned}$$

Substituting and simplifying, we get

$$\begin{aligned}F_l^- &= [b-a(2N_0+1)\Delta]e^{-Gl} + \sum_{m=0}^{\infty} e^{-Gl/2}e^{Gm/2} \\ &\quad \times \int_0^{\pi} \frac{d\theta}{\pi}[2\varepsilon_m F_m \cosh(\sqrt{\lambda}\Delta) - 2G_m \frac{(2N_0+1)}{\sqrt{\lambda}}\sinh(\sqrt{\lambda}\Delta)] \\ &\quad \times \cos(l\theta+\phi)\cos(m\theta+\phi) \\ G_l^- &= \varepsilon_l a e^{-Gl} + \varepsilon_l \sum_{m=0}^{\infty} e^{-Gl/2}e^{Gm/2} \\ &\quad \times \int_0^{\pi} \frac{d\theta}{\pi}[2G_m \cosh(\sqrt{\lambda}\Delta) - 2\varepsilon_m F_m \frac{\sqrt{\lambda}}{2N_0+1}\sinh(\sqrt{\lambda}\Delta)] \\ &\quad \times \cos(l\theta+\phi)\cos(m\theta+\phi)\end{aligned}$$

Due to matching at the boundary, the above equations are equal to F_{l+1}^+ and G_{l+1}^+, respectively. Thus the $(j+1)$ amplitudes are

$$\begin{aligned}F_l^+ &= [b-a(2N_0+1)\Delta]e^{-G(l-1)} + 2\sum_{m=0}^{\infty} e^{G/2(m+1-l)} \\ &\quad \times \int_0^{\pi} \frac{d\theta}{\pi}[\varepsilon_m F_m \cosh(\sqrt{\lambda}\Delta) - G_m \frac{(2N_0+1)}{\sqrt{\lambda}}\sinh(\sqrt{\lambda}\Delta)] \\ &\quad \times \cos[(l-1)\theta+\phi]\cos(m\theta+\phi) \qquad (3.88) \\ G_l^+ &= \varepsilon_{l-1} a e^{-G(l-1)} + 2\varepsilon_{l-1}\sum_{m=0}^{\infty} e^{G/2(m+1-l)} \\ &\quad \times \int_0^{\pi} \frac{d\theta}{\pi}[G_m \cosh(\sqrt{\lambda}\Delta) - \varepsilon_m F_m \frac{\sqrt{\lambda}}{2N_0+1}\sinh(\sqrt{\lambda}\Delta)] \\ &\quad \times \cos[(l-1)\theta+\phi]\cos(m\theta+\phi) \qquad (3.89)\end{aligned}$$

These equations, plus (3.76) and (3.80) for G_0^+ and F_0^+, totally determine $\vec{X}^{j+1}$ in terms of $\vec{X}^j$. We can write them compactly as

$$\vec{X}^{j+1} = N(\Delta)\vec{X}^j + a\vec{L} + b\vec{K} \tag{3.90}$$

which is in the form (3.81) which we sought.

Since $\vec{X}^{j+1} = \vec{X}^j$ for the CF case, we get

$$\vec{X}^{CF} = aU\vec{L} + bU\vec{K} \tag{3.91}$$

where

$$U = (I - N)^{-1}. \tag{3.92}$$

Choice of the field F fixes Δ according to

$$\Delta = \frac{\omega_0}{cF\ell_0} \tag{3.93}$$

which in turn determines N and U. Now inspection of (3.91) gives the impression that we are free to choose both a and b. However, given b and Δ, there is a unique value for a which will produce an $\vec{X}^{CF}$ satisfying the sum rule (3.64). Hence, as expected, density and field determine the current.

To find a, we define

$$\vec{X}_a = \begin{pmatrix} \vec{F}_a \\ \vec{G}_a \end{pmatrix} = U\vec{L} \tag{3.94}$$

$$\vec{X}_b = \begin{pmatrix} \vec{F}_b \\ \vec{G}_b \end{pmatrix} = U\vec{K} \tag{3.95}$$

so that

$$\vec{X}^{CF} = a\vec{X}_a + b\vec{X}_b. \tag{3.96}$$

The sum rule requires

$$\Sigma_G = a\frac{e^G}{1 - e^{-G}} = a\sum_{l=0}^{\infty}(G_a)_l + b\sum_{l=0}^{\infty}(G_b)_l$$

or in more compact notation

$$af = a\Sigma_{Ga} + b\Sigma_{Gb}$$

so that

$$a = b\frac{\Sigma_{Gb}}{f - \Sigma_{Ga}}. \tag{3.97}$$

We set $b = 1$ since it simply scales the solution with the density. Then, given Δ, Eq. (3.97) suffices to determine a and hence $\vec{X}^{CF}$. As a check we can apply a similar approach to Σ_F to get

$$a = \frac{f - \Sigma_{Fb}}{\Sigma_{Fa}}. \tag{3.98}$$

For moderate fields the two expressions (3.97) and (3.98) could be calculated to agree to four or more figures. The low-field case was problematic, as discussed in the next section.

3.6 Numerical Results

In order to generate numbers with the above solution we need to specify the phonon energy ω_0, the lattice temperature T, and the dimensionless electric field $1/\Delta$. There are no boundary conditions other than periodicity for the CF case. We choose $\omega_0 = 0.063$eV, the value for optical phonons in silicon.

Figure 3.2 shows the dimensionless current vs. the dimensionless field, for different lattice (phonon) temperatures: 100, 200, and 300 K. The solid line is the result from (3.97) and (3.98) above. For $1/\Delta \lesssim 0.1$, or $\Delta \gtrsim 10$, we find that the good agreement between the two sum rules begins to fail. The reason is that the entries of the matrix N vary as $\exp(\Delta)$ and so get very large for small fields (large Δ). The resulting inversion to obtain U becomes inaccurate at small fields, giving unreliable results. Numerically, for silicon, assuming $\ell_0 \sim 100$Å, this occurs for fields $F \lesssim 6 \times 10^3$ V/cm. Note that the field enters the solution only in the form $\exp(1/F)$, which cannot be expanded in positive powers of F.

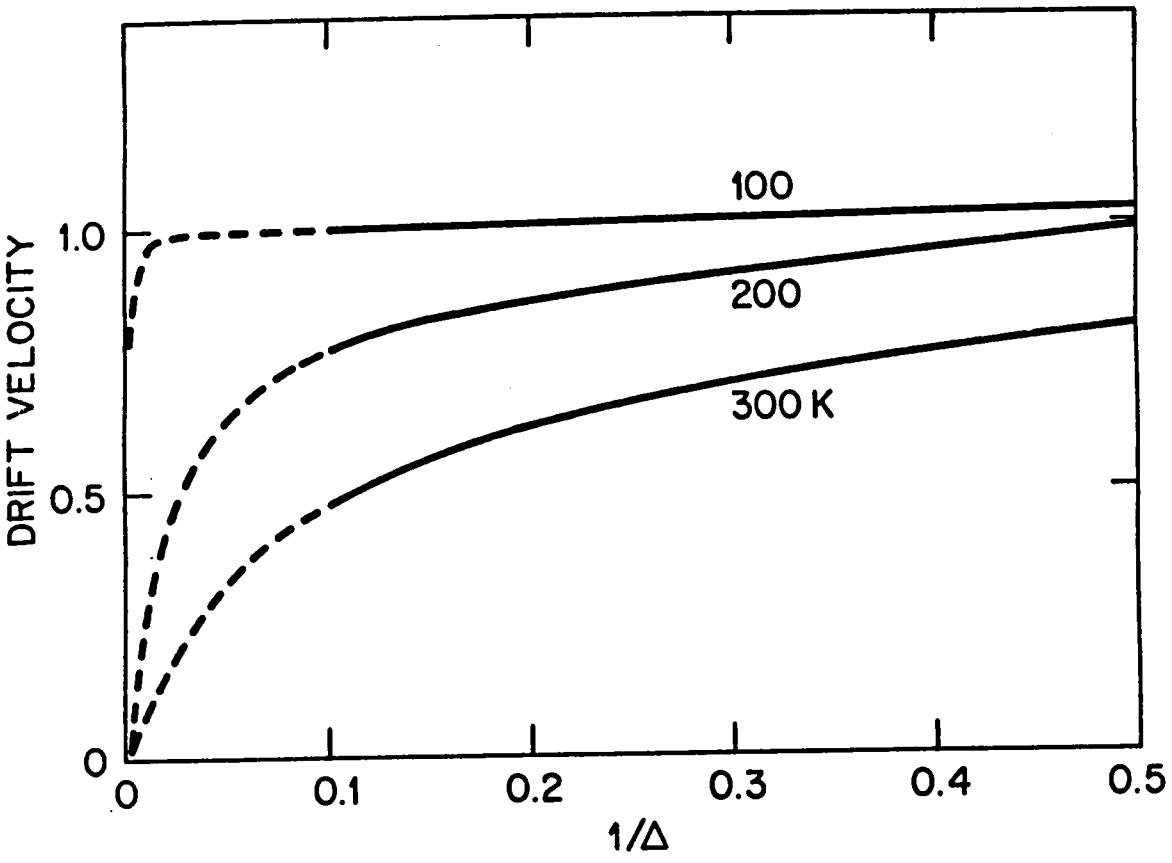

Figure 3.2: Current as a function of field $1/\Delta$ for three lattice temperatures. The solid lines are from the full (matrix) Boltzmann solution; they join the low-field approximation of Mahan at $1/\Delta \sim 0.1$. Current saturation is apparent; the saturation current is only weakly temperature-dependent.

The dashed lines in Fig. 3.2 are from an analytical, small-field perturbation solution obtained by Mahan [43] to second order in F. The low-field expansion agrees well with the high- field results at $1/\Delta \simeq 0.1$. We find, in agreement with previous experimental and theoretical results (Chapter 2), that the current saturates at large fields, and that the saturation value is at most weakly temperature-dependent. This saturation current is expected to prevail until other mechanisms come into play at very large fields, such as impact ionization or velocity runaway (Chapter 4).

When the values of F_l obtained from $\vec{X}^{CF}$ are plotted on a semilog scale, the results are well fitted by a straight line for all fields examined, implying that

$$F_l \sim \exp(-l\omega_0/T_e),$$

ie, the electrons have a Maxwellian distribution which allows the definition of an electron temperature T_e. Plots of T_e vs. field are shown in Figure 3.3, for phonon temperatures T_p =100, 200, and 300 K.

We find the somewhat surprising result that, for small fields, the electron temperature is lower that the lattice temperature, even when carrier energy is measured in the lattice frame. The T_e results are plotted, for low fields, down to the point at which the solution begins to fail. The lowest temperatures found, respectively, for T_p =100, 200, and 300 K, are 100, 196, and 293 K. The phenomenon of "field-induced electron cooling" has been obtained in other theoretical calculations (Chapter 2); the effect, if real, is small and would be difficult to measure.

Finally, for illustrative purposes we plot in Figure 3.4 the amplitudes F_l and G_l for a single stage; the parameters in this case are T=300K and $\Delta = 5$. The results were obtained from Eq. (3.90), replacing Δ by z. We note that the amplitudes match (as they should) if an identical stage is repeated on either side. Note also the discontinuity in dG_1/dz and dF_1/dz across the boundary, due to the creation of the new level.

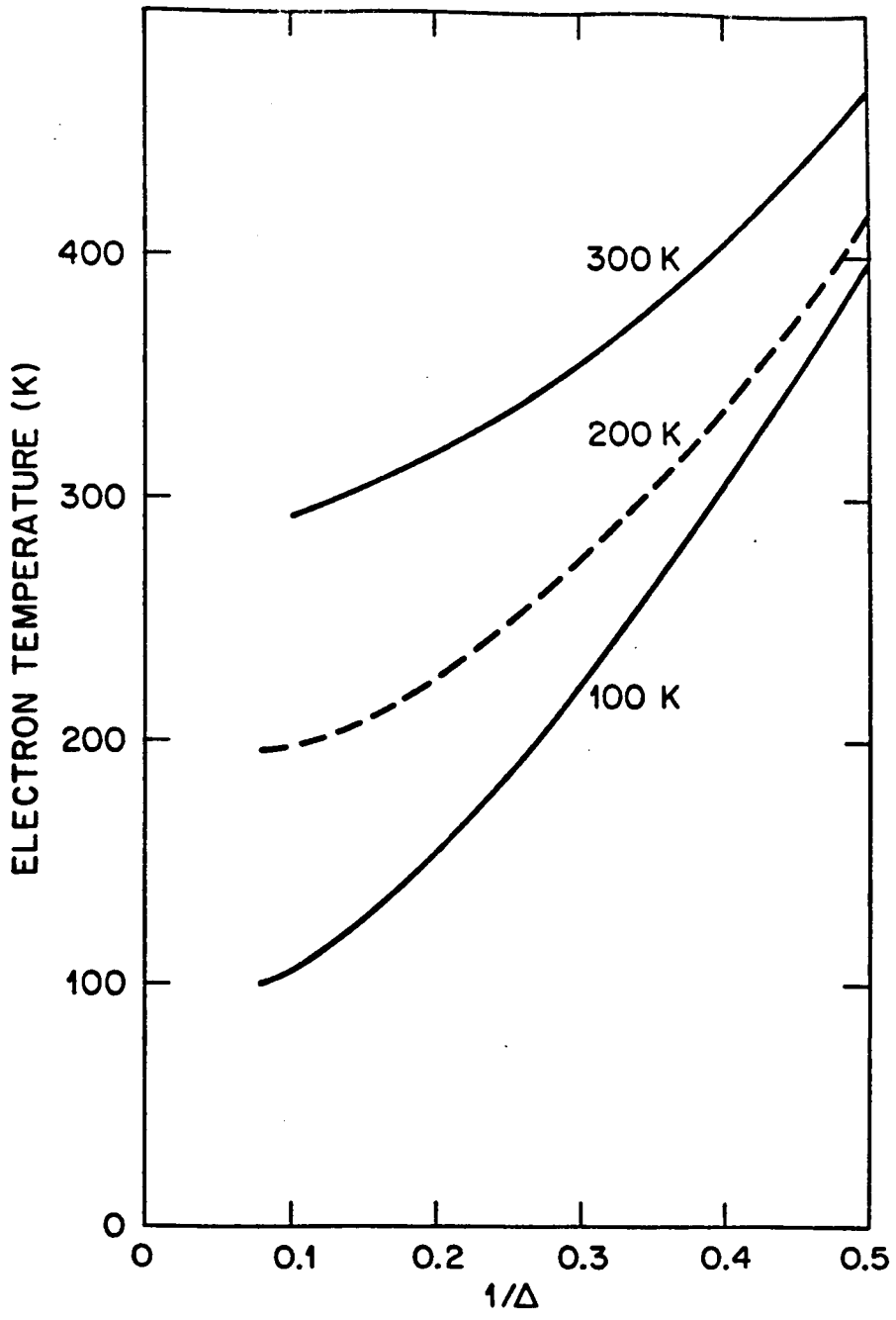

Figure 3.3: Electron temperature vs. field $1/\Delta$, for three lattice temperatures. The electron temperature is less than the lattice temperature for small fields.

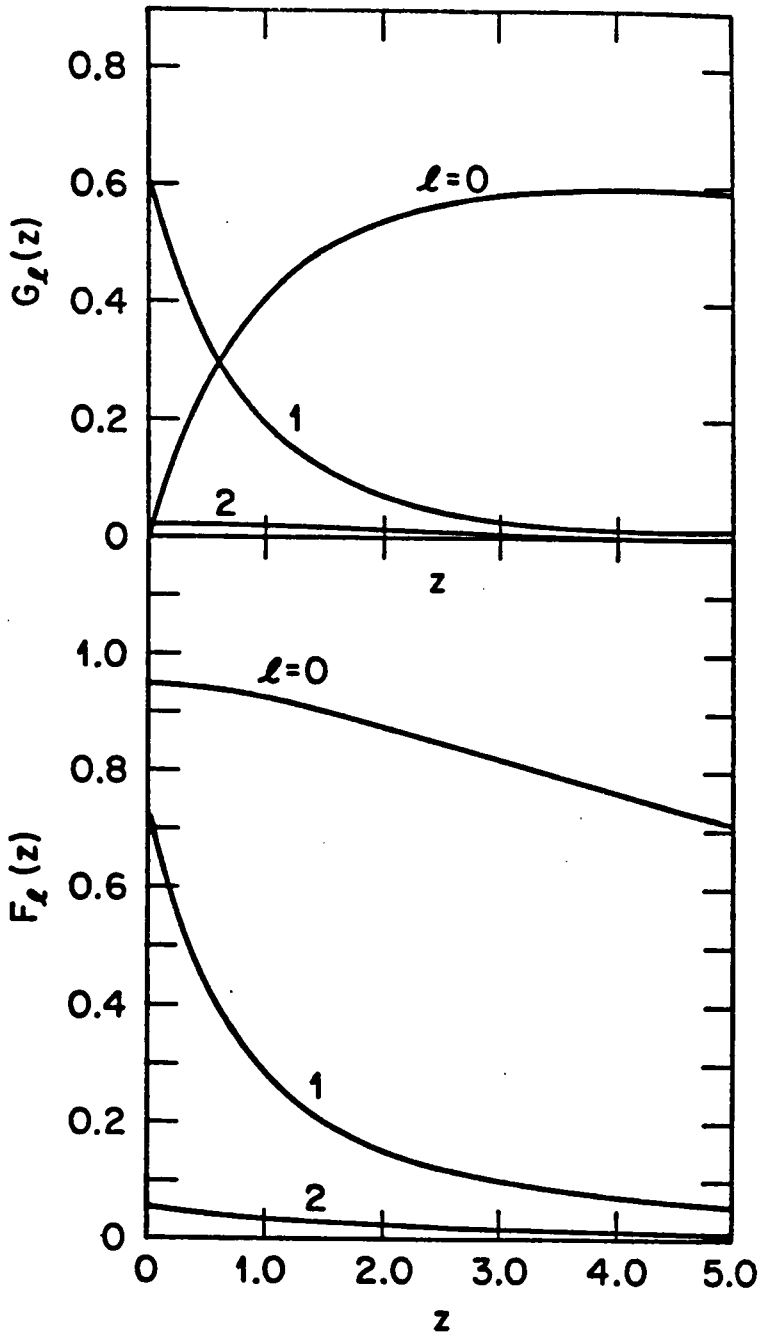

Figure 3.4: Constant-field solution: density and current amplitudes. The current and density amplitudes, $G_l(z)$ and $F_l(z)$, respectively, are shown for the CF case in a single stage for T=300K and $1/\Delta = 0.2$. The complete solution consists of repeated stages identical to this one.

3.7 Discussion and Summary

We have presented a solution to the Boltzmann equation for one-dimensional flow subject to optical phonon scattering. We assume forward and backward scattering are equally probabable ($\alpha = 1$), thus complementing the earlier work by Mahan [2] which assumed forward scattering only ($\alpha = 0$). We have carried the solution through to completion for the constant-field case, while a self-consistent solution for the case of arbitrary field profile has remained elusive.

The constant-field results show the well-known phenomenon of current saturation in a realistic way. The approach to saturation is retarded with increasing lattice temperature, while the saturation current is nearly temperature- independent. The good agreement of our results with experiment thus adds further weight to the importance of optical phonons in high-field transport.

The CF solutions have a Maxwellian shape with a well-defined electron temperature T_e. This quantity is found to be slightly lower than the lattice temperature at moderate fields; it then increases with increasing field in roughly parabolic fashion. The phenomenon of "electron cooling" has been predicted before, by various models; to our knowledge it has not been observed. Our model differs from previous predictions in three ways. We do not measure energy with respect to CM motion, as do others; we find the amount of cooling *increases* with increasing lattice temperature; and, the model begins to fail numerically roughly in the center of the region in field for which cooling is predicted. The problem is interesting and deserves more attention; however the predicted magnitude of cooling is small, and, if it is accurate, probably cannot be detected.

A comparison of the present results with the CF results for $\alpha = 0$ will be done in Chapter 4. The $\alpha = 1$ case is analogous to isotropic (deformation potential) scattering in higher dimension, while the forward-scattering ($\alpha = 0$) case is more representative of polar scattering. The more general case $0 < \alpha < 1$, while soluble

by the same technique, is more complicated and has not been done; one expects results intermediate to the two extreme cases.

An important difference in the $\alpha = 0$ case is that f^+ and f^- are decoupled, thus halving the dimension of the problem and the number of boundary conditions required [2]. Without backscattering, information flows only in one direction; hence one can assume an equilibrium distribution just to the left of the point where a finite field begins. This assumption, plus the simpler boundary conditions at the match point, enabled a solution of the $\alpha = 0$ case for arbitrary field profile.

The same has not been possible with backscattering included. The distribution can be assumed known only asymptotically far from a disturbance in either direction. Thus, with the doubled requirement for boundary conditions, it appears that a solution must specify the distributions at $z = \pm\infty$ and then solve for the intervening values so as to be consistent with both limits.

Chapter 4

Runaway

4.1 Introduction

In previous work we have obtained exact solutions to the Boltzmann equation in one dimension, for the case of constant electric field and scattering by dispersionless optical phonons. In this work the parameter α characterizes the relative probability of backward scattering to that of forward scattering; we obtained solutions for $\alpha = 0$ [2] and $\alpha = 1$ [43]. Similar theoretical works include a recent, one-dimensional relaxation-time solution [34] and a number of 3-D calculations [35,47,48,49,50,51].

It was early recognized by Fröhlich [19] that optical phonons by themselves cannot stabilize the carrier population in the face of arbitrarily large fields. For sufficiently large fields, an electron is expected to gain more energy between scattering events than it can lose to an optical phonon upon scattering; hence the velocity distribution becomes unstable at large fields. This situation is given the name "velocity runaway" or simply "runaway".

The prediction by Fröhlich of runaway from optical phonons is supported by several subsequent calculations, including an elaborate quantum-mechanical treatment by Thornber and Feynman [22], a numerical calculation by Ferry [50] based on a method of Rees [52], and a recent Monte Carlo calculation by Fitting and Friemann

[51]. Experimental study of runaway is clearly more difficult, since other dissipative phenomena invariably arise in bulk materials to mask the electron-phonon instability. In devices with small channel length, runaway should appear in the form of an increase in measured velocity with increasing channel length, in contrast to the velocity overshoot phenomenon in which electron velocity drops with increasing channel length [23].

The most thoroughly studied material, both experimentally and theoretically, on the question of runaway is silicon dioxide [16,20,48,50,51,53-57]. A rather clear picture has emerged from the recent work by the IBM workers [20,54,55,56,57], involving electron velocity runaway setting in at about the theoretically predicted threshold field [20,51,53], followed by stabilization of the carrier population at high energies due to nonpolar coupling to acoustic phonons [20,56,57]. This picture is credible since (i) the sharp increase in electron energy at threshold has been observed [20]; (ii) the probability of acoustic phonon emission is approximately proportional to the carrier energy [59]: (iii) the nonpolar scattering is isotropic, and thus more effective at stabilizing the carrier velocities than the predominantly forward polar optical scatering [56].

In our one-dimensional theory, anisotropic, forward scattering corresponds to the $\alpha = 0$ case, while isotropic scattering is modeled by setting $\alpha = 1$. We find it of interest to examine the question of runaway in one dimension for the two extremes.

4.2 Results and Discussion

For $\alpha = 0$, the threshold field for runaway is predicted from the relation (energy gained per mean free path) = (energy lost to phonon), or

$$\left(\frac{1}{\Delta}\right)_{Th} = \frac{eE_{Th}\ell_0}{\hbar\omega_0} = 1$$

where $1/\Delta$ is a dimensionless parameter related to the electric field E, the scattering length ℓ_0, and the phonon energy $\hbar\omega_0$, and Th signifies "at threshold." We have

solved the $\alpha = 0$ case in two ways: (i) by finding the spatial dependence of the distribution, beginning at the point $x = 0$ where the field begins [2]; and (ii) by determining the steady distribution which results from a constant field of infinite spatial extent. The former calculation (i) involves beginning with an equilibrium distribution at the lattice temperature at $x = 0$ (where there is no field for $x < 0$) and finding the distribution for each subsequent stage using the method of Ref. [2]. The latter method (ii) is that employed in Ref. [43]: a steady solution is assumed to exist which is periodic, with the period being one stage ($= \hbar\omega_0/eE$); the periodicity is then exploited to find the solution using matrix inversion [43].

Figure 4.1 shows the results from calculations of type (i) which are pertinent to the question of runaway. The condition of stability implies that solution (i) converges to that in (ii) for large x; this condition is illustrated for $1/\Delta = 0.8$ in Fig. 4.1a. Instability (runaway) is reflected in as absence of solution (ii), while the distribution found in (i) is characterized by an average energy which increases without limit with increasing x, as shown for $1/\Delta = 1.2$ (Fig. 4.1b).

For the case $\alpha = 1$ we have not solved the case (i) that the field is a step function in x, but only the steady-field case (ii) [43]. Figure 4.2 compares results for the steady-field solution (ii), for $\alpha = 0$ and $\alpha = 1$. We have plotted the inverse electron temperature vs. electric field ($1/\Delta$) for each case. The electron temperature is obtained from the slope of a semi-log plot of the electron distribution ($\log f_l$ vs. l); whenever a steady solution is obtained, such plots are linear, corresponding to a Maxwellian electron distribution characterized by a temperature T_e.

We see from Fig. 4.2 that $T_e \to \infty$ as $E \to E_{Th}$ for the forward-scattering case $\alpha = 0$ (with no steady solution for $E > E_{Th}$), indicating that forward scattering alone cannot stabilize the carrier distribution. For the case $\alpha = 1$ (isotropic scattering), a stable carrier distribution may be found up to the largest field examined, so that there is no evidence of runaway for this case.

Hence our results for the 1-D Boltzmann equation are in accord with the earlier

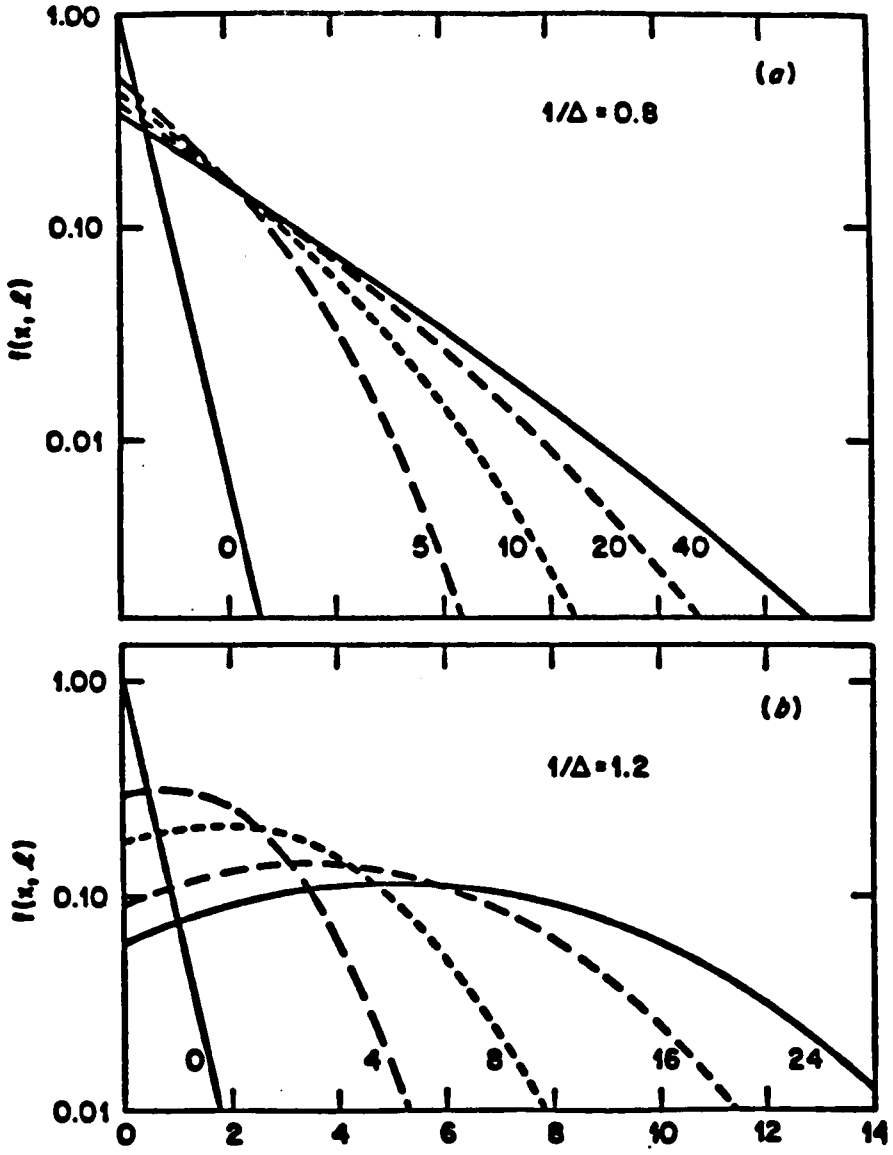

Figure 4.1: Evolution of the electron distribution from a step in field. The curves show the particle distribution $f(x,l)$ at a distance x from where a constant field begins. The number by each curve gives the distance x in units of the number of stages; $G = \hbar\omega_0/k_BT_L = 2.50$, and $\alpha = 0$ (no backscattering). (a) $1/\Delta = 0.8$. Here the field is less than the critical value (1.0) and there is no runaway; the distribution approaches a Maxwellian form at large x. (b) $1/\Delta = 1.2$. Runaway occurs when $1/\Delta > 1$. At increasing distance the peak of the distribution moves to increasing energy.

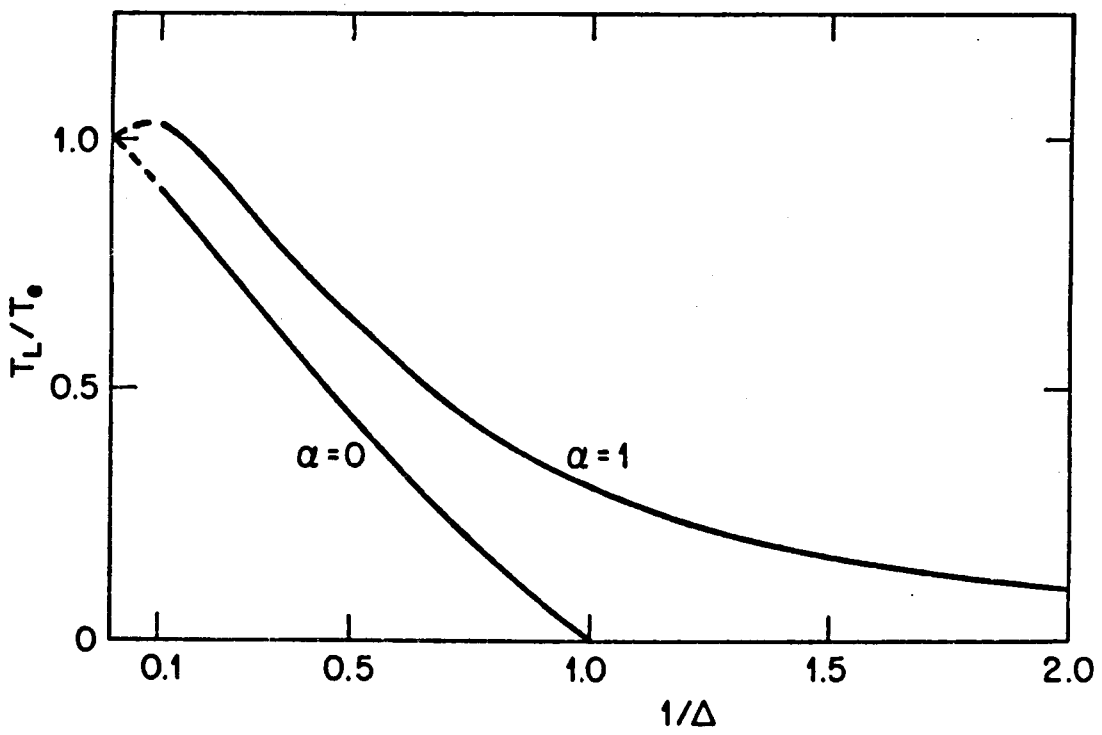

Figure 4.2: Runaway as reflected in electron temperature. The inverse electron temperature $1/T_e$, normalized to the lattice temperature T_L (300K), is plotted vs. the field parameter $1/\Delta$; $G = 2.43$. $\alpha = 0$ represents no backscattering; $\alpha = 1$ represents isotropic (in 1D) scattering. For forward scattering only, $T_e \rightarrow \infty$ as $1/\Delta \rightarrow 1.0$, signifying runaway. For $\alpha = 1$ the distribution is stable to arbitrarily large fields. The low-field behavior (dashed line, $1/\Delta < 0.1$) is extrapolated.

predictions of runaway from polar optical phonons, and with the understanding of runaway which has been obtained for SiO_2. Since polar coupling results predominantly in forward scattering, it is best modeled by the case $\alpha = 0$, which gives runaway above a threshold field ($1/\Delta = 1$) [58]. No runaway is found for the case of isotropic scattering ($\alpha = 1$), which we have shown, in one dimension at least, to be capable of stabilizing the carrier distribution for very large fields.

Results of a 1-D calculation are suggestive at best. Those real systems which are best modeled by one-dimensional flow are probably dominated by anisotropic, forward scattering, and hence more prone to runaway. Such systems should include the more strongly polar crystals, ie ionic crystals among insulators, and III-V and II-VI semiconductors. In the case of semiconductors other scattering mechanisms (intervalley and nonpolar optical) need to be considered as well [60,61].

Chapter 5

Time-dependent Theory of Hot Electrons Using the Discrete Boltzmann Equation

5.1 Introduction

Excitation of semiconductors by light of energy $\hbar\omega_{ex} > E_g$, where E_g is the band gap of the material, results in a nonequilibrium population of photoexcited carriers, which then relax towards equilibrium via various scattering mechanisms [29,62]. The study of such systems under photoexcitation is of considerable interest for the information which may be gained concerning the scattering mechanisms and dynamics of nonequilibrium carriers in semiconductors. In polar semiconductors, under certain, commonly met conditions, the scattering of electrons in the conduction band is dominated by polar optical phonon scattering. These conditions are that ε_c (the electron energy relative to the bottom of the band) is greater than $\hbar\omega_{op}$, the phonon energy (assumed constant), but less than that energy which is sufficient for intervalley transitions; and that carrier densities, either from doping or from photoexcitation, are low, so that carrier-carrier scattering is not important.

The influence of optical phonon scattering appears in various forms, all of which involve periodic oscillations in spectra: oscillatory photoconductivity [63,64,65], oscillations in photoluminescence intensity vs. energy of photoexcitation [66,65], and oscillations in luminescence intensity vs. luminescence energy [67,68,69,70,71]. The last-mentioned phenomenon is observed only for low carrier densities [68,69,70,71]. If the carrier density is too large, then carrier-carrier scattering, in which energy exchange occurs in arbitrary amounts, tends to wash out the discrete line structure of photoluminescence spectra; in the high-density limit, the spectra may be analyzed as arising from a Maxwellian distribution at a temperature above the lattice temperature [62,65]. The various scattering processes which affect the hot carrier distribution, and their interpretation in terms of observed photoluminescence spectra, have been discussed in several review articles [29,62,75].

The present calculation applies to the low-carrier-density limit. The system most commonly studied is lightly-doped p-gallium arsenide [69–74]. Steady photoexcitation yields a photoluminescence spectrum consisting of a series of broadened lines, beginning below the excitation energy $\hbar\omega_{ex}$, and spaced by the optical phonon energy $\hbar\omega_{op}$. These lines have been shown [73] to arise from recombination of electrons in the conduction band with neutral acceptors, ie. from the (e, A^0) transition. Since the acceptor level is essentially k-independent, one obtains almost direct information on the hot electron distribution in the steady state; that is,

$$I(\varepsilon) \propto n(\varepsilon) W_{eA}(\varepsilon) \tag{5.1}$$

where I is the luminescence intensity, n the electron distribution and W_{eA} the transition rate from conduction band to acceptor level. Hence one must assume a model for the (e, A^0) transition, based on a model for the acceptor wave function, in order to obtain $n(\varepsilon)$ from $I(\varepsilon)$. The commonly employed model [29,66,69,76] uses hydrogenic wave functions for the acceptor level and incorporates an effective acceptor mass m_A [77,142]. Within the limits of a model for W_{eA}, then, one obtains information on the electron distribution from luminescence spectra.

In this paper we show that an analytical solution to the Boltzmann equation due to Mahan [2] may be applied to the dynamics of photoexcited carriers in semiconductors. Mahan's solution applies to systems with no time dependence, and one-dimensional spatial dependence, in which optical phonon scattering is dominant. Since the optical phonon energy is treated as a constant, only discrete energy levels need be considered; hence the term "discrete Boltzmann equation" (DBE). In the following we show that the DBE applies equally well to systems which are isotropic (no spatial dependence), but time-dependent, as long as optical phonons remain the dominant scattering mechanism. Using the DBE we will obtain the time-dependent electron distribution for both pulsed and steady photoexcitation.

Since the LO-phonon scattering time (τ_{op}) $\sim$ 100 fs [69], direct time-resolved photoluminescence spectra from photoexcited carriers have not been obtained on a time scale which enables the observation of phonon-dominated transients. Carrier dynamics have been studied on nano- and picosecond time scales [65,78,79,80]. Photoexcited phonon populations have been studied on the subpicosecond time scale by Kash et al [81] and Collins and Yu [82]. Erskine, Taylor and Tang measured carrier lifetimes, due to phonon and intervalley scattering, on the order of tens of femtoseconds, using a pulse correlation technique [83]. Finally, we mention the experiment of Oudar et al [84], who measured subpicosecond relaxation phenomena for photoexcited carriers at energies $\varepsilon_c < \hbar\omega_{op}$.

Theoretical treatments of photoexcited carriers have been confined primarily to numerical solutions [29,85,86]. Levinson and Levinsky have shown that, where the phonon population is small (low T, and small non-equilibrium densities),

$$n(\varepsilon_n) \sim \begin{cases} \tau_{op}(\varepsilon_n)\,, & \varepsilon_n < \varepsilon^* \\ 0\,, & \varepsilon_n > \varepsilon^* \end{cases} \tag{5.2}$$

where ε_n is the discrete carrier energy = $(\varepsilon^* - n\hbar\omega_{op})$, and ε^* is the energy of the photoexcited electrons [87,88]. Eq. (5.2) is valid only for the steady-state solution under steady illumination. It describes a rectangular distribution (if $\tau_{op} \sim$

independent of ε), which, to the level of approximation assumed, shows agreement with experimental results [67,69,71], and with our calculation (see below). Our solution neglects the non-equilibrium phonons generated by the excited electrons, but incorporates scattering from thermal phonons at large T [2].

The theoretical treatment of Collins and Yu [82] is most similar to ours. They find an analytical solution to the Boltzmann equation for a discrete electron distribution (ie, scattering only by LO phonons), which is linearized in the distribution function. Their work differs from ours in the following respects. (i) They consider only spontaneous emission of phonons, which restricts the applicability of the result to low T. (ii) Their solution is only valid for a pulsed excitation $\delta(t)$. (iii) They extended their formulation to incorporate intervalley scattering and non-parabolic band structures, and solved the resulting equations numerically. (iv) They also derived and solved the linearized Boltzmann equation for the phonon distribution, and compared the results with experimental Raman-scattering data.

Our method, as noted above, is not restricted to low temperatures. Further, it may be applied to excitations of arbitrary time dependence, although in the following we treat only pulsed and steady excitations.

5.2 Pulsed Excitation

In the case that the distribution depends only upon time, the Boltzmann equation is

$$\frac{df}{dt} = \left(\frac{df}{dt}\right)_{\text{scatt.}} \tag{5.3}$$

Discretizing the above, we get [2]

$$\begin{aligned} \frac{d}{dt} f_l &= -\frac{f_l}{\tau_l}[N_0 + (N_0+1)\Theta(l-1)] \\ &\quad + \frac{f_{l-1}}{\tau_{l-1}}[N_0\Theta(l-1)] + \frac{f_{l+1}}{\tau_{l+1}}(N_0+1) \end{aligned} \tag{5.4}$$

where $\Theta(x)$ is the step function, N_0 = the phonon occupation number = $[\exp(G) - 1]^{-1}$, and $G = \hbar\omega_{op}/kT$.

Next we make the reasonable assumption [89] that τ_l = constant = τ; then, normalizing time so that $\tau = 1$, we get

$$\dot{\vec{f}} = -M\vec{f} \tag{5.5}$$

where M is an infinite, tridiagonal matrix identical to that of Eq. (5.7) in Ref. [2]. Hence one knows immediately, from Ref. [2], that

$$f_l(t) = C_0 e^{Gl} + e^{-Gl/2}\int_0^\pi \frac{d\theta}{\pi} C(\theta) e^{-\lambda(\theta)t}\cos(l\theta + \phi) \tag{5.6}$$

where

$$\lambda(\theta) = \frac{e^G + 1 - 2e^{G/2}\cos\theta}{e^G - 1}$$

and

$$\tan\phi = \frac{e^{G/2} - \cos\theta}{\sin\theta}$$

using the spectrum of eigenvalues and eigenfunctions of M. The eigenvalues of M consist of a discrete value $\lambda = 0$, and a continuous spectrum of values $\lambda = \lambda(\theta)$. The constants C_0 and $C(\theta)$ then need to be determined by initial conditions.

If we rewrite (5.6) as

$$\vec{f}(t) = C_0\vec{f}_0 + \int_0^\pi \frac{d\theta}{\pi} C(\theta) e^{-\lambda_\theta t}\vec{f}_\theta \tag{5.7}$$

where $\vec{f}_0, \vec{f}_\theta$ are eigenvectors corresponding to $\lambda = 0, \lambda = \lambda(\theta)$, respectively, then we find that

$$\tilde{f}_0\vec{f}_0 = 1 \tag{5.8}$$

$$\tilde{f}_0\vec{f}_\theta = 0 \tag{5.9}$$

$$\tilde{f}_\theta\vec{f}_0 = 0 \tag{5.10}$$

$$\tilde{f}_\theta\vec{f}_{\theta'} = \frac{\pi}{2}\delta(\theta - \theta') \tag{5.11}$$

if

$$\tilde{f}_0 = (1 - e^{-G})(\ 1\ \ 1\ \ 1\ \ \cdots\ ) \tag{5.12}$$

and

$$\left(\tilde{f}_\theta\right)_l = e^{Gl/2}\cos(l\theta + \phi) \tag{5.13}$$

ie these are the left eigenvectors of M. Then, evaluating (5.7) at $t = 0$ and multiplying on the left by $\tilde{f}_\theta$, we get

$$C_\theta = 2\tilde{f}_\theta \vec{f}(0) = 2\sum_{l=0}^{\infty} e^{Gl/2}\cos(l\theta + \phi) f_l(0). \tag{5.14}$$

If we multiply by $\tilde{f}_0$ we get

$$C_0 = \tilde{f}_0 \vec{f}(0) = (1 - e^{-G})\sum_{l=0}^{\infty} f_l(0). \tag{5.15}$$

Now we imagine an initial distribution $\vec{f}(0)$ injected into an empty band by a short pulse of light, where the pulse time is small compared to τ. For monochromatic light we have that

$$f_l(0) = a\delta_{ln} \tag{5.16}$$

ie the light populates only the nth level. Clearly, $C_0 = a(1 - e^{-G})$. Eq. (5.14) becomes

$$C_\theta = 2e^{Gn/2}\cos(n\theta + \phi) \tag{5.17}$$

so that

$$f_l(t) = C_0 e^{-Gl} + e^{-Gl/2}e^{Gn/2}\int_0^\pi \frac{d\theta}{\pi} 2e^{-\lambda_\theta t}\cos(l\theta + \phi)\cos(n\theta + \phi). \tag{5.18}$$

Eq. (5.18) is the complete solution for the initial condition (5.16).

5.3 Steady Excitation

In the case of continuous illumination, which is more typical of experiments, carriers are injected into the conduction band at a steady rate. Hence we rewrite (5.5) as

$$\dot{\vec{f}} + M\vec{f} = \vec{k} \tag{5.19}$$

where $\vec{k}$ is a constant vector representing the steady injection of carriers by photoexcitation; for monochromatic illumination $\vec{k}$ has only one nonzero entry.

Eq. (5.19) has no steady-state solution, since we are exciting a system possessing a $\lambda = 0$ eigenvalue with the frequency $\omega = 0$. More physically, we have not provided a mechanism for carriers to leave the band; without one, the population grows indefinitely. Hence we must add a term representing radiative recombination; however, we will neglect other possibilities (eg, intervalley transitions). So (5.19) becomes

$$\dot{\vec{f}} + (M^0 + M')\vec{f} = \vec{k} \tag{5.20}$$

where M^0 is the matrix of Section 2 [Eq. (7), Ref. [2]] and M' is a diagonal matrix representing recombination. We write (5.20) in a form suggesting a perturbative treatment, since radiative transitions are very slow relative to phonon scattering (ie, $M'_{ll} \ll M^0_{ll}$).

Thus we let

$$\lambda_0 = \lambda_0^0 + \lambda_0' = \lambda_0' \tag{5.21}$$

$$\lambda_\theta = \lambda_\theta^0 + \lambda_\theta' \tag{5.22}$$

and

$$\vec{f}_0 = \vec{f}_0^0 + \vec{f}_0' \tag{5.23}$$

$$\vec{f}_\theta = \vec{f}_\theta^0 + \vec{f}_\theta' \tag{5.24}$$

and similarly for left eigenvectors. If we assume that (5.8)-(5.11) hold for the *perturbed* system, and the band is assumed empty at $t = 0$, then it is easily shown that the solution to Eq. (5.20) is

$$\begin{aligned} \vec{f}(t) &= (\tilde{f}_0\vec{k})\left(\frac{1-e^{-\lambda_0 t}}{\lambda_0}\right)\vec{f}_0 \\ &\quad + \int_0^\pi \frac{d\theta}{\pi}(2\tilde{f}_\theta\vec{k})\left(\frac{1-e^{-\lambda_\theta t}}{\lambda_\theta}\right)\vec{f}_\theta \end{aligned} \tag{5.25}$$

which, given the perturbed eigensystem, is a complete solution.

First-order perturbation theory gives

$$\lambda_0' = (1-e^{-G})\sum_{l=0}^{\infty} M_{ll}' e^{-Gl} \tag{5.26}$$

$$\lambda_\theta' = 0. \tag{5.27}$$

Since [2] $\lambda_\theta^0 \simeq 1$, while $\lambda_0' \simeq 10^{-6}$, we see that Eq. (5.25) consists of a part which evolves slowly, at the rate λ_0, and a fast part which is basically driven by phonon scattering. Physically, the occurrence of the two very different time scales reflects the fact that the phonon scattering is very much faster (by $\sim 10^6$) than recombination.

As a first approximation, then, we set $\vec{f}_\theta' = \tilde{f}_\theta' = \vec{0}$, ie we assume no perturbation to the phonon dynamics. The perturbation on $\vec{f}_0$ is found to be

$$(\vec{f}_0')_l = -\sum_{m=0}^{\infty} M_{mm}' e^{-Gm/2} e^{-Gl/2} \int_0^\pi \frac{d\theta}{\pi} \frac{2\cos(l\theta+\phi)\cos(m\theta+\phi)}{\lambda_\theta^0} \tag{5.28}$$

while

$$(\tilde{f}_0')_l = (1-e^{-G})e^{Gl}(\vec{f}_0')_l. \tag{5.29}$$

As noted above, $\lambda_\theta^0 \simeq 1$; the approximation improves with decreasing temperature [90]. If we remove λ_θ^0 from (5.28), the remaining integral is known analytically [2], and we get

$$\begin{aligned}(\vec{f}_0')_l &\simeq -M_{ll}' e^{-Gl} + e^{-GL}\sum_{m=0}^{\infty} M_{mm}' e^{-Gm} \\ &= (-M_{ll}' + \lambda_0')e^{-Gl}\end{aligned} \tag{5.30}$$

which is parallel to $\vec{f}_0^0$; hence

$$\tilde{f}_0 \simeq \tilde{f}_0^0 = (1-e^{-G})(\ 1\quad 1\quad 1\quad \cdots\ ) \tag{5.31}$$

Eqs. (5.25)–(5.27), (5.30), (5.31) thus constitute an approximate solution for steady excitation.

5.4 Numerical Results

First, we show a numerical example for the solution in Sec. 2 to a pulsed initial state. The pulsed solution (5.18) requires only the specification of $G = (\hbar\omega_{op})/kT$, and an initial density a. Fig. 5.1 shows a solution for $\hbar\omega_{op}$ =.037 eV (GaAs), T=300K, $a = 1/(1 - e^{-G})$ and n (the pulsed level) = 5. It should be emphasized that the distribution is actually a set of discrete points; the continuous curves are added as an aid to the eye. The distribution relaxes smoothly towards the equilibrium distribution (e^{-Gl}); however note that it is still significantly different from equilibrium after 10 scattering times.

It should be noted that this solution, normalized to an energy-independent scattering time τ_{op}, is nevertheless *not* equivalent to the relaxation-time approximation [86]. Fig. 5.2 shows the relaxation time solution to the DBE, for the same initial condition; it consists of a decaying spike and a growing Maxwell-Boltzmann distribution. In the relaxation time approximation interactions between energy levels are not modeled, unlike the present formalism; the result is a more rapid, but less physical, approach to equilibrium.

To our knowledge, experimental resolution of the carrier distribution on this time scale ($\tau_{op} \sim 100$ fs) has not been achieved. We may compare our results with those obtained by Lugli and Ferry [85], who have solved the same problem using a Monte Carlo technique, both with and without e-e scattering; their results without e-e scattering are qualitatively similar to ours. Ulbrich has solved a similar problem numerically, except that the initial spike is at low energy (5 meV) and scattering is by acoustic phonons [76].

The second example we treat is the solution for steady illumination (5.25). It requires a knowledge of the matrix elements M'_{ll}, ie the recombination rates. We choose to model transitions from the conduction band to an acceptor impurity level, as this phenomenon is typical of experiments [69–74]. For these transition rates we used expressions from Dumke [142], normalized to $\tau_{op} = 10^{-13}$ sec.

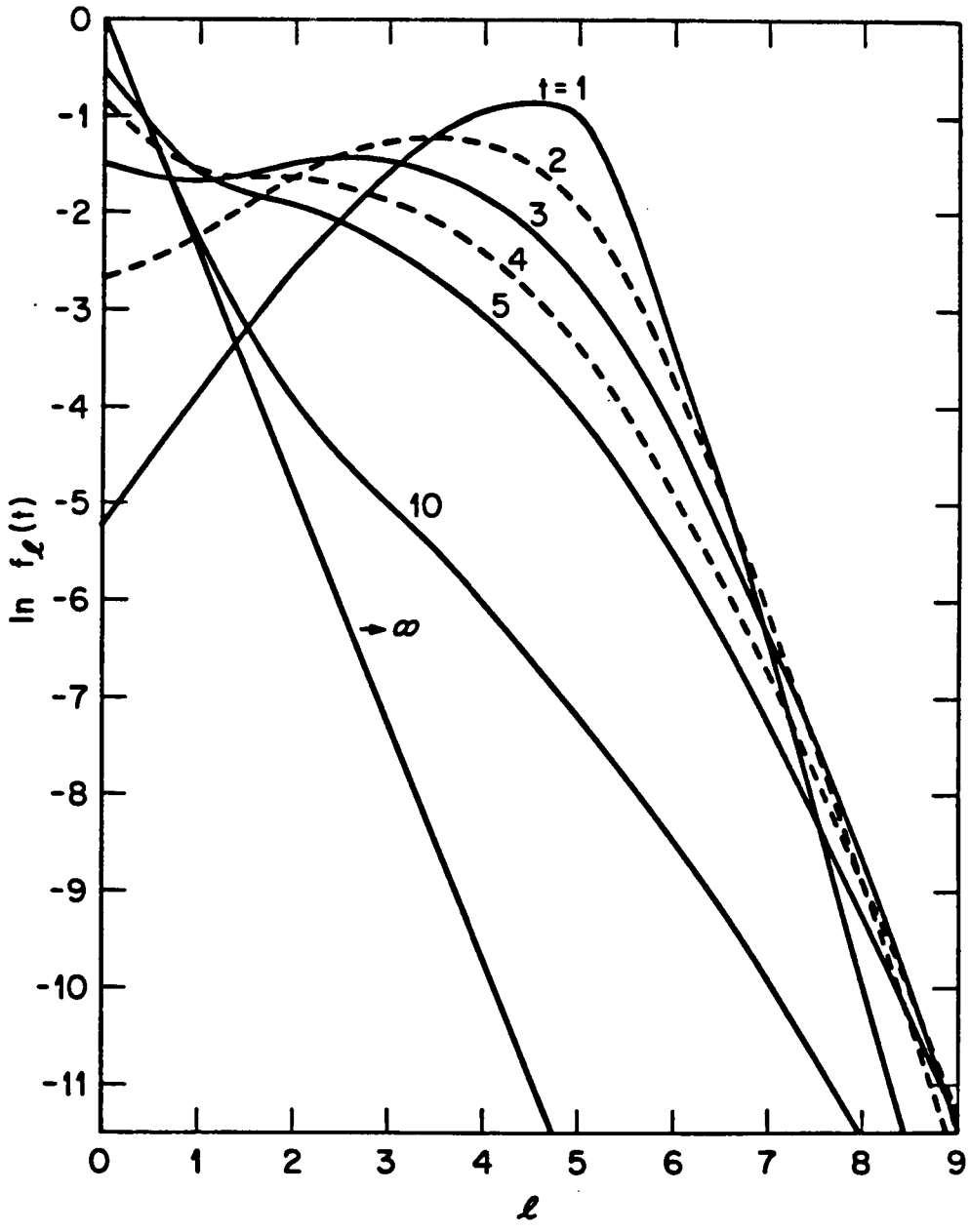

Figure 5.1: Time-dependent solution for pulsed excitation. The electron distribution decays from an initial spike at $l = 5$, $t = 0$; $\hbar\omega_{op} = .037$ eV, T = 300K. The distribution is discrete in energy; the smooth curves are a visual aid.

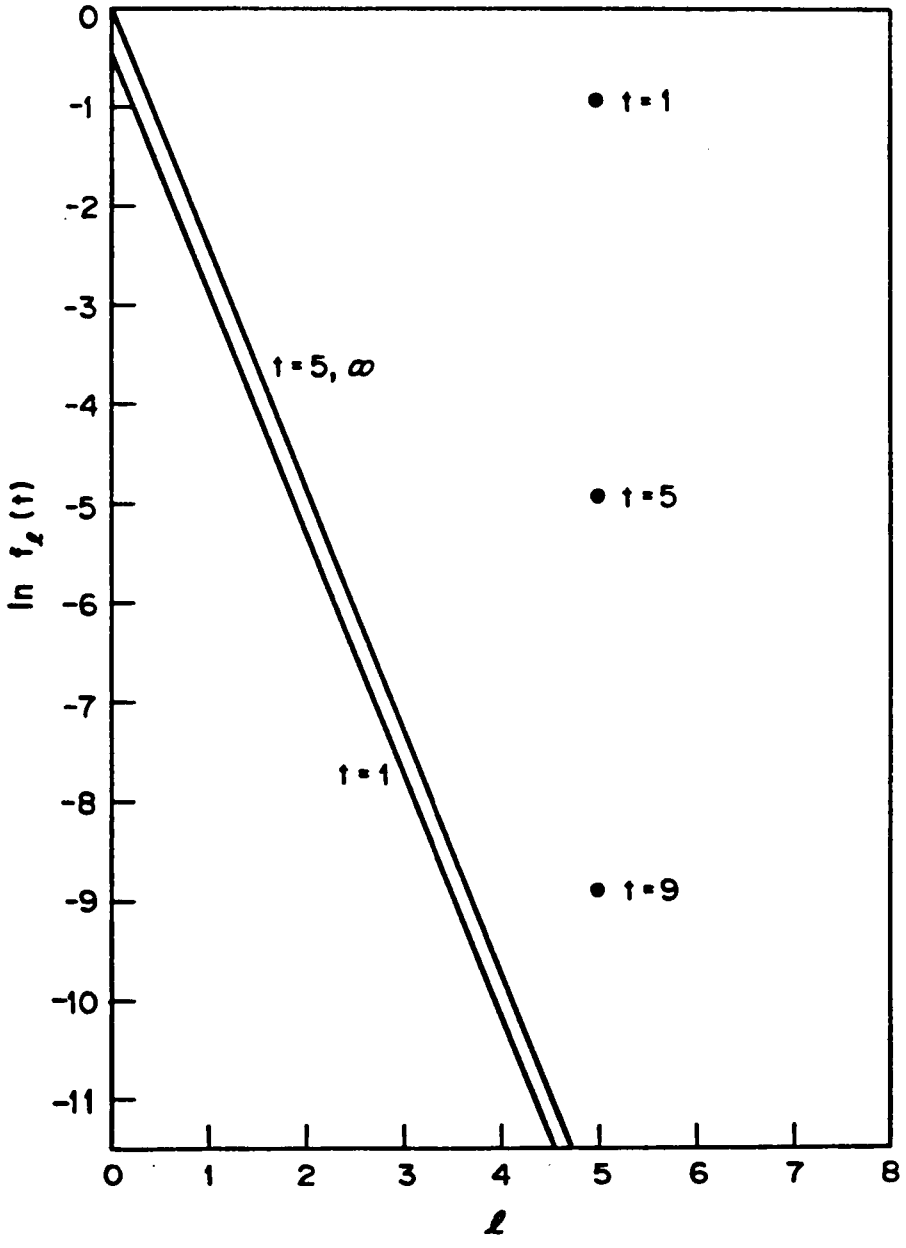

Figure 5.2: Relaxation-time approximation. The same conditions apply as in Fig. 5.1; the absence of interaction among the levels is evident.

In Figs. 5.3 and 5.4 we show time-dependent solutions for an initially unoccupied band, into which carriers are injected at a steady rate at the level $l = 8$ ($\varepsilon = 8\hbar\omega_{op}$), for GaAs, at T=77K and 300K, respectively. The distribution achieves a broad plateau, at either temperature, after $\sim 10\tau_{op}$. However at room temperature the plateau is masked by a slow-growing quasithermal distribution which appears after much longer times ($\sim 10^7\tau_{op}$). At 77K this same distribution appears but falls more rapidly with energy, so that the plateau persists; note the resemblance to the rectangular distribution mentioned in Sec. 1.

The approximations used in the perturbation solution are considered acceptable if the results converge to the steady-state distribution. The latter may be obtained by solving (5.20) subject to $\dot{\vec{f}} = 0$, ie

$$M\vec{f} = (M^0 + M')\vec{f} = \vec{k}. \tag{5.32}$$

Eq. (5.32) is soluble by matrix inversion, as the addition of M' makes the matrix nonsingular. For temperatures below $\sim$ 50K, we find that it is not a good approximation to use the unperturbed $\vec{f_\theta}$ and $\tilde{f}_\theta$ eigenvectors in the time-dependent solution [Eq. (5.25)]. We have analytical expressions for these vectors, to first order in M', but have not implemented them numerically.

Steady-state results are easily available at any temperature from (5.32). Also, it is possible to drop the assumption that τ_{op} is independent of energy, in the steady-state case. Fig. 5.5 shows the steady-state distribution for injection at $l = 8$, for T=30K. Results are plotted for three cases:

(i) τ_{op} = constant

(ii) Mean free path = constant = $v(\varepsilon)\tau(\varepsilon)$ where $v(\varepsilon)$ is the group velocity. This gives

$$\frac{1}{\tau_l(\varepsilon)} = \frac{v_l(\varepsilon)}{\text{constant}} = \frac{\sqrt{l+\delta l}}{\text{constant}} \tag{5.33}$$

In the results shown in Fig. 5.5 we used $\delta l = 1/2$ so that $1/\tau_0 \neq 0$, and normalized to $1/\tau_8 = 1$.

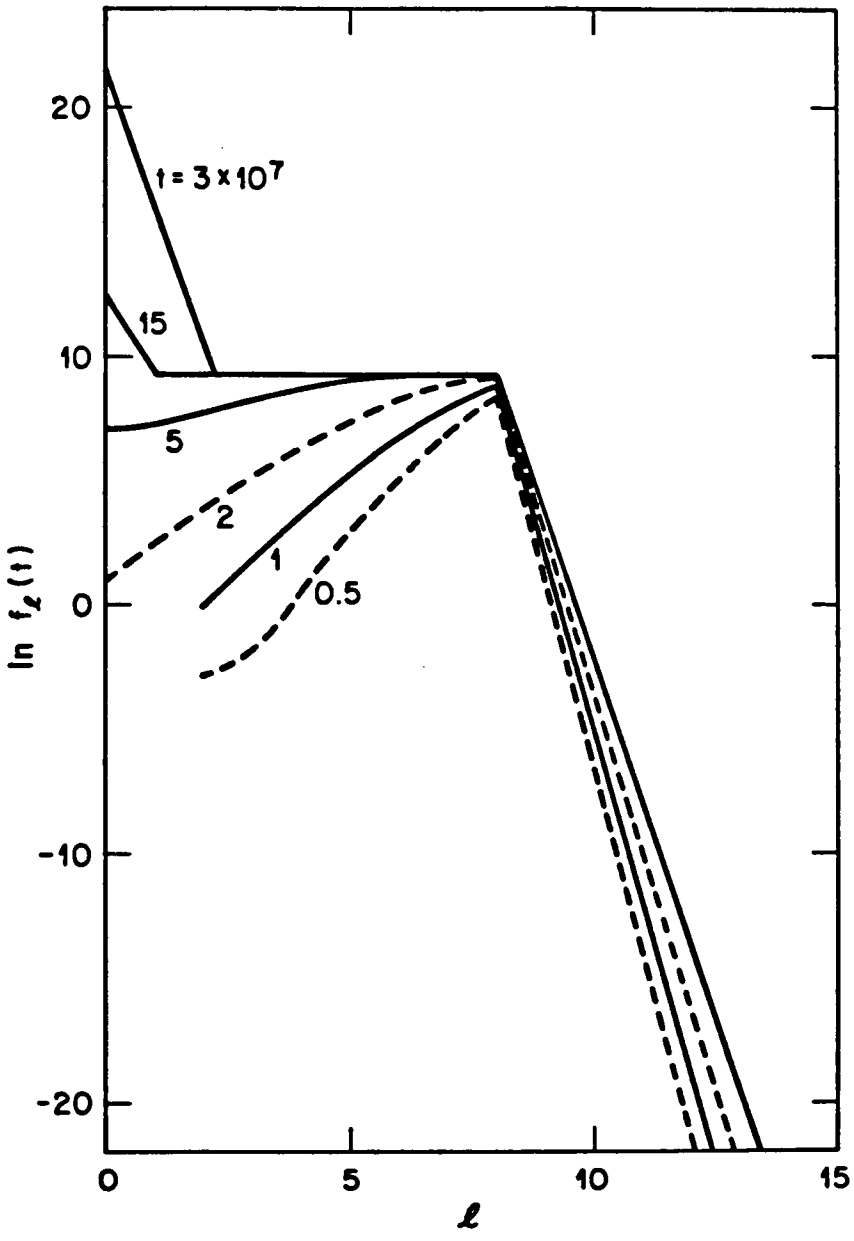

Figure 5.3: Electron distribution vs. time, for steady injection at $l = 8$; GaAs, T=77K.

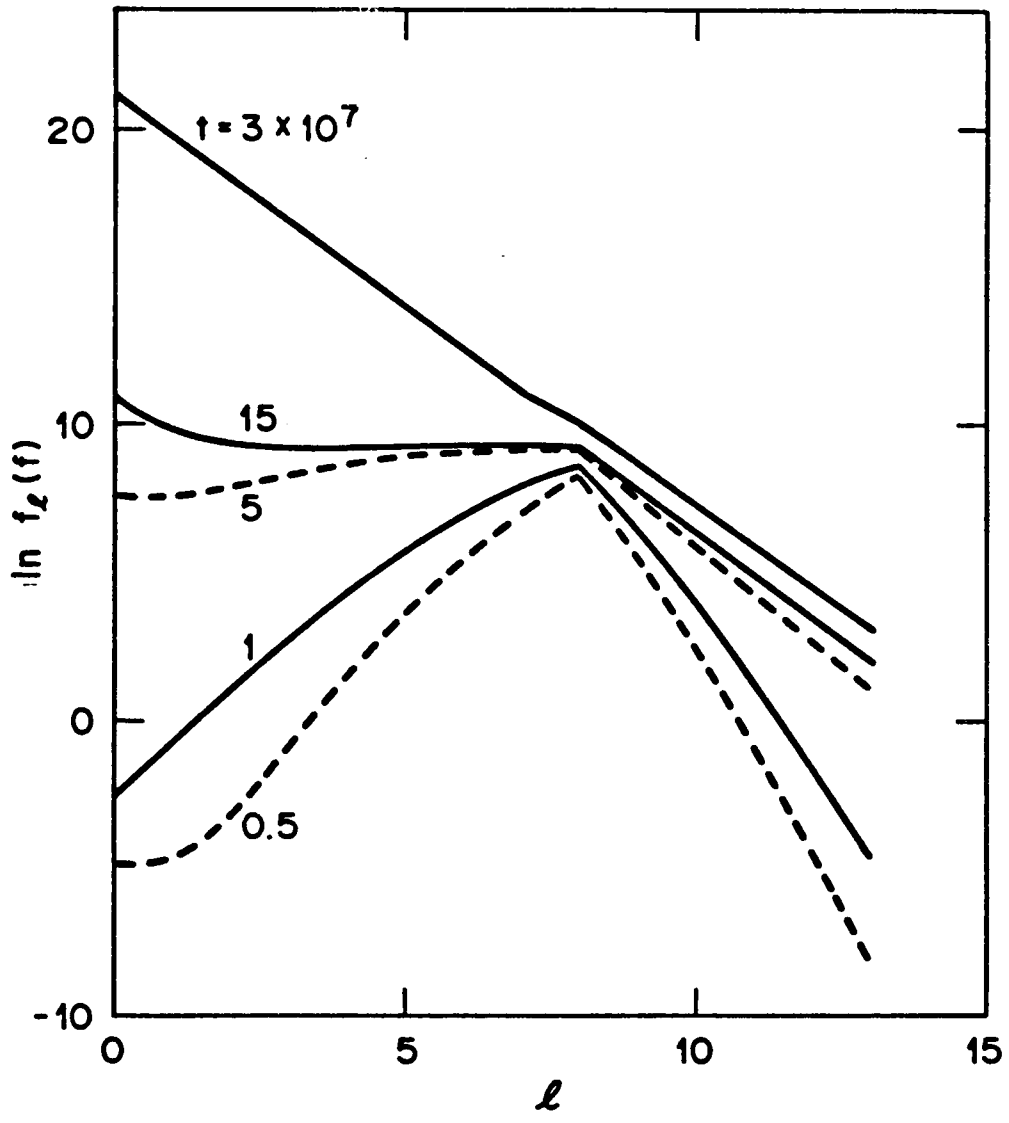

Figure 5.4: Electron distribution vs. time, for steady injection at $l = 8$; GaAs, T=300K.

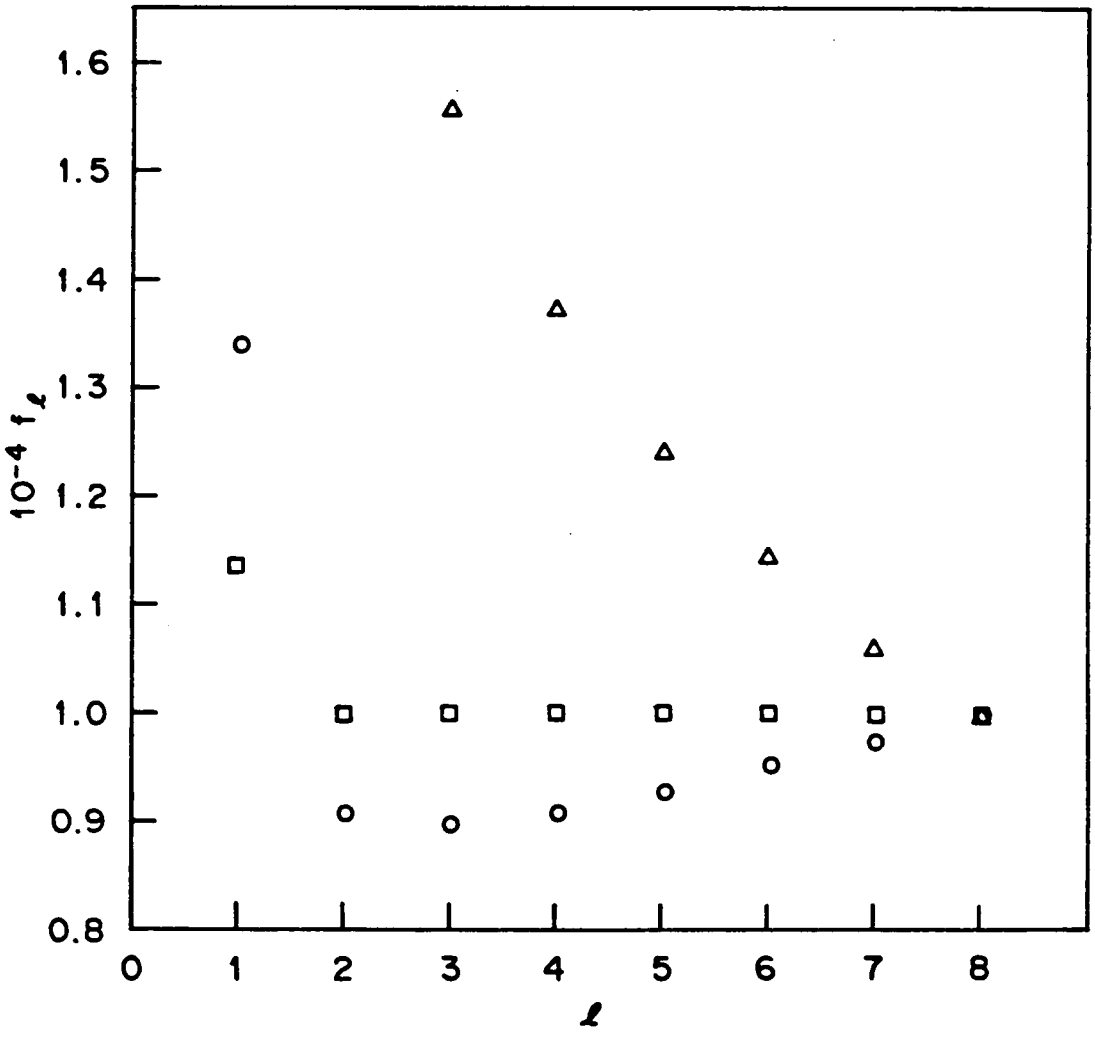

Figure 5.5: Steady-state distribution for constant excitation at $l = 8$, GaAs, T=30K; using various expressions for τ_{op}. (See text). (□) τ = constant; (△) mfp = constant; (o) $1/\tau = -2\Im(\Sigma)$.

(iii) $1/\tau_{op} = -2\Im(\Sigma)$ or

$$\frac{1}{\tau_{op}} = \frac{(\text{const})}{\sqrt{l+1/2}}\left[N_0 \ln\left|\frac{(l+3/2)^{1/2}+(l+1/2)^{1/2}}{(l+3/2)^{1/2}-(l+1/2)^{1/2}}\right|\right.$$
$$\left.+(N_0+1)\ln\left|\frac{(l-1/2)^{1/2}+(l+1/2)^{1/2}}{(l+1/2)^{1/2}-(l-1/2)^{1/2}}\right|\right] \qquad (5.34)$$

where $\Im(\Sigma)$ is the imaginary part of the electron self-energy, obtained for single-phonon scattering by Mahan [91], and as in (ii), we used $\delta l = 1/2$ and set $\tau_8 = 1$.

Fig. 5.6 shows the discrete luminescence spectra obtained from the distributions of Fig. 5.5, using Eq. (5.1) and the transition rates M'_{ll}. The results resemble the spectra in Ref. [73]; however, the differences among models (i)–(iii) for τ_{op} are less obvious in these spectra than they are in Fig. 5.5. There are other published spectra for which the resemblance is weaker. In Ref. [72] the peaks are very broad and not well resolved, while in Ref. [69] (Fig. 1) only the first three peaks are not masked by luminescence from electrons excited from the light-hole band. Figure 3 of the same source [69], the luminescence spectrum of carriers injected by intervalley transitions from the L valley, is not similar to our Fig. 5.6, being considerably flatter.

The Leningrad workers used Eq. (5.1) and models for W_{cA} to obtain the distribution $n(\varepsilon)$ from their spectra [69,71]. Using an expression for W_{cA} similar to ours, they obtained a distribution (Fig. 4, Ref. [69]) very much like that of (iii) in Fig. 5.5; the agreement is not as good with a different model [71]. Nevertheless both models used by them, and the three reported here in the steady-state calculation, give essentially indistinguishable results on the coarser scale of Fig. 5.3, ie a very flat distribution above the "pileup" at the bottom of the band.

We have not done time-dependent calculations for T<77K. The steady-state results merely approximate a rectangular electron distribution more and more closely as T→0, showing no qualitative difference from the temperature regime in which we have time-dependent results. Further work on the low-temperature, time-dependent solution may be warranted as experimental techniques advance to yield comparable information experimentally. Similarly, more detailed comparison of steady-state re-

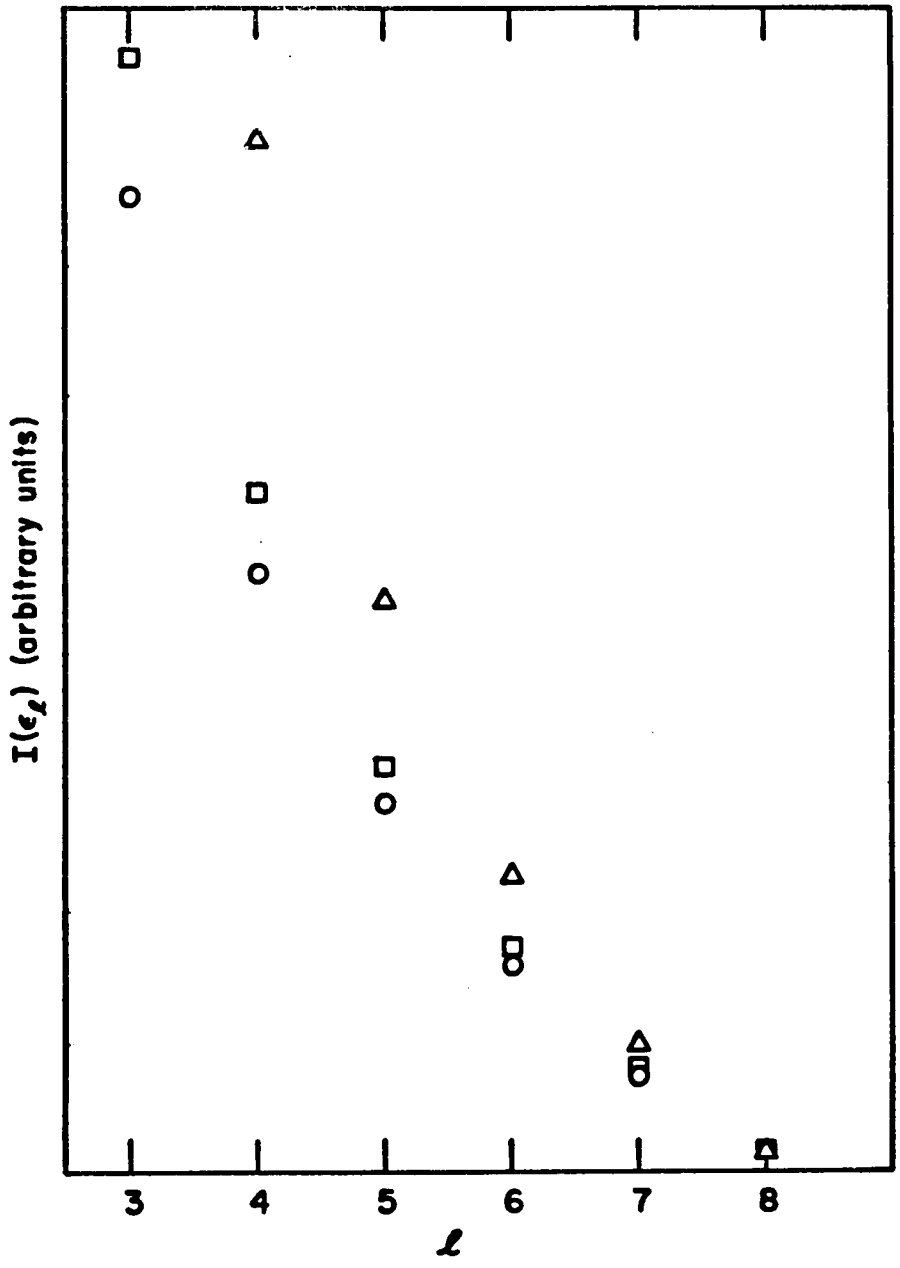

Figure 5.6: Luminescence spectra for constant illumination. The spectra plotted correspond to the distributions of Fig. 5.5, obtained from Eq. (5.1) and M'_{ll} (see text).

sults requires better modeling of the transition rate between the conduction band and the acceptor level.

5.5 Conclusions

We have presented a theory for the time dependence of the nonequilibrium electron distribution, which is valid for the case of dilute carrier concentrations such that carrier-carrier scattering is unimportant. Our solution is analytical and thus avoids the computational burden of numerical solutions. It is also more general than previous analytical work in the following ways. Both the time-dependent and the steady-state solution are readily obtained in our approach, with the steady solution serving as an independent check of the time-dependent calculation. Our DBE solution is not restricted to low temperatures. We have solved both the case of steady excitation and the delta-function case; and the approach may be extended to a time-dependent excitation of arbitrary form (eg, a broadened pulse). Hence, although it will perhaps always be necessary to resort to numerical solutions in order to incorporate all possible scattering mechanisms, our approach represents an attractive and flexible solution for systems in which optical phonon scattering is dominant.

Such systems correspond to an important class of experimentally realizable cases which have been and remain of considerable interest, both for their pertinence to the understanding of practical devices involving hot electrons, and for the improvement in understanding of basic physical processes which they offer. Further steps toward the merging of theoretical and experimental insight will require, on the theoretical side, refinements in models for recombination rates, and on the experimental side, advances in femtosecond spectroscopy.

Part II

Dynamic Screening in the Electron Gas

Chapter 6

Introduction to Part II

The concept of screening is of fundamental importance in understanding the response of solids (and plasmas) to charged perturbations. The basic, intuitively obvious notion is that charge carriers (henceforth, electrons) which can move or distort their configuration in response to a perturbing electric field, will do so in such a way as to cancel the field at large distances [4]. A more difficult problem is to describe accurately and quantitatively the screening response of electrons to a given perturbation.

The problem of a point charge impurity is clearly one of the simplest that can be posed; and yet this problem is both highly pertinent in describing real physical phenomena in solids, and not yet fully solved. Hence the point impurity problem remains one of current interest.

We simplify the problem considerably by restricting our consideration to metals. The Fermi temperature of metals is sufficiently large ($\sim 10^4$K) that we can neglect temperature effects and treat the problem at T=0. In order to simplify further we concentrate on the electron-electron interaction and neglect the lattice: we take the "jellium" model, consisting of a homogeneous sea of electrons imbedded in a rigid, structureless background of positive charge. This model has some validity as a representation for simple metals (s and p electrons).

The case of a *static*, point impurity has been the subject of considerable effort. Friedel [92], using scattering theory, first predicted that the screening charge around an impurity would be oscillatory in r, and gave its asymptotic limit for large r as

$$\delta\rho(r) \sim \frac{\cos(2k_F r + \phi)}{r^3}$$

where k_F is the Fermi wavevector, and ϕ is (for a spherically symmetric impurity potential) the s-wave phase shift [4]. Subsequently the commonest approach has been to use the linear screening approximation as embodied in the (linear) dielectric function $\epsilon(q)$. The earliest example of this approach is the work of Langer and Vosko [93], who found $\delta\rho(r)$ in two models. One is called the "random phase approximation" or RPA [4]; the RPA is essentially a mean-field (Hartree) theory which neglects both exchange and the effects of local correlations between electrons. Langer and Vosko also used the work of Hubbard [94] to include some effects of exchange on the screening: in modern notation, they modified the RPA form with a "local-field correction" $G(q)$ [4].

Further work in linear dielectric theory has concentrated primarily on improving the local-field factor $G(q)$, to include not only exchange but correlation effects as well. Examples which include $\delta\rho$ calculations are [95,96,97]. The $\delta\rho$ results for various $G(q)$ tend to be qualitatively quite similar.

There have been efforts to go beyond the linear approximation; since the smallest impurity charge is of magnitude one (which cannot be considered infinitesimal!), it cannot be assumed that linear-response theory is adequate. Sjölander and Stott [98] performed calculations for both finite and infinite impurity mass. They used essentially a mean-field approach in two versions; they found large differences from the linear result. Their work was extended by Bhattacharyya and Singwi [99], who obtained good agreement with positron-annihilation data by including three-body correlations.

Density-functional theory (DFT) [100], which has shown success in a wide variety of applications [101], has been applied to the point-impurity problem. Almbladh et

al [102] found the screening of a proton in the electron gas, using the local-density approximation (LDA) [Kohn and Sham in [100]] for the exchange-and-correlation potential. Jena and Singwi [103] treated the same problem, using the first-order term in a gradient expansion for which the LDA is zeroth-order; their results were very similar. Variations on the point-impurity problem include the work of Bryant and Mahan [104], who gave special treatment in the LDA to the valence electrons of the central ion; and that of Norskov [105], who, using a Green's-function formulation of the DFT, was able to treat non-spherically-symmetric perturbations such as two close protons. Finally we mention work on the somewhat different problem of determining the excitation spectrum of the jellium/point-impurity system, which has been approached using a dielectric formulation [106], and using DFT [107].

Thus we find the point-impurity problem applied to a variety of physical questions: Knight shifts due to positive muons [103], NMR spectra [108], positron annihilation rates in metals [98,99], heats of solution [102] and other properties [105] of hydrogen in metals, soft x-ray absorption (SXA) and emission (SXE) spectra [104], and the stopping power of metals for impinging (slow) ions [109]. We also find a clear consensus that, for these static screening calculations, the linear approximation gives results which are markedly different from those of the less restricted nonlinear theories. This appears to be a clear signal that even Z=1 is too large for linear-response theory.

Dynamic screening calculations are less frequently found in the literature. Time-dependent calculations are readily performed in the linear approximation using the dynamic dielectric function $\epsilon(q,\omega)$. An example is the RPA calculation of the perturbed wake of a fast-moving ion in the electron gas by Mazarro et al [110].

The work of Noguera et al [111] is similar to the present work. They calculate the dynamic screening of a suddenly-created dipole system consisting of a point core hole and an ejected photoelectron which has a constant, classical velocity. A linear screening model is used, with the plasmon-pole approximation for the dielectric

function. The classical model for the photoelectron is most appropriate when the latter is highly energetic. Our work applies to the same regime, since we assume that the photoelectron leaves the core hole with infinite velocity. We then concentrate on the dynamic screening response of the electron gas to the core hole, in the linear approximation.

A self-consistent, time-dependent nonlinear theory, which is equal in rigor to the DFT of the ground state, remains to be developed and tested [101,112]; a linearized version has been presented [113]. Calculations of dynamic screening in metals which are similar in approach to a time-dependent DFT include the quasistatic version of Ying [114], and a linearized model by Mukhopadhyay and Lundqvist [115]. From the results found in the static case, we expect linear models to be of limited validity; hence progress in a nonlinear dynamic theory is desirable.

The dynamic screening of conduction electrons is clearly of fundamental interest. In x-ray spectra, for example, we find a variety of coupled physical processes of widely varying energy (and hence time) scales; some of these processes are included in the screening response. Most theories (see Chapter 7) of x-ray spectra neglect the dynamics of screening. The effects of transients in screening on the resulting spectra are thus not well understood.

The present work is an attempt to accurately depict the dynamics of core-hole screening in the electron gas. It is plausible, but remains to be tested, that the *transient* nature of the screening behavior may be well described by a linear theory, although the amplitudes are not. Chapter 7 is an article which has been submitted for publication, containing a description of the approach employed, the numerical results, and their implications. It is followed by two appendices giving, respectively, the details of the analytical derivations, and the numerical methods employed.

Chapter 7

Time-dependent Screening in the Electron Gas

7.1 Introduction

The absorption and emission of X-rays by simple metals have received extensive theoretical and experimental attention, particularly since the prediction of threshold singularities in absorption (SXA) and emission (SXE) spectra by Mahan [116] and Nozieres and DeDomenicis [117] (MND). The field has been reviewed by Mahan [118] in an early article, and more recently by Wilkins [119].

In this paper we wish to consider the various processes that are involved in the absorption of an X-ray photon by a metal, and in particular the time scales that are relevant for these processes. We shall see that the various theoretical approaches may be characterized by the approximations used for these time scales; and we shall present a description of the time dependence of the screening response of the electron gas, which is based on the assumption that the ejected photoelectron has infinite velocity, i.e., that it leaves the vicinity of the core hole instantly.

The first event in X-ray absorption is the actual absorption of the photon, with concomitant transfer of energy to a (we assume only one) core electron. The time

scale for this process is [111] $\tau_x \lesssim 10^{-20}$ s. As this time is much smaller than any other pertinent time scale it is universally approximated as $\tau_x = 0$. We then consider several events which may or may not overlap in time: the relaxation of the remaining core electrons (characterized by τ_{ce}), the departure of the energetic electron (τ_e), and the screening response of the conduction electrons in the metal (τ_{sc}). Since the energy scale is much larger for core than for conduction electrons, it is generally reasonable [111] to take $\tau_{ce} \ll \tau_{sc}$. It is commonly assumed [104,111] that $\tau_{sc} \sim \omega_p^{-1}$, where ω_p is the plasma frequency of the electron gas; we will return to this question below. The problem is that

$$0 \lesssim \tau_e < \infty$$

with the lower limit applying to a highly energetic photoelectron (far from threshold), and the upper limit being the adiabatic limit which is approached as the X-ray energy approaches the ionization threshold from above [120]. Thus we may have $\tau_e \gtrsim \tau_{ce}$, and $\tau_e \gtrsim \tau_{sc}$.

On a longer time scale we again find several processes which may compete [121]: the relaxation of the lattice via phonon emission [122] (τ_p), and the decay of the core hole through either Auger (τ_A) or radiative (τ_r) mechanisms [123]. These time scales are more pertinent to the emission process and will generally be treated as infinite in the following.

The MND theory takes $\tau_{sc} = \tau_x = 0$, i.e., the core hole is assumed to appear fully screened, and conduction electron phase shifts are calculated accordingly [124,125]. This theory is generally successful in describing SXA and SXE spectra near threshold (where $\tau_e \to \infty$). Farther from threshold one uses the "final-state rule," a one-particle formalism, to calculate spectra [126,127,128]; this theory also neglects the dynamics of screening. It is perhaps remarkable that these theories succeed as well as they do, since between them they include an energy region (and hence a region of τ_e) where $\tau_e \sim \tau_{sc}$. In this region it seems unlikely that a model based solely upon static screening would yield the correct physics. This apparent

contradiction is partially resolved by the work of Minnhagen [125] and Shung and Langreth [129], who show that the theory, at least as applied to X-ray photoemission spectra (XPS), is compatible with dynamical screening for some distance from threshold.

Gadzuk and Sunjic (GS) [120] have attempted to deal with a wide range of photoelectron departure rates using a parameter η (where $\eta \sim 1/\tau_e$). They predict observable differences from the prediction of the "sudden" ($\eta \to \infty$, $\tau_e \to 0$) theory for XPS spectra, for $\eta \lesssim 2E_F$, where E_F is the Fermi energy. It is not clear, however, that photoelectrons with $\eta < 2E_F$ are sufficiently energetic to escape the solid surface and be detected. A further problem is that their calculation is based upon a theory [130] which again assumes instantaneous screening, i.e., $\eta \gg \tau_{sc}^{-1} \sim \omega_p \sim E_F$; hence the reliability of the results for $\eta < E_F$ is unclear.

Finally, we mention the work of Noguera et al [111]. They gave the ejected electron a classical (constant) velocity $\vec{v}$ and then used linear response theory to find the response of the electron gas to the two perturbing point charges,

$$\rho_{ext}(\vec{r},t) = e\Theta(t)(\delta(\vec{r}) - \delta(\vec{r} - \vec{v}t)), \tag{7.1}$$

where the first term is the core hole, and $\Theta(t)$ is the step function. With this semiclassical model they could incorporate both dynamic screening and a wide range of τ_e (by varying $|\vec{v}|$); thus they could study the interaction of the two processes at comparable time scales. This enabled them to estimate the parameter η of GS, and also to examine critically the theory of EXAFS (extended X-ray absorption fine structure) [131].

The present work is an improvement on that of Noguera et al. in that we use better dielectric functions to model the dynamic screening process, though we retain the linear screening formalism. However, we do not treat the outgoing electron, i.e., we let $\tau_e \to 0$ (or $|\vec{v}| \to \infty$) in (7.1). Thus we treat, in linear response, the time dependence of the screening charge response to the perturbing charge

$$\rho_{ext}(\vec{r},t) = e\delta(\vec{r})\Theta(t). \tag{7.2}$$

7.2 Theory

In linear response theory

$$\rho_t(\vec{q},\omega) = \rho_{ext}(\vec{q},\omega) + \rho_s(\vec{q},\omega) = \frac{\rho_{ext}(\vec{q},\omega)}{\epsilon(\vec{q},\omega)}$$

or

$$\rho_s(\vec{q},\omega) = \rho_{ext}(\vec{q},\omega)\left[\frac{1}{\epsilon(\vec{q},\omega)} - 1\right], \tag{7.3}$$

where ρ is a charge density and subscripts t, ext, s refer to "total," "external," and "screening," respectively.

The Fourier transform of (7.2) gives

$$\rho_{ext}(\vec{q},\omega) = \frac{i}{\omega + i\delta}, \tag{7.4}$$

where δ is a positive infinitesimal and we have let e (the electronic charge) $= 1$.

Substituting (7.4) into (7.3) and taking the inverse transform, we get, after some manipulation (see Appendix B),

$$\begin{aligned}\rho_s(r,t) &= \frac{1}{\pi^3 r}\Theta(t)\int_0^\infty dq q \sin qr \\ &\quad \times \int_0^\infty \frac{d\omega}{\omega}\left[\Im\left(\frac{1}{\epsilon(q,\omega)}\right)\right][1-\cos(\omega t)].\end{aligned} \tag{7.5}$$

The spectral function $\Im(1/\epsilon)$ consists of a continuum part, representing e-h pair excitations, and a plasmon peak for certain values ω_q [4]. Hence we can find the separate contributions to ρ_s from each type of excitation:

$$\begin{aligned}\rho_s^{eh} &= \frac{\Theta(T)}{\pi^3 R}\int_0^\infty dq q \sin qr \\ &\quad \times \int_{\Omega_1}^{\Omega_2}\frac{d\Omega}{\Omega}\left[\Im\left(\frac{1}{\epsilon(Q,\Omega)}\right)\right][1-\cos(\alpha'\Omega T)],\end{aligned} \tag{7.6}$$

$$\rho_s^p = -\frac{\Theta(T)}{\pi^2 R}\int_0^{Q_c} Q dQ \sin QR\left[\frac{1-\cos(\alpha'\Omega_Q T)}{\Omega_Q|\epsilon_1'|_{\Omega_Q}}\right]. \tag{7.7}$$

Here we have changed to dimensionless quantities (see Appendix B); the charge densities are scaled to k_F^3, where k_F is the Fermi wavevector.

Now we take

$$\epsilon(q,\omega) = 1 - \frac{v_q P(q,\omega)}{1 + v_q G(q) P(q,\omega)} \tag{7.8}$$

where v_q is the Fourier transform of the Coulomb potential, $P(q,\omega)$ is the Lindhard function [132], and $G(q)$ is the (static) local-field correction to the RPA [133]. Using (7.8), we can numerically integrate (7.6) and (7.7) to find the two charge densities.

7.3 Results and Discussion

For the function $G(q)$ in Eq. (7.8) we have used two choices: $G = 0$ (the random phase approximation or RPA) and a parameterized version due to Vashishta and Singwi [134], $G = G_{VS}(q)$. Other parameterized expressions for $G(q)$ are available [96,135,136]; however, since the results for $G = 0$ and for $G = G_{VS}$ differ only slightly, these other choices were not explored.

The electron density is reflected in the parameter r_s, which is small for high densities. We chose to examine a moderately high density, $r_s = 3$ (close to Li at $r_s = 3.24$), and a low density, $r_s = 6$ (close to Cs at $r_s = 5.63$) [137].

In Figs. 7.1–7.3 we show the time development of the three densities ρ_{eh}, ρ^p, and $\rho' = \rho^{eh} + \rho^p$, in the RPA approximation, for $r_s = 3$. Note that the plasmon part is expanded in scale by a factor of 30.

In Figs. 7.4–7.6 we attempt to render more clearly the time dependence of the three quantities, by plotting the values at $R = 0$ vs $T = \omega_p t$. The absolute values at $R = 0$ cannot be considered reliable when computed from linear response theory [102]; however, the time dependence is more likely to be reliable. The time dependence of the values at $R = 0$ is illustrative of the behavior for general R, as may be seen in Figs. 7.1–7.3.

Several points are of interest from the results of Figs. 7.1–7.6. First, the e-h contribution essentially determines the behavior of the total screening charge ρ'; the plasmon part is on the order of 3%. From Figs. 7.1–7.3 we see that the

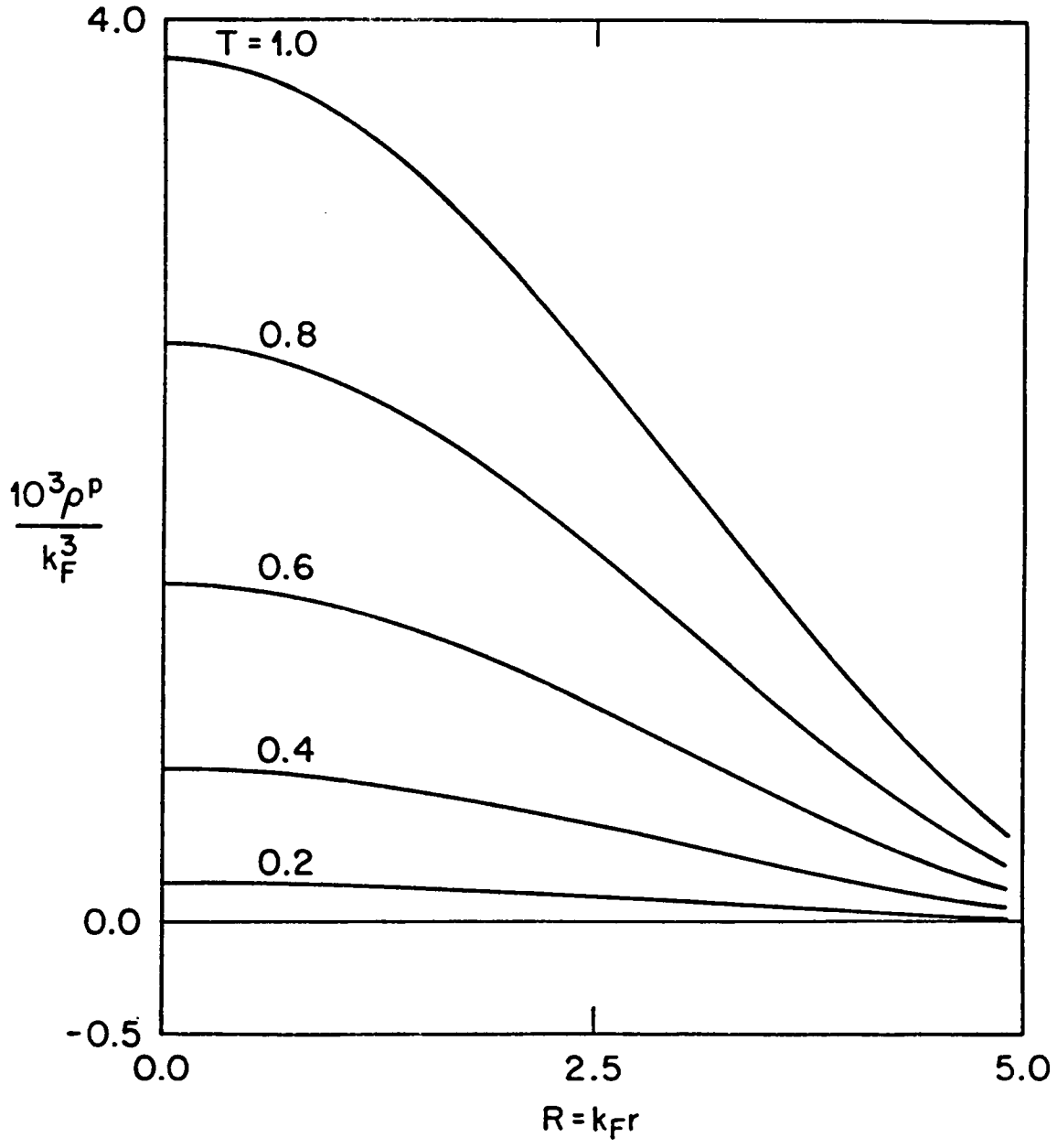

Figure 7.1: Plasmon screening charge for small R and T; RPA, $r_s = 3$.

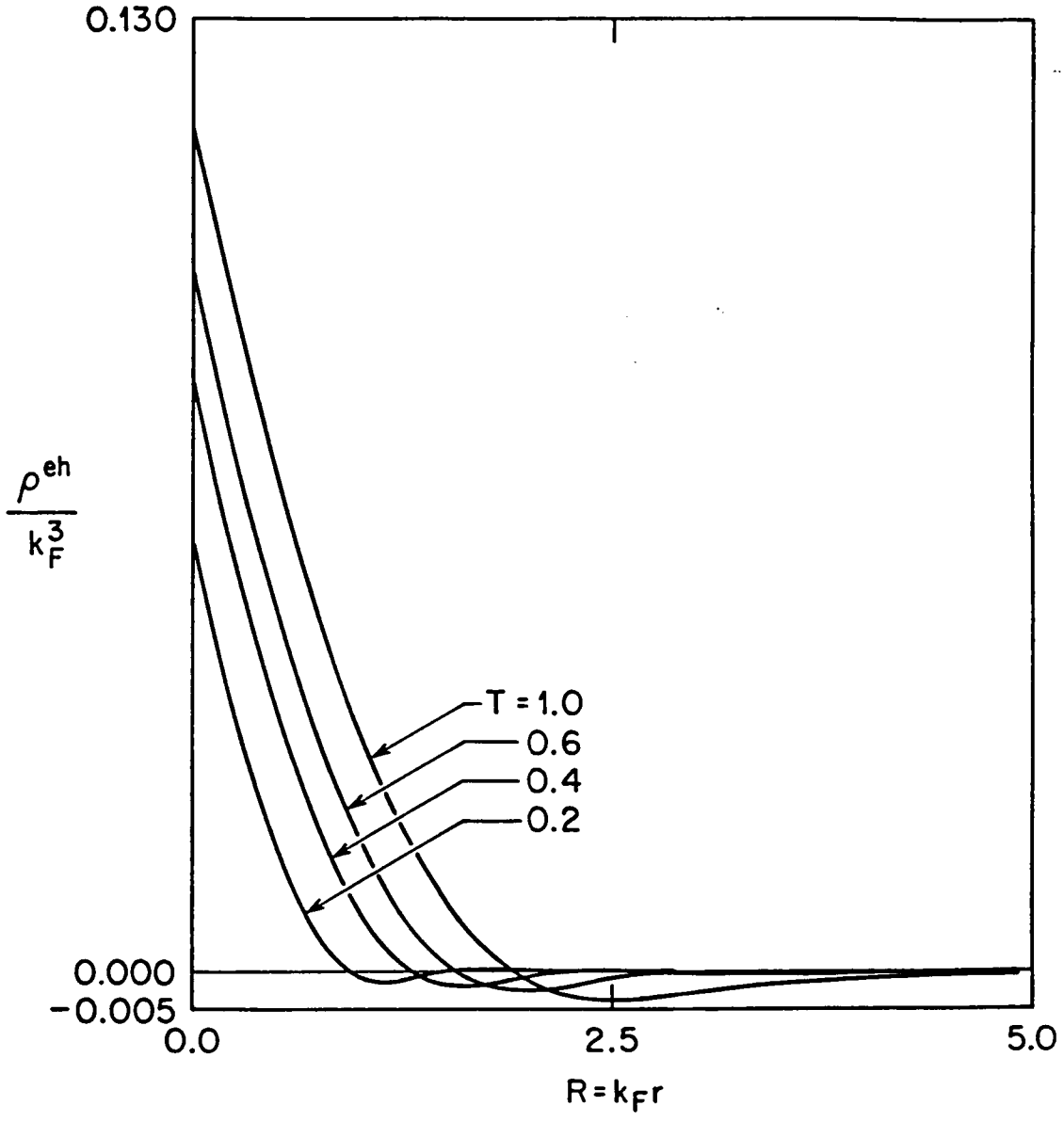

Figure 7.2: Electron-hole pair screening charge for small R and T; RPA, $r_s = 3$.

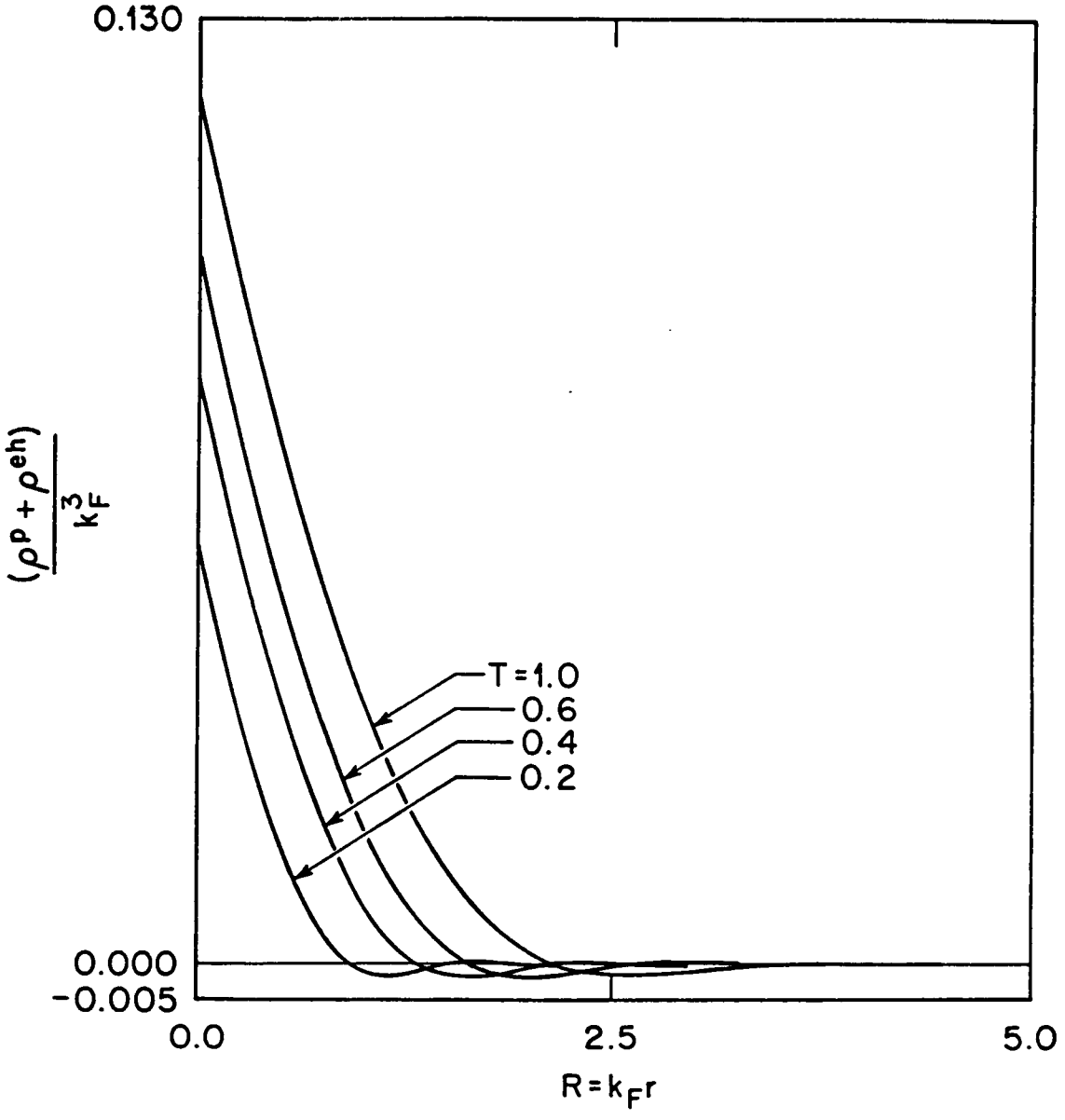

Figure 7.3: Total screening charge for small R and T; RPA, $r_s = 3$.

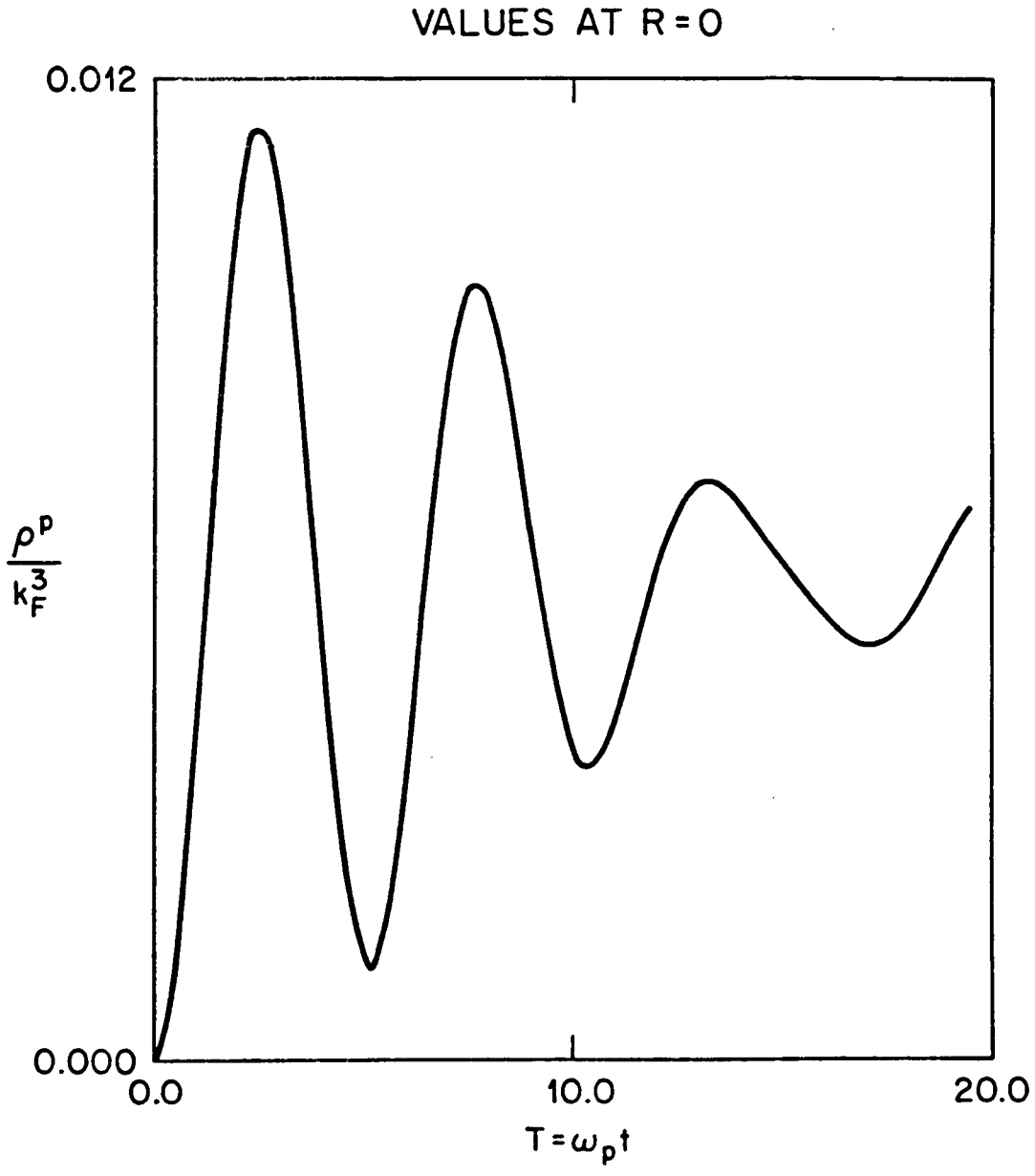

Figure 7.4: Time dependence of plasmon screening charge at $R = 0$; RPA, $r_s = 3$.

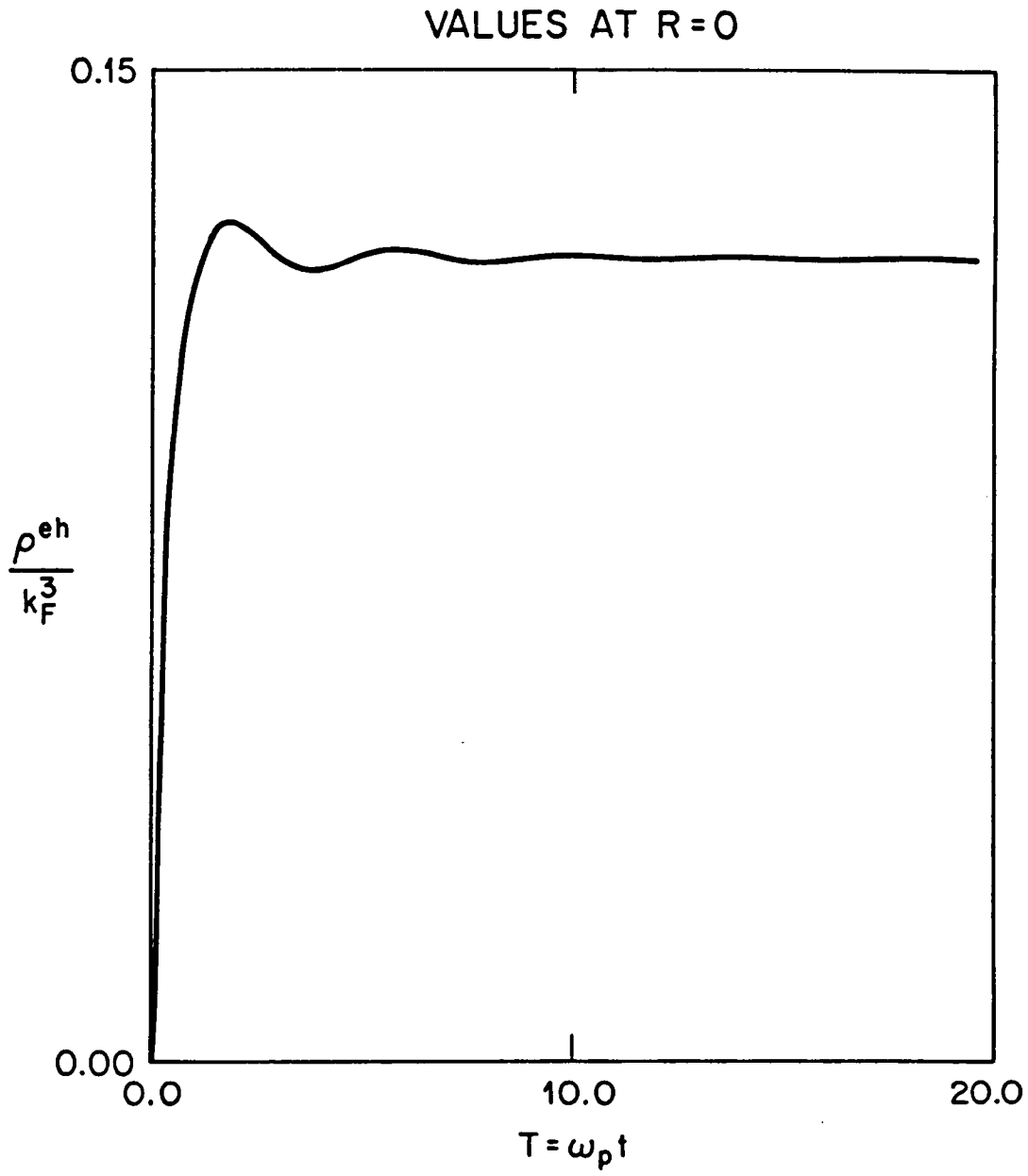

Figure 7.5: Time dependence of e-h screening charge at $R = 0$; RPA, $r_s = 3$.

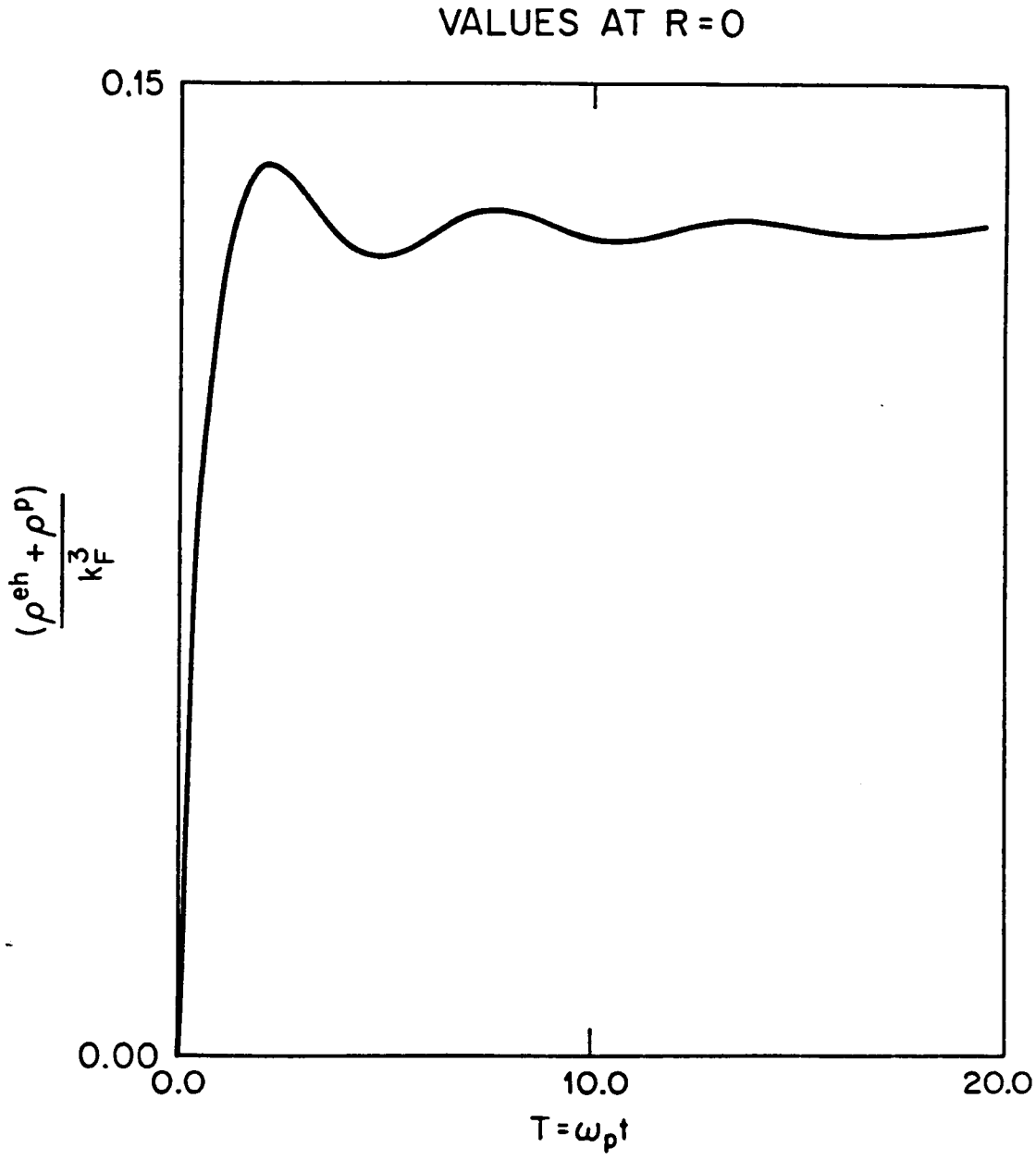

Figure 7.6: Time dependence of total screening charge at $R = 0$; RPA, $r_s = 3$.

spatial oscillations in ρ^{eh} and ρ^{p} tend to interfere destructively, leading to small net oscillations in ρ'. This was found to be true even at $T \to \infty$ [138].

The plasmon part, unsurprisingly, is more lightly damped than ρ^{eh} in both space and time. For $T > 6$, further oscillations in time are essentially due to plasmons; however, they are of order 10^{-2}.

The rise time (τ_{sc}) of ρ' is essentially that of ρ^{eh}; the first peak in Fig. 7.6 occurs at $T \sim 2$ or $t \sim 2\omega_p^{-1}$. On the fast-rising, heavily-damped e-h part there is superimposed a small, long-time "ringing" from the plasmons. In the ideal electron gas this ringing could persist to the time scale of core hole decay (for some metals [123] $\tau_A \sim 10\omega_p^{-1}$). In real metals, however, the plasmon excitations are expected to be more heavily damped, due both to band structure effects [139] and to the presence of an imaginary part in a realistic, dynamic local-field correction $G(q,\omega)$ [133,140]. Hence we expect, since $\tau_r \gtrsim \tau_A$, that there would be little observable effect from persistent screening transients in the emission spectra of simple metals. A similar conclusion was reached by Yue and Doniach [141] using many-body perturbation theory.

For $r_s = 3$, the results for $G = G_{VS}$ are very close to those in the RPA, differing slightly in vertical scale [138]; hence they are not shown. The plasmon ringing is somewhat more lightly damped using the local-field correction. This difference in plasmon damping is more pronounced in the low-density case, $r_s = 6$. Figure 7.7 shows the time dependence of $\rho'(R = 0)$ for $r_s = 6$, using $G = G_{VS}(q)$; it may be compared with Fig. 7.6. The reduction in plasmon damping seen in Fig. 7.7 arises from the decreased dispersion of the plasmon curve for this case. The plasmon dispersion curves for $r_s = 6$, calculated numerically from the equation $\epsilon_1 = 0$, are plotted in Fig. 7.8; the reduction in dispersion with the addition of G_{VS} is evident.

Thus we find that, using the more realistic dielectric function ($G = G_{VS}$), the long-time ringing is more pronounced at low electron density. This observation is reminiscent of the tendency for enhanced long-range spatial oscillations with

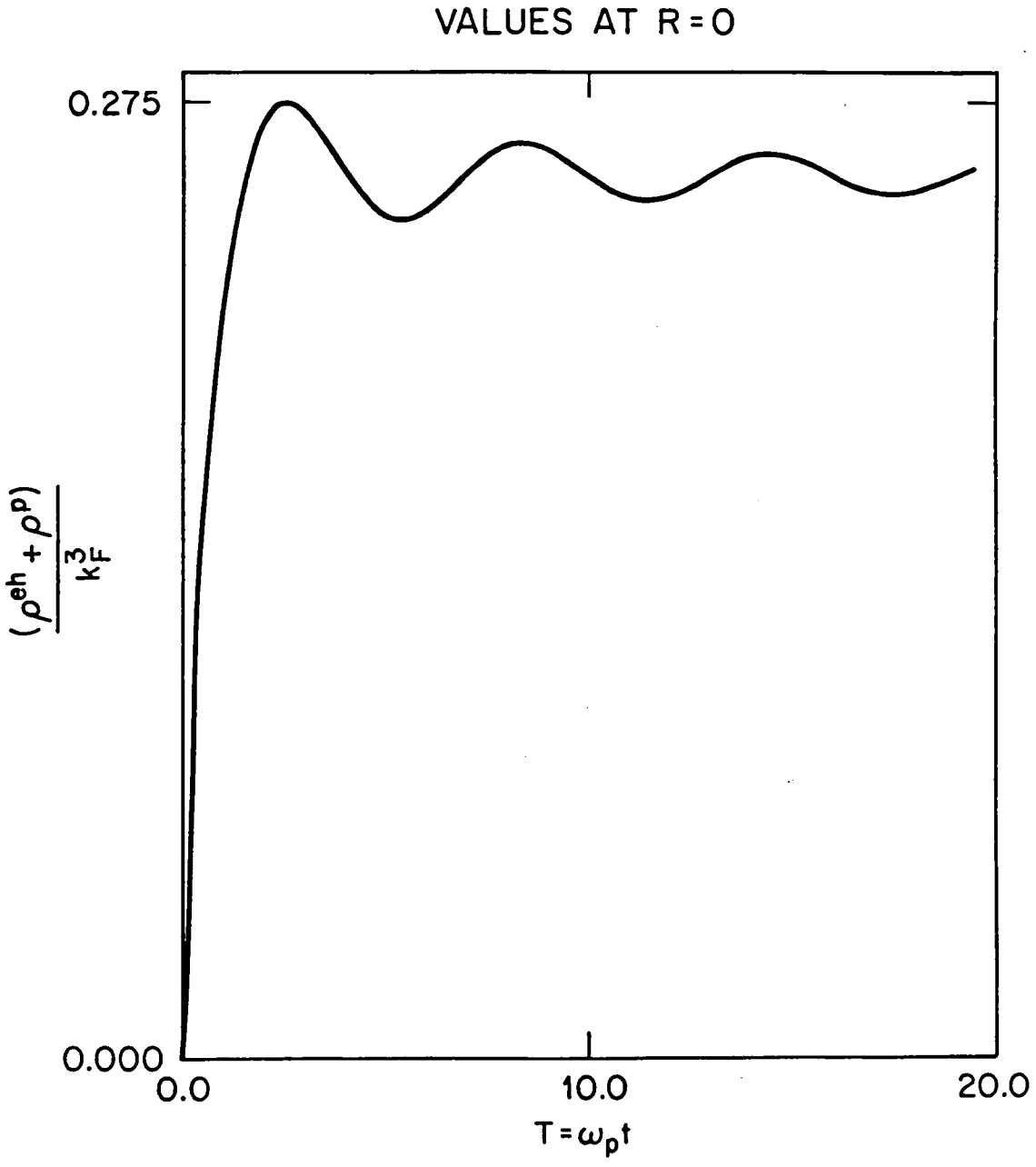

Figure 7.7: Time dependence of total screening charge at $R = 0$; $G = G_{VS}$, $r_s = 6$.

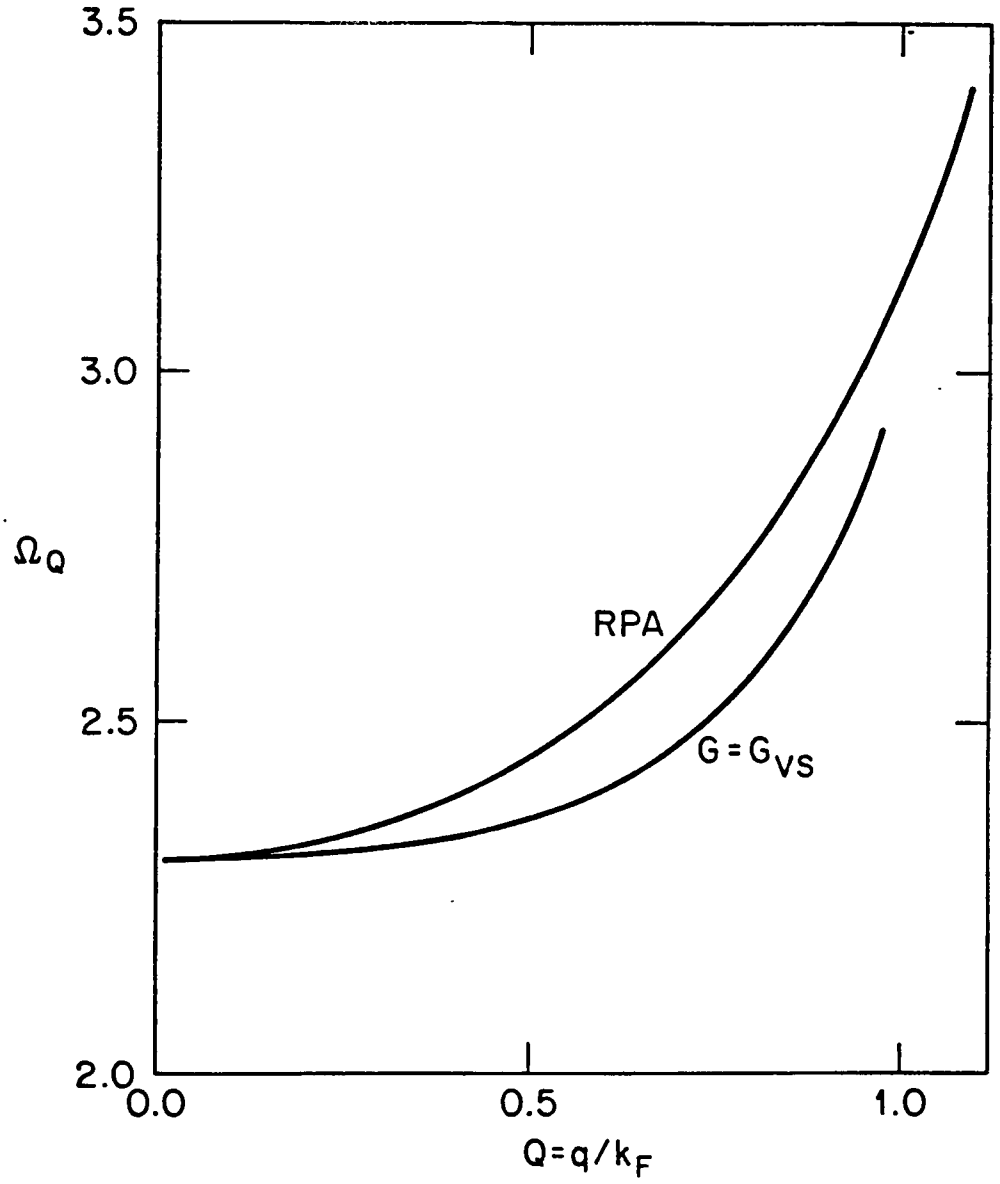

Figure 7.8: Plasmon dispersion for low density, with and without local-field correction.

decreasing gas density, seen in static screening calculations [138]. We note that the rise time of the screening charge, and the relative weight of the plasmon part, changes little in doubling r_s.

We note finally that our results corroborate the intuitive notion that $\tau_{sc} \sim \omega_p^{-1}$, as well as the results of Noguera et al [111]. They find that a screening time t_0 can be determined which is independent of photoelectron velocity v, and that

$$t_0 = 0.15 \left(\frac{2\pi}{\omega_p} \right) \simeq \omega_p^{-1}.$$

In our model the photoelectron has infinite velocity. Neglecting its interaction with the dynamic screening process enables us to calculate more carefully the response of the gas to the hole; our calculation is thus valid for $\tau_\epsilon \ll \tau_{sc}$. Noguera et al., using a semiclassical model, find that τ_{sc} (t_0 in their notation) is *independent* of τ_ϵ (which is proportional to $1/v$) over the entire range of τ_ϵ, including $\tau_\epsilon \sim \tau_{sc}$. The interesting question, not addressed by their model, is whether significant resonance or interference effects may arise from the interaction of a *quantum-mechanical* photoelectron with the core hole and the screening gas, in the energy regime $\tau_\epsilon \sim \tau_{sc}$.

Bibliography

Bibliography

[1] For some recent controversy on the validity of linear response theory see N. G. van Kampen, Phys. Norv. 5, 10 (1971); W. M. Visscher, Phys. Rev. A 10, 2461 (1974).

[2] G. D. Mahan, J. Appl. Phys. 58, 2242 (1985)

[3] O. Madelung, *Introduction to Solid-State Theory*, Springer-Verlag, Berlin, 1978.

[4] G. D. Mahan, *Many-Particle Physics*, Plenum, New York, 1981.

[5] B. R. Nag, *Electron Transport in Compound Semiconductors*, Springer-Verlag, New York, 1980, Chapter 11.

[6] E. M. Conwell, *High Field Transport in Semiconductors*, Academic Press, New York, 1967.

[7] *Proceedings of the Second International Conference on Hot Electrons in Semiconductors*, in Solid-State Electr. 21 (1), 1978.

[8] D. K. Ferry, J. R. Barker, and C. Jacoboni, eds., *Physics of Nonlinear Transport in Semiconductors*, Plenum, New York, 1980.

[9] L. Reggiani, ed., *Hot-Electron Transport in Semiconductors*, Springer-Verlag, Berlin, 1985.

[10] *Proceedings of the Fourth International Conference on Hot Electrons in Semiconductors*, Physica 134B+C, 1985.

[11] H. Fröhlich, Proc. Roy. Soc. A 188,521(1947).

[12] E. J. Ryder and W. Shockley, Phys. Rev. 81, 139 (1951).

[13] E. J. Ryder, Phys. Rev. 90, 766 (1953)

[14] F. F. Fang and A. B. Fowler, J. Appl. Phys. 41, 1825 (1970).

[15] J. P. Nougier and M. Rolland, Phys. Rev. B 8, 5728 (1973).

[16] R. C. Hughes, Phys. Rev. Lett. 30, 1333 (1973).

[17] S. Komiyama, T. Kurosawa, and T. Masumi, in [9].

[18] R. A. Höpfel, J. Shah, D. Block, and A. C. Gossard, Appl. Phys. Lett. 48, 148 (1986).

[19] H. Fröhlich, Proc. Roy. Soc. A 160, 230 (1937); H. Fröhlich, Proc. Roy. Soc. A 172, 94 (1939).

[20] D. J. DiMaria, M. V. Fischetti, M. Arienzo, and E. Tierney, J. Appl. Phys. 60, 1719 (1986).

[21] J. M. Ziman, *Principles of the Theory of Solids*, 2nd ed., Cambridge University Press, Cambridge, 1972, p. 195.

[22] K. K. Thornber and R. P. Feynman, Phys. Rev. B 1, 4099 (1970).

[23] S. Y. Chou, D. A. Antoniadis, and H. I. Smith, IEEE Trans. EDL-6, 665 (1985).

[24] H. U. Baranger and J. W. Wilkins, Phys. Rev. B 30, 7349 (1984).

[25] A. F. J. Levi, J. R. Hayes, P. M. Platzman, and W. Weigmann, Phys. Rev. Lett. 55, 2071 (1985); M. Heiblum, M. I. Nathan, D. C. Thomas, and C. M. Knoedler, Phys. Rev. Lett. 55, 2200 (1985).

[26] V. V. Paranjape and T. P. Ambrose, Phys. Lett. 8, 223 (1964); V. V. Paranjape and E. De Alba, Proc. Phys. Soc. 85, 945 (1965).

[27] A. C. Baynham, P. N. Butcher, W. Fawcett, and J. M. Loveluck, Proc. Phys. Soc. 92, 783 (1967).

[28] X. L. Lei and C. S. Ting, Phys. Rev. B 32, 1112 (1985); Phys. Rev. B 30, 4809 (1984).

[29] R. G. Ulbrich, in [7, p. 51] is a recent review.

[30] C. H. Yang, J. M. Carlson-Swindle, S. A. Lyon, and J. M. Worlock, Phys. Rev. Lett. 55, 2359 (1985).

[31] W. H. Knox, C. Hirlimann, D. A. B. Miller, J. Shah, D. S. Chemla, and C. V. Shank, Phys. Rev. Lett. 56, 1191 (1986).

[32] J. Shah, A. Pinczuk, A. C. Gossard, and W. Weigmann, Phys. Rev. Lett. 54, 2045 (1985).

[33] W. Pötz and P. Kocevar, Phys. Rev. B 28, 7040 (1983); W. Pötz, preprint.

[34] S. A. Trugman and A. J. Taylor, Phys. Rev. B 33, 5575 (1986).

[35] G. A. Baraff, Phys. Rev. 128, 2507 (1962); Phys. Rev. 133, A26 (1964).

[36] E. J. Aas and K. Blotekjaer, J. Phys. Chem. Solids 35, 1053 (1974).

[37] P. K. Basu, J. Appl. Phys. 48, 350 (1977); P. Lugli and D. K. Ferry, Phys. Rev. Lett. 56, 1295 (1986).

[38] J. R. Barker, J. Phys. C 6, 2663 (1973).

[39] S. K. Sarker, Phys. Rev. B 32, 743 (1985); S. K. Sarker, J. H. Davies, F. S. Khan, and J. W. Wilkins, Phys. Rev. B 33, 7263 (1986).

[40] W. Cai, M. C. Marchetti, and M. Lax, Phys. Rev. B 34, 8573 (1986); and preprint.

[41] D. Y. Xing and C. S. Ting, Phys. Rev. B 35, 3971 (1987); C. S. Ting and T. W. Nee, preprint.

[42] G. D. Mahan, Phys. Rep. 145, 251 (1987).

[43] G. D. Mahan and G. S. Canright, Phys. Rev. B 35, 4365 (1987).

[44] G. S. Canright and G. D. Mahan, Phys. Rev. B 36, 2870 (1987).

[45] G. S. Canright and G. D. Mahan, Phys. Rev. B 36, 1025 (1987).

[46] W. E. Boyce and R. C. DiPrima, *Elementary Differential Equations and Boundary Value Problems*, 2nd ed., John Wiley & Sons, 1969.

[47] W. P. Dumke, Phys. Rev. 167, 783 (1968).

[48] D. K. Ferry, Phys. Rev. B 8, 1544 (1973).

[49] D. K. Ferry, Appl. Phys. Lett. 27, 689 (1975).

[50] D. K. Ferry, J. Appl. Phys. 50, 1422 (1979).

[51] H. J. Fitting and J. U. Friemann, Phys. Stat. Sol. (a) 69, 349 (1982).

[52] H. D. Rees, J. Phys. Chem. Solids 30, 643 (1969).

[53] W. T. Lynch, J. Appl. Phys. 43, 3274 (1972).

[54] T. N. Theis, D. J. DiMaria, J. R. Kirtley, and D. W. Dong, Phys. Rev. Lett. 52, 1445 (1984).

[55] D. J. DiMaria, T. N. Theis, J. R. Kirtley, F. L. Pesavento, and D. W. Dong, J. Appl. Phys. 57, 1214 (1985).

[56] M. V. Fischetti, D. J. DiMaria, S. D. Brorson, T. N. Theis, and J. R. Kirtley, Phys. Rev. B 31, 8124 (1985).

[57] S. D. Brorson, D. J. DiMaria, M. V. Fischetti, F. L. Pesavento, P. M. Solomon, and D. W. Dong, J. Appl. Phys. 58, 1302 (1985).

[58] For SiO_2, if $E_{Th} \sim 1.5$MV/cm [20], and we consider only the LO phonons at $\hbar\omega_0 \cong .15$ eV [35], then this criterion implies that the mean free path $\ell_0 \sim 10$Å; other measurements indicate $\ell_0 \sim 30$Å(Ref. [57], and references therein).

[59] Ref. [143], p. 137.

[60] Ref. [5], Ch. 6.

[61] J. M. Ziman, *Electrons and Phonons*, Oxford Press, Oxford, Ch. X (1979).

[62] J. Shah, Solid State Electr. 21, 43 (1978).

[63] R. E. Nahory, Phys. Rev. 178, 1293 (1969).

[64] R. W. Shaw, Phys. Rev. B 3, 3283 (1971).

[65] C. Weisbuch, Solid State Electr. 21, 179 (1978).

[66] R. Ulbrich, Phys. Rev. Lett. 27, 1512 (1971).

[67] D. N. Mirlin, I. Ya. Karlik, L. P. Nikitin, I. I. Reshina, and V. F. Sapega, JETP Lett. 32, 31 (1980).

[68] D. Olego and M. Cardona, Phys. Rev. B 22, 886 (1980).

[69] D. N. Mirlin, I. Ya. Karlik, L. P. Nikitin, I. I. Reshina, and V. F. Sapega, Solid State Commun. 37, 757 (1981).

[70] B. P. Zakharchenya, J. Luminescence 24/25, 669 (1981).

[71] B. P. Zakharchenya, D. N. Mirlin, V. I. Perel, and I. I. Reshina, Sov. Phys. Usp. 25, 143 (1982).

[72] E. A. Imhoff, M. I. Bell, and R. A. Forman, Solid State Commun. 54, 845 (1985).

[73] G. Fasol, K. Ploog, and E. Bauser, Solid State Commun. 54, 343 (1985).

[74] G. Fasol and H. P. Hughes, Phys. Rev. B 33, 2953 (1986).

[75] M. Voos, R. F. Leheny, and J. Shah, in *Handbook on Semiconductors*, vol. 2, M. Balkanski, ed., North-Holland, Amsterdam, 1982.

[76] R. Ulbrich, Phys. Rev. B 8, 5719 (1973).

[77] H. B. Bebb and E. W. Williams, in *Semiconductors and Semimetals*, vol. 8, ed. by R. K. Willardson and A. C. Beer, Academic Press, New York, Ch. 4 (1972).

[78] C. V. Shank, R. L. Fork, R. F. Leheny, and J. Shah, Phys. Rev. Lett. 42, 112 (1979).

[79] R. F. Leheny, J. Shah, R. L. Fork, C. V. Shank, and A. Migus, Solid State Commun. 31, 809 (1979).

[80] D. von der Linde and R. Lambrick, Phys. Rev. Lett. 42, 1090 (1979).

[81] J. A. Kash, J. C. Tsang, and J. M. Hvam, Phys. Rev. Lett. 54, 2151 (1985).

[82] C. L. Collins and P. Y. Yu, Phys. Rev. B 30, 4501 (1984).

[83] D. J. Erskine, A. J. Taylor, and C. L. Tang, Appl. Phys. Lett. 45, 55 (1984).

[84] J. L. Oudar, A. Migus, D. Hulin, G. Grillon, J. Etchepare, and A. Antonetti, Phys. Rev. Lett. 53, 384 (1984).

[85] P. Lugli and D. K. Ferry, Physica 134B, 364 (1985).

[86] Ref. [5], Ch. 7.

[87] Y. B. Levinson and B. N. Levinsky, Solid State Commun. 16, 713 (1975).

[88] Y. B. Levinson and B. N. Levinsky, Sov. Phys. JETP 44, 156 (1976).

[89] W. Fawcett, A. Boardman, and S. Swain, J. Phys. Chem. Solids 31, 1964 (1970).

[90] At $T = 77$K, $0.88 \leq \lambda_\theta^0 \leq 1.13$, assuming $\hbar\omega_{op} = .037$ eV (GaAs).

[91] Ref. [4], p. 631.

[92] J. Friedel, Nuovo Cim. (Suppl.) 2, 287 (1958).

[93] J. S. Langer and S. H. Vosko, J. Phys. Chem. Solids, 12, 196 (1959).

[94] J. Hubbard, Proc. Roy. Soc. A 243, 336 (1957).

[95] K. S. Singwi and M. P. Tosi, Phys. Rev. 181, 784 (1969).

[96] K. S. Singwi, A. Sjölander, M. P. Tosi, and R. H. Land, Phys. Rev. B 1, 1044 (1970).

[97] R. P. Singh and M. Yussouff, Phys. Stat. Sol. (b) 101, K93 (1980).

[98] A. Sjölander and M. J. Stott, Phys. Rev. B 5, 2109 (1972); and references therein.

[99] P. Bhattacharyya and K. S. Singwi, Phys. Rev. Lett. 29, 22 (1972).

[100] P. Hohenberg and W. Kohn, Phys. Rev. 136, B864 (1964); W. Kohn and L. J. Sham, Phys. Rev. 140, A1133 (1965).

[101] For a review see A. K. Rajagopal, Adv. Chem. Phys. 41, 59 (1980); and references therein.

[102] C. O. Almbladh, U. von Barth, Z. D. Popovic, and M. J. Stott, Phys. Rev. B 14, 2250 (1976).

[103] P. Jena and K. S. Singwi, Phys. Rev. B 17, 3518 (1978).

[104] G. W. Bryant and G. D. Mahan, Phys. Rev. B 17, 1744 (1978).

[105] J. K. Norskov, Phys. Rev. B 20, 446 (1979); Solid- State Commun. 25, 995 (1978); Solid-State Commun. 24, 691 (1971).

[106] E. A. Sziklas, Phys. Rev. 138, A1070 (1965).

[107] B. Vinter, Phys. Rev. B 17, 2429 (1978).

[108] G. Grüner and M. Minier, Adv. Phys. 26, 231 (1977).

[109] N. Barberan and P. M. Echenique, J. Phys. B 19, L81 (1986); P. M. Echenique, R. M. Nieminen, and R. H. Ritchie, Solid-State Commun. 37, 779 (1981). Ions whose velocity $v < v_F$ (the Fermi velocity) are considered to be statically screened in this work.

[110] A. Mazarro, P. M. Echenique, and R. H. Ritchie, Phys. Rev. B 27, 4117 (1983).

[111] C. Noguera, D. Spanjaard, and J. Friedel, J. Phys. F 9, 1189 (1979).

[112] E. Runge and E. K. U. Gross, Phys. Rev. Lett. 52, 997 (1984).

[113] E. K. U. Gross and W. Kohn, Phys. Rev. Lett. 55, 2850 (1985).

[114] S. C. Ying, Nuovo Cimento B 23, 270 (1974).

[115] G. Mukhopadhyay and S. Lundqvist, Nuovo Cimento B 27, 1 (1975).

[116] G. D. Mahan, Phys. Rev. 163, 612 (1967).

[117] P. Nozières and C. T. DeDomenicis, Phys. Rev. 178, 1097 (1969).

[118] G. D. Mahan, in *Solid State Physics*, ed. by H. Ehrenreich, F. Seitz, and D. Turnbull (Academic, New York, 1974) p. 75.

[119] J. W. Wilkins, in *X-Ray and Atomic Inner-Shell Physics*, ed. by B. Crasemann (AIP, New York, 1982).

[120] J. W. Gadzuk and M. Šunjić, Phys. Rev. B 12, 524 (1975).

[121] G. D. Mahan, Phys. Rev. B 15, 4587 (1977).

[122] T. A. Callcott, E. T. Arakawa, and D. L. Ederer, Phys. Rev. B 16, 5185 (1977).

[123] P. H. Citrin, G. K. Wertheim, and Y. Baer, Phys. Rev. B 16, 4526 (1977).

[124] G. D. Mahan, Phys. Rev. B 11, 4814 (1975).

[125] P. Minnhagen, J. Phys. F 7, 2441 (1977).

[126] U. von Barth and G. Grossmann, Solid State Commun. 32, 645 (1979); Phys. Rev. B 25, 5150 (1982).

[127] G. D. Mahan, Phys. Rev. B 21, 1421 (1980).

[128] L. C. Davis and L. A. Feldkamp, Phys. Rev. B 23, 4279 (1981).

[129] K. Shung and D. C. Langreth, Phys. Rev. B 23, 1480 (1981).

[130] E. Müller-Hartmann, T. V. Ramakrishnan, and G. Toulouse, Phys. Rev. B 3, 1102 (1971).

[131] C. Noguera and D. Spanjaard, J. Phys. F 11, 1133 (1981).

[132] J. Lindhard, K. Dan. Vidensk. Selsk. Mat. Fys. Medd. 28 (8), 1 (1954).

[133] S. Ichimaru, Rev. Mod. Phys. 54, 1017 (1982).

[134] P. Vashishta and K. S. Singwi, Phys. Rev. B 6, 875 (1972).

[135] K. Utsumi and S. Ichimaru, Phys. Rev. A 26, 603 (1982); I. Nagy, J. Phys. C: Solid State Phys. 19, L481 (1986).

[136] M. Mostoller (unpublished) has obtained an analytic expression for the local-field correction of Geldart and Taylor (Can. J. Phys. 48, 167 (1970)).

[137] For $G = G_{VS}$ (and for most other theories besides RPA) the value $r_s = 6$ is somewhat beyond the stability limit for the electron gas; i.e., the compressibility becomes negative (Ref. [4]).

[138] For $T = \infty$ we let the cosine term = 0 in Eqs. (6) and (7); the results, when summed, were identical to those obtained from static calculations for the same G and r_s. See [93] and [96].

[139] P. C. Gibbons and S. E. Schnatterly, Phys. Rev. B 15, 2420 (1977); P. C. Gibbons, Phys. Rev. B 17, 549 (1978).

[140] A. A. Kugler, J. Stat. Phys. 12, 35 (1975); J. E. Alvarellos, and F. Flores, J. Phys. F: Met. Phys. 15, 1929 (1985); B. Dabrowski, Phys. Rev. B 34, 4989 (1986).

[141] J. T. Yue and S. Doniach, Phys. Rev. B 8 4578 (1973).

[142] W. P. Dumke, Phys. Rev. 132,1998(1963).

[143] C. Kittel, *Quantum Theory of Solids*, John Wiley & Sons, New York, 1963.

[144] P. A. Stark, *Introduction to Numerical Methods*, Macmillan, New York, 1970.

[145] W. H. Press, B. P. Flannery, S. A. Teukolsky, and W. T. Vetterling, *Numerical Recipes: The Art of Scientific Computing*, Cambridge University Press, Cambridge, 1986.

[146] I. S. Gradshteyn and I. M. Ryzhik, *Table of Integrals, Series, and Products*, 4th ed., Academic Press, New York, 1980.

[147] M. Abramowitz and I. A. Stegun, *Handbook of Mathematical Functions*, Dover, New York, 1970.

Appendices

Appendix A

Mathematical Details for Section 5.3

In this appendix we provide the details of the derivations in Section 5.3. In particular we shall present the perturbation analysis in order to show the nature of the approximations made.

First we describe briefly the matrix elements $M'_{ll} = 1/\tau_l$, where τ_l is the lifetime of energy level l for radiative recombination with an acceptor level. Dumke [142] obtains the transition probability per unit time, per electromagnetic mode, for spontaneous emission as

$$W_{c,A} = \frac{64\sqrt{2}\pi^3 e^2 \hbar^4 |P_{cv}|^2 \delta(\hbar\omega + E_A - E_G - E_c)}{n^2 m^2 \hbar\omega (m_A E_A)^{3/2}[1 + (m_c E_c/m_A E_A)]^4} \tag{A.1}$$

where $|P_{cv}|^2$ is the average of the (squared) matrix element of the momentum operator between valence and conduction bands, $\hbar\omega$ is the emitted photon energy, E_A is the acceptor level measured from the top of the valence band, E_G the band gap, E_c the conduction electron energy from the bottom of the conduction band, n is the index of refraction, m the bare electron mass, m_A an equivalent acceptor mass, and m_c the effective conduction band mass.

The inverse lifetime is then obtained by summing over electromagnetic modes

and multiplying by the acceptor concentration n_A:

$$\frac{1}{\tau_{E_c}} = n_A \int d(\hbar\omega) W_{c,A} \rho(\hbar\omega) \tag{A.2}$$

where

$$\rho(\hbar\omega) = n^3\omega^2/\pi^2\hbar c^3$$

is the photon density of states per unit volume. The matrix element $|P_{cv}|^2$ is obtained for isotropic bands from the f-sum rule [143]:

$$\frac{m}{m_c} - 1 = \frac{2}{m}|P_{cv}|^2 \sum_\gamma \frac{1}{E_{c,0} - E_{\gamma,0}} \tag{A.3}$$

where γ is a valence band index, and a single conduction band is assumed; the subscript 0 means the $k = 0$ value.

We choose to model gallium arsenide. We take $n = (12.6)^{1/2}$, $E_G = 1.51$eV, E_A=0.04eV, m_A=0.47m, m_c=.072m, $n_A = 10^{17}\text{cm}^{-3}$. We include three hole bands in (A.3): a light-hole and heavy- hole band, and a split-off band at Δ=0.34eV below the light and heavy bands. Then, normalizing to the phonon scattering rate $1/\tau_{op} = 10^{13}\text{sec}^{-1}$, we get

$$\frac{1}{\tau_{E_c}} = \frac{4.17 \times 10^{-6}(E_c + 1.49)}{(1 + 4.55E_c)^4} \tag{A.4}$$

(E_c in eV), which becomes $1/\tau_l = M'_{ll}$ when E_c is expressed in terms of the integer index l. Note that M'_{ll} is on the order of 10^{-6}, which justifies the first-order perturbation theory employed in the following.

Next we derive Eq. (5.18). We write

$$\vec{f}(t) = c_0(t)\vec{f_0} + \int_0^\pi \frac{d\theta}{\pi} c_\theta(t)\vec{f_\theta} \tag{A.5}$$

Then

$$\begin{aligned} \dot{\vec{f}} + M\vec{f} &= \dot{c}_0\vec{f_0} + \int_0^\pi \frac{d\theta}{\pi}\dot{c}_\theta\vec{f_\theta} \\ &\quad + \lambda_0 c_0\vec{f_0} + \int_0^\pi \frac{d\theta}{\pi}\lambda_\theta c_\theta \vec{f_\theta} \\ &= \vec{k} \end{aligned} \tag{A.6}$$

Multiplying by $\tilde{f}_0$ gives

$$\dot{c}_0 + \lambda_0 c_0 = \tilde{f}_0 \vec{k}$$

which is solved to give

$$c_0 = e^{-\lambda_0 t} \int_0^t dt' e^{\lambda_0 t'} \tilde{f}_0 \vec{k}(t') \tag{A.7}$$

if $\vec{k}$ is time-dependent; or, for constant $\vec{k}$,

$$c_0 = \tilde{f}_0 \vec{k} \left(\frac{1 - e^{-\lambda_0 t}}{\lambda_0} \right) \tag{A.8}$$

In the above it is assumed $c_0(0) = c_\theta(0) = 0$, ie the band is initially unoccupied. A similar derivation gives

$$c_\theta = \begin{cases} 2e^{-\lambda_\theta t} \int_0^t dt' e^{\lambda_\theta t'} \tilde{f}_\theta \vec{k}(t') & \vec{k} \text{ time-dependent} \\ 2\tilde{f}_\theta \vec{k} \left(\frac{1-e^{-\lambda_\theta t}}{\lambda_\theta} \right) & \vec{k} \text{ constant} \end{cases} \tag{A.9}$$

Eqs. (A.5), (A.8), and (A.9) are equivalent to Eq. (5.18).

Finally we find the eigensystem of $M = M^0 + M'$ by perturbation theory. The perturbed system is defined by Eqs. (5.21–5.24) and we wish it to satisfy the orthogonality relations (5.8–5.11), as does the unperturbed system. We wish to solve

$$M \vec{f}_\lambda = \lambda \vec{f}_\lambda \tag{A.10}$$

or

$$(M^0 + M')(\vec{f}^0_\lambda + \vec{f}'_\lambda) = (\lambda^0 + \lambda')(\vec{f}^0_\lambda + \vec{f}'_\lambda) \tag{A.11}$$

which to first order gives

$$(M^0 - \lambda^0)\vec{f}'_\lambda + (M' - \lambda')\vec{f}^0_\lambda = 0 \tag{A.12}$$

Multiplying by $\tilde{f}^0_\lambda$ gives

$$\lambda' = \frac{\tilde{f}^0_\lambda M' \vec{f}^0_\lambda}{\tilde{f}^0_\lambda \vec{f}^0_\lambda} \tag{A.13}$$

This expression is meaningful if the denominator is finite. For $\lambda = \lambda_0 = 0$, the denominator is unity, and we get Eq. (5.26). For $\lambda = \lambda(\theta)$, we write

$$\lambda'_\theta = \lim_{N \to \infty} \frac{\sum_{l=0}^N M'_{ll} \cos^2(l\theta + \phi)}{\sum_{l=0}^N \cos^2(l\theta + \phi)} \tag{A.14}$$

We know the denominator grows without bound. The numerator, however, is finite, since [see Eq. (A.4)]

$$M'_{ll}(l \to \infty) \longrightarrow (const) \times l^{-3}$$

Hence we obtain

$$\lambda'_\theta = 0. \tag{A.15}$$

Now we seek the perturbed right and left eigenvectors. We assume the perturbation vectors are orthogonal to the corresponding unperturbed vectors. For example, we expand $\vec{f}'_0$ as

$$\vec{f}'_0 = \int_0^\pi \frac{d\theta}{\pi} d_0(\theta) \vec{f}^0_\theta \tag{A.16}$$

Substituting into (A.12) gives

$$\int_0^\pi \frac{d\theta}{\pi} d_0(\theta) \lambda^0_\theta \vec{f}^0_\theta = -(M' - \lambda'_0) \vec{f}^0_0$$

Multiplying by $\tilde{f}^0_{\theta'}$, and then dropping the prime, gives

$$d_0(\theta) \lambda^0_\theta = -2 \tilde{f}^0_\theta M' \vec{f}^0_0$$

or

$$d_0(\theta) = -\frac{2}{\lambda^0_\theta} \sum_{l=0}^{\infty} e^{-Gl/2} M'_{ll} \cos(l\theta + \phi) \tag{A.17}$$

which, combined with (A.16), gives Eq. (5.28). A similar derivation, starting from the transpose of Eq. (A.16), gives Eq. (5.29). We note that

$$\tilde{f}_0 \vec{f}_0 = \tilde{f}^0_0 \vec{f}^0_0 + \tilde{f}'_0 \vec{f}^0_0 + \tilde{f}^0_0 \vec{f}'_0 = 1 \tag{A.18}$$

since the latter two terms are orthogonal vector products.

Now expand

$$\vec{f}'_\theta = a_0 \vec{f}^0_0 + P \int_0^\pi \frac{d\theta'}{\pi} a_\theta(\theta') \vec{f}^0_{\theta'} \tag{A.19}$$

where the symbol P means to omit the point $\theta = \theta'$ from the integral. Substitution into (A.12) gives

$$-a_0\lambda^0_\theta \vec{f}^0_0 + P\int_0^\pi \frac{d\theta'}{\pi} a_\theta(\theta')[\lambda^0_{\theta'} - \lambda^0_\theta]\vec{f}^0_{\theta'} = 0 \tag{A.20}$$

Now multiply by $\tilde{f}^0_{\theta''}$, where $\theta'' \neq \theta$; we get

$$\frac{1}{2} a_\theta(\theta'')[\lambda^0_{\theta''} - \lambda^0_\theta] = -\tilde{f}^0_{\theta''} M' \vec{f}^0_\theta$$

or

$$a_\theta(\theta') = 2\sum_{m=0}^{\infty} \frac{\cos(m\theta+\phi)\cos(m\theta'+\phi')M'_{mm}}{\lambda^0_\theta - \lambda^0_{\theta'}} \tag{A.21}$$

Multiplying (A.20) by $\tilde{f}^0_0$ gives

$$\begin{aligned} a_0 &= \frac{\tilde{f}^0_0 M' \vec{f}^0_\theta}{\lambda^0_\theta} \\ &= \frac{\sum_{m=0}^{\infty}(1-e^{-G})M'_{mm}e^{-Gm/2}\cos(m\theta+\phi)}{\lambda^0_\theta} \end{aligned} \tag{A.22}$$

so that, finally,

$$\begin{aligned} (\vec{f}'_\theta)_l &= P\int_0^\pi \frac{d\theta'}{\pi} \frac{e^{-Gl/2}\cos(l\theta'+\phi')}{\lambda^0_\theta - \lambda^0_{\theta'}} \\ &\quad \times 2\sum_{m=0}^{\infty} \cos(m\theta+\phi)\cos(m\theta'+\phi')M'_{mm} \\ &\quad + \frac{e^{-Gl}}{\lambda^0_\theta} \\ &\quad \times \sum_{m=0}^{\infty}(1-e^{-G})M'_{mm}e^{-Gm/2}\cos(m\theta+\phi) \end{aligned} \tag{A.23}$$

A similar calculation gives

$$(\tilde{f}'_\theta)_l = e^{Gl}(\vec{f}'_\theta)_l \tag{A.24}$$

Since the cost/benefit ratio of computing these quantities seems high, they are neglected in the remainder of the calculation. However their denominators (which are $\propto e^{-G/2}$) can become very small at low temperatures. Hence the neglect of $\vec{f}'_\theta$ and $\tilde{f}'_\theta$ leads to poor results at low temperature, as discussed in Section 5.4. We

have verified the following relationships:

$$\tilde{f}_0 \vec{f}_\theta = \tilde{f}_\theta \vec{f}_0 = 0 \tag{A.25}$$

$$\tilde{f}_\theta \vec{f}_{\theta'} = \frac{\pi}{2}\delta(\theta - \theta') \tag{A.26}$$

Hence the perturbed system satisfies (5.8)–(5.11).

Appendix B

Details of Section 7.2

This appendix contains details of the derivations in Sec. 7.2. We drop the vector notation in $\epsilon(q,\omega)$ as there is no angular dependence; then, putting (7.4) into (7.3) and double transforming gives

$$\begin{aligned}\rho_s(r,t) &= \frac{1}{(2\pi)^4}\int d^3q \int d\omega e^{i\vec{q}\cdot\vec{r}} e^{-i\omega t}\left(\frac{1}{\epsilon(q,\omega)}-1\right)\left(\frac{i}{\omega+i\delta}\right) \\ &= \frac{1}{4\pi^3 r}\int_0^\infty dq q \sin qr \int_{-\infty}^\infty d\omega e^{-i\omega t}\left(\frac{1}{\epsilon(q,\omega)}-1\right)\left(\frac{i}{\omega+i\delta}\right). \quad \text{(B.1)}\end{aligned}$$

Next we note that

$$B(q,\omega) \equiv \left(\frac{1}{\epsilon(q,\omega)}-1\right)$$

has the required properties for the Kramers-Kronig relations (i.e., it is the transform of a causal function, and it vanishes as $\omega \to \infty$) [4]. So, letting

$$B(q,\omega) = B_1(q,\omega) + iB_2(q,\omega)$$

we have that

$$B(q,\omega) = -\frac{1}{\pi}\int_{-\infty}^\infty d\omega' \frac{B_2(q,\omega')}{\omega-\omega'+i\delta},$$

which combined with (7.5) gives

$$\rho_s(r,t) = \frac{1}{4\pi^3 r}\int_0^\infty dq q \sin qr \int_{-\infty}^\infty d\omega e^{-i\omega t}$$

$$\times \left(\frac{i}{\omega + i\delta}\right)\left(-\frac{1}{\pi}\int_{-\infty}^{\infty} d\omega' \frac{B_2(q,\omega')}{\omega - \omega' + i\delta}\right)$$

$$= \frac{1}{4\pi^3 r}\int_0^{\infty} dq q \sin qr \int_{-\infty}^{\infty} d\omega' B_2(q,\omega')$$

$$\times \left[\frac{-i}{\pi}\int_{-\infty}^{\infty} d\omega \frac{e^{-i\omega t}}{(\omega + i\delta)(\omega - \omega' + i\delta)}\right].$$

Contour integration gives the quantity in square brackets as

$$2\left(\frac{1 - e^{-i\omega' t}}{\omega'}\right)\Theta(t)$$

so that

$$\rho_s(r,t) = \frac{1}{2\pi^3 r}\Theta(t)\int_0^{\infty} dq q \sin qr \int_{-\infty}^{\infty} \frac{d\omega}{\omega} B_2(q,\omega)(1 - e^{-i\omega t}). \tag{B.2}$$

Now, since

$$B_2(q,\omega) = -\frac{\epsilon_2(q,\omega)}{\epsilon_1^2 + \epsilon_2^2}, \tag{B.3}$$

where $\epsilon(q,\omega) = \epsilon_1(q,\omega) + i\epsilon_2(q,\omega)$, then $B_2(q,\omega)$ is an odd function of ω. This fact, applied to (B.2), gives Eq. (7.5) of the main text.

In Eqs. (7.6) and (7.7), $R = k_F r, Q = q/k_F, T = \omega_p t, \Omega = \omega/E_F, \omega_q$ is defined by $\epsilon_1(q,\omega_q) = 0$ and $\epsilon_2(q,\omega_q) = 0$;

$$\omega_p = \lim_{q\to 0} \omega_q$$

(i.e., the long-wavelength plasma frequency), Ω_Q is defined analogously to ω_q,

$$\alpha' = \frac{\alpha^2}{(12 r_s)^{1/2}},$$

$$\alpha = \left(\frac{9\pi}{4}\right)^{1/3},$$

and r_s is a dimensionless quantity defined by [4]

$$\frac{4}{3}\pi(r_s a_0)^3 = \frac{1}{n_0},$$

where n_0 is the uniform unperturbed density of the electron gas, and a_0 is the Bohr radius;

$$\begin{aligned} \Omega_1 &= \max(0, Q^2 - 2Q) \\ \Omega_2 &= Q_2 + 2Q \\ |\epsilon_1'|_{\Omega_Q} &= \left| \frac{d\epsilon_1(Q,\Omega)}{d\Omega} \right|_{\Omega=\Omega_Q} . \end{aligned}$$

The limits on the Ω integral in (7.6) are the upper and lower bounds for the e-h continuum. To get (7.7), use (B.3) to note that

$$\lim_{\epsilon_2 \to 0} B_2 = -\pi\delta(\epsilon_1) = -\frac{\pi\delta(\Omega - \Omega_Q)}{\left| \frac{d\epsilon_1(Q,\Omega)}{d\Omega} \right|_{\Omega=\Omega_Q}}.$$

The upper limit (Q_c) in (7.7) is the point at which the plasmon curve meets the e-h continuum; i.e.,

$$Q_c^2 + 2Q_c = \Omega_{Q_c}.$$

Finally, we can recover the steady-state result for ρ_s from (7.5) as follows. For $t \to \infty$, the term $\cos(\omega t)$ will integrate to zero. Hence

$$\rho_s(r, \infty) = \frac{1}{2\pi^3 r} \int_0^\infty dq q \sin qr \int_{-\infty}^\infty \frac{d\omega}{\omega} B_2(q, \omega)$$

[cf Eq. (B.2)]. Since the residue of B_2 is zero at $\omega = 0$, the ω integral is equal to its principal part. Then a Kramers-Kronig transformation gives

$$\begin{aligned} \rho_s(r, \infty) &= \frac{1}{2\pi^2 r} \int_0^\infty dq q \sin qr B_1(q, 0) \\ &= \frac{1}{2\pi^2 r} \int_0^\infty dq q \sin qr \left(\frac{1}{\epsilon(q,0)} - 1 \right). \end{aligned} \tag{B.4}$$

The standard result [95] is Eq. (B.4) multiplied by (-1) to convert negative (electronic) charge densities to positive particle densities. We have done the same.

Appendix C

Numerical Methods for Chapter 7

In this appendix we give the details of the numerical methods used to obtain the results in Chapter 7.

We can find $d\epsilon_1/d\Omega$ analytically. In the RPA we have

$$\epsilon_1 = 1 + \beta[1 + u(\Omega) \cdot L_p + v(\Omega) \cdot L_m] \tag{C.1}$$

where

$$\beta = \frac{2r_s}{\pi\alpha}\frac{1}{Q^2} \tag{C.2}$$

$$u(\Omega) = \left(\frac{1}{2Q} - \frac{Q}{8} - \frac{\Omega}{4Q} - \frac{\Omega^2}{8q^3}\right) \tag{C.3}$$

$$v(\Omega) = \left(\frac{1}{2Q} - \frac{Q}{8} + \frac{\Omega}{4Q} - \frac{\Omega^2}{8q^3}\right) \tag{C.4}$$

$$L_p = \ln\left[\frac{\Omega + (Q^2 + 2Q)}{\Omega + (Q^2 - 2Q)}\right] \tag{C.5}$$

and

$$L_m = \ln\left[\frac{\Omega - (Q^2 + 2Q)}{\Omega - (Q^2 - 2Q)}\right], \tag{C.6}$$

the expression for L_m being valid for the plasmon region where $\Omega > Q^2 + 2Q$. So

$$\frac{d\epsilon_1}{d\Omega} = \beta[u'L_p + v'L_m + uL_p' + vL_m']$$

which amounts to

$$\frac{d\epsilon_1}{d\Omega} = \beta\left[-\frac{1}{4Q}(1+\frac{\Omega}{Q^2})L_p + \frac{1}{4Q}(1-\frac{\Omega}{Q^2})L_m + u\frac{(-4Q)}{Q^4-4Q^2+2Q^2\Omega+\Omega^2} + v\frac{4Q}{Q^4-4Q^2-2Q^2\Omega+\Omega^2}\right] \quad \text{(C.7)}$$

Now write

$$\epsilon(Q,\Omega) = 1 + v_q P(Q,\Omega) \quad \text{(C.8)}$$

so

$$\epsilon_1'(Q,\Omega) = v_q P_R'(Q,\Omega) \quad \text{(C.9)}$$

where

$$P = P_R + iP_I \quad \text{(C.10)}$$

and the prime signifies differentiation with respect to frequency. We introduce this notation in order to go beyond RPA. Let

$$\begin{aligned}\epsilon_G(Q,\Omega) &= 1 - \frac{v_q P(Q,\Omega)}{1+v_q G(Q) P(Q,\Omega)} \\ &= \epsilon_{G_1} + i\epsilon_{G_2}\end{aligned} \quad \text{(C.11)}$$

denote the real and imaginary parts of the dielectrc function which incorporates the local-field correction $G(Q)$. In the plasmon region

$$\epsilon_{G_2} = \epsilon_2 = P_I = 0.$$

Hence

$$\epsilon_{G_1} = 1 - \frac{v_q P_R}{1+v_q G P_R} = \frac{1+v_q H P_R}{1+v_q G P_R}$$

where $H = H(Q) = G(Q) - 1$; then we get

$$\epsilon_{G_1}' = -\frac{v_q P_R'}{(1+v_q G P_R)^2} = \frac{\epsilon_1'}{(1+v_q G P_R)^2} \quad \text{(C.12)}$$

where the omission of the subscript G in any ϵ implies RPA, which is obtained by setting $G(Q) = 0$.

The quantity ϵ'_{G_1} is useful in two ways. It enters directly into the calculation of the plasmon part of the screening in Eq. (7.7). It also may be used as part of a Newton-Raphson (NR) subroutine [144] to find the zeroes of $\epsilon_1(\Omega)$, ie to find the plasmon curve Ω_Q.

The value Q_c at which the plasmon curve enters the continuum is also the zero of a function, ie we set

$$Q^2 + 2Q - \Omega_Q = 0; \tag{C.13}$$

however we cannot take the derivative of this function. Hence we used a modification of Brent's algorithm from Press et al [145] (henceforth PFTV) to find Q_c and Ω_{Q_c}.

In the course of carrying out the numerical integration it was found that the NR algorithm (which is iterative) was too slow to be called repeatedly. Hence the entire Ω_Q curve, up to Ω_{Q_c}, was fitted by a 30-term Chebyshev polynomial using a fitting routine from PFTV [145]; the coefficients were then used to calculate Ω_Q in the course of the integration. The disagreement between fitted and NR values for Ω_Q was always less than 10^{-4}. The determination of Q_c and the Chebyshev fit needs to be done only once for each choice of density (r_s) and local- field factor $G(Q)$.

The plasmon integral, being a single integral, was readily accomplished. A variable-step-size Runge-Kutta method was used since the integrand was observed (by plotting it) to be oscillatory with a varying frequency. All the integration routines were obtained from PFTV [145].

The e-h double integral was treated as nested single integrals, with an outer (Q) integral and an inner (Ω) integral. The outer integral was broken into three parts as follows. A large-Q approximation was used for $Q > Q_L = 20$, enabling most of the integration to be done analytically as described below. The interval $0 \leq Q \leq 20$ was divided into two parts because the Q integrand (ie the inner integral) has a discontinuous slope at $Q = Q_c$, due to the sudden entrance of plasmon-like spectral weight. Each low-Q part was integrated using the same approach: Romberg

integration for the inner integral and Gaussian integration for the outer integral. This combination was found to be the fastest of several tested. It was possible to vary the order of the Gaussian integration automatically since algorithms were available [145] to calculate the abscissae and weight factors; hence the number of points was increased until a convergence criterion (10^{-4}) was satisfied.

Next we develop the large-Q integral. We note that Ω is of order Q^2 in the e-h region; hence, for large Q, we get

$$\begin{aligned} \epsilon_1 &= 1 + O(Q^{-2}) \\ \epsilon_2 &= O(Q^{-1}), \end{aligned}$$

so that

$$-\Im\left(\frac{1}{\epsilon}\right) = \frac{\epsilon_2}{\epsilon_1^2 + \epsilon_2^2} \approx \epsilon_2 \tag{C.14}$$

where $\Im$ means imaginary part.

Furthermore, for large Q, $\epsilon_2 \approx \epsilon_{G_2}$; so we neglect any G-dependence. The large-Q integral is then

$$\begin{aligned} I_L &= \frac{r_s}{\alpha\pi^3 R}\int_{Q_L}^{\infty} Q dQ \sin QR \\ &\quad \times \int_{\Omega_1}^{\Omega_2} \frac{d\Omega}{\Omega}\frac{1}{Q^3}\left(1 + \frac{\Omega}{2} - \frac{\Omega^2}{4Q^2} - \frac{Q^2}{4}\right) \\ &\quad \times [\cos(\alpha'\Omega T) - 1] \end{aligned} \tag{C.15}$$

or

$$I_L = I_T - I_\infty \tag{C.16}$$

where I_T has the cosine term in the square brackets, and I_∞ the term unity.

The inner integral in I_∞ gives

$$\frac{8}{3Q} + O(Q^{-3});$$

hence

$$I_\infty = \frac{8}{3}\frac{r_s}{\alpha\pi^3 R}\int_{Q_L}^{\infty} dQ \frac{\sin QR}{Q^3}$$

or

$$I_\infty = \frac{8}{3}\frac{r_s}{\alpha\pi^3 R} \times \left[\frac{\sin(Q_L R)}{2Q_L^2} + \frac{R\cos(Q_L R)}{2Q_L} + \frac{R^2}{2}\mathrm{si}(Q_L R)\right] \quad \text{(C.17)}$$

using Gradshteyn and Ryzhik [146]; $\mathrm{si}(x)$ is the sine integral, and we have used the fact that $\mathrm{si}(\infty)=0$ [147]. It follows that

$$I_\infty(R=0) = \frac{8}{3}\frac{r_s}{\alpha\pi Q_L} \quad \text{(C.18)}$$

Next we seek

$$I_T = \frac{r_s}{\alpha\pi^3 R}\int_{Q_L}^{\infty}\frac{dQ}{Q^2}\sin QR \times \int_{\Omega_1}^{\Omega_2} d\Omega\left(\frac{1}{2} - \frac{\Omega}{4Q^2} - \frac{Q^2}{4\Omega} + \frac{1}{\Omega}\right) \times \cos(\alpha'\Omega T) \quad \text{(C.19)}$$

We call the inner integral I_Ω; it is

$$I_\Omega = \frac{Q}{B}\cos A\sin B - \frac{2}{B}\sin A\cos B + \frac{2}{B^2}\sin A\sin B + (1-\frac{Q^2}{4})[\mathrm{ci}(A+B) - \mathrm{ci}(A-B)] \quad \text{(C.20)}$$

where

$$A = \alpha' Q^2 T \quad \text{(C.21)}$$

$$B = 2\alpha' QT \quad \text{(C.22)}$$

and $\mathrm{ci}(x)$ is the cosine integral. We wrote simple iterative routines, using algorithms from Abramowitz and Stegun [147], to calculate $\mathrm{ci}(x)$ and $\mathrm{si}(x)$.

The Q integral of I_T cannot be done analytically; we used Gaussian integration. The $R=0$ value is obtained, as in the low-Q integrals, by replacing

$$\frac{\sin QR}{R} \longrightarrow Q.$$

As a check, we can verify analytically that

$$\lim_{T\to 0} I_T = I_\infty.$$

We further note that I_T should become negligible for large T. We find in fact that

$$I_T(T=1) \approx 10^{-3} I_\infty;$$

hence we neglect I_T for $T > 1$.

Finally we discuss the large-T behavior of the small-Q integrals; this is needed to examine the long-time transient behavior, for which the $R = 0$ value was chosen as representative (Chapter 7). For large values of T the Gauss/Romberg combination failed to give reliable results, due to the strongly oscillating Ω integrand. Hence we derived and used an algorithm which applies to integrals of the form

$$I = \int_{x_0}^{x_M} dx f(x) \cos(Ax)$$

by treating small pieces of $f(x)$ as parabolic segments, integrating each piece analytically, and summing the results. The algorithm is thus a trig-modified Simpson's Rule; it is

$$\begin{aligned} I &= f_0 \left\{ -\frac{1}{A^3\Delta^2}[S_2 + S_0(A^2\Delta^2 - 1)] + \frac{1}{2A^2\Delta}(C_2 + 3C_0) \right\} \\ &+ \sum_{\substack{n=0 \\ even}}^{M-2} f_{n+1} \left\{ \frac{2}{A^3\Delta^2}(S_{n+2} - S_n) - \frac{4}{2A^2\Delta}(C_{n+2} + C_n) \right\} \\ &+ \sum_{\substack{n=2 \\ even}}^{M-2} f_n \left\{ \frac{1}{A^3\Delta^2}(S_{n-2} - S_{n+2}) + \frac{1}{2A^2\Delta}(C_{n+2} + 6C_n + C_{n-2}) \right\} \\ &+ f_M \left\{ \frac{1}{A^3\Delta^2}[S_M(A^2\Delta^2 - 1) + S_{M-2}] \right. \\ &\left. + \frac{1}{2A^2\Delta}(3C_M + C_{M-2}) \right\} \end{aligned} \tag{C.23}$$

where $f_n = f(x_n)$, $x_n = x_0 + n\Delta$, $x_M = x_0 + M\Delta$, $M = 2m$, m =integer;

$$\Delta = \frac{x_M - x_0}{M} = \frac{x_M - x_0}{2m};$$

$C_n = \cos(Ax_n)$, $S_n = \sin(Ax_n)$. Eq. (C.23) was used rather than Romberg's method for large T, giving results which were well-behaved at large T and which joined smoothly onto the small-T results.

Vita

Geoffrey St. John Canright was born in Los Angeles, California on June 24, 1949. He graduated from Palisades High School in June of 1966. After studying at UCLA he transferred to UC Berkeley where he received a B.S. in Psychology in 1972. Subsequently he worked as a carpenter, mechanic, plant manager, electrician, machine designer and field service engineer before returning to academic work.

In 1979 he joined the Oak Ridge National Laboratory (ORNL) as an engineer in the Instrumentation and Controls (I&C) Division, and simultaneously initiated pursuit of a B.S. in Electrical Engineering, which was obtained from the University of Tennessee (UT) in December 1981. He graduated first in his college with a 4.0 GPA. In 1982 he took the position of Instructor in Electrical Engineering at UT, concurrently doing graduate work in the same department. In the 1983–1984 academic year he worked as a consultant to the I&C Division in the area of electrical load management, and simultaneously consulted with the Metals and Ceramics (M&C) Division on the properties of amorphous magnetic alloys. In the latter project he was instrumental in obtaining his own funding from the Department of Energy.

In September 1984 he joined the Physics Department at UT, but continued to work at the M&C Division of ORNL until January 1986, at which time he joined the research group of Dr. Gerald Mahan, Distinguished Professor of Physics. Mr. Canright received the degree of Doctor of Philosophy with a major in Physics in December 1987.

The author is a member of Tau Beta Pi, Sigma Pi Sigma, and the American Physical Society. He is the principal author or coauthor of eight journal articles. After graduation he will join Indiana University at Bloomington as a postdoctoral fellow.